NATURAL AND SYNTHETIC SILICA INCORPORATED CHITOSAN COMPOSITE SCAFFOLDS FOR BONE TISSUE ENGINEERING APPLICATIONS

**A Thesis Submitted to
the Graduate School of Engineering and Science of
Izmir Institute of Technology
in Partial Fulfillment of the Requirements for the Degree of**

DOCTOR OF PHILOSOPHY

in Bioengineering

**by
Sedef TAMBURACI**

**July 2016
İZMİR**

We approve the thesis of **Sedef TAMBURACI**

Examining Committee Members:

_____
Prof. Dr. Funda TIHMINLIOĞLU
Department of Chemical Engineering, İzmir Institute of Technology

_____
Assoc. Prof. Dr. Engin ÖZÇİVİCİ
Department of Bioengineering, İzmir Institute of Technology

_____
Prof. Dr. Ayşe Semra KOÇTÜRK
Faculty of Medicine, Department of Medical Biochemistry, Dokuz Eylül University

_____
Assist. Prof. Dr. Ahu ARSLAN YILDIZ
Department of Bioengineering, İzmir Institute of Technology

_____
Prof. Dr. Oğuz BAYRAKTAR
Department of Chemical Engineering, Ege University

28 July 2016

_____   _____
Prof. Dr. Funda TIHMINLIOĞLU   **Prof. Dr. Hasan HAVITÇIOĞLU**
Supervisor,   Co-Supervisor,
Department of Chemical Engineering,   Faculty of Medicine, Department of
İzmir Institute of Technology   Orthopedics and Traumatology,
                                              Dokuz Eylül University

_____   _____
Prof. Dr. Volga BULMUŞ   **Prof. Dr. Bilge KARAÇALI**
Head of the Department of Biotechnology   Dean of the Graduate School of
and Bioengineering   Engineering and Sciences

ACKNOWLEDGMENTS

ABSTRACT

NATURAL AND SYNTHETIC SILICA INCORPORATED CHITOSAN COMPOSITE SCAFFOLDS FOR BONE TISSUE ENGINEERING APPLICATIONS

Recently bone tissue engineering studies have focused on the development of 3D scaffolds that can organize the tissue regeneration in natural way with appropriate porosity and reinforced the structure. Natural polymer-based composites have been focused with more attention than synthetic polymer composites for bone tissue engineering applications because of their biocompatibility and biodegradability. In this work, the goal was to combine the useful biomaterial properties of both chitosan and silica to design biocomposite organic/inorganic biomaterials for bone tissue engineering applications. The composite scaffolds were fabricated by freeze drying method bu using two different silicas; natural silica; Diatomite and synthetic silica, octa (tetramethylammonium) polyhedral oligomeric silsesquioxanes (OctaTMA-POSS).

The effects of silica type and loading on the mechanical, morphological, chemical, surface properties, wettability and biocompatibility of composite scaffolds were investigated and characterized by using SEM, AFM, contact angle analysis, swelling study, protein adsorption assay, biodegradation and biomineralization tests. WST-1 cytotoxicity, cell proliferation with rezasurin and alkaline phosphatase activity assays were performed to determine biological activity of the composite scaffolds. *In vitro* biomineralization on scaffolds was determined by Von Kossa and Alizarin red staining. POSS and diatomite incorporation increased the surface roughness. Chitosan-silica composites exhibited 82-90% porosity. Wet chitosan-silica composite scaffolds exhibited higher compression moduli compared to pure chitosan scaffold in 67.3-81.4kPa and 78.1 to 107.6kPa range respectively. Average pore size range of chitosan-diatomite and chitosan-POSS composite scaffolds was obtained as 15-180μm and 220-300μm, respectively. Results indicated that chitosan-silica composites did not show any cytotoxic effect on 3T3, MG-63 and Saos-2 cell lines. Chitosan-silica composites were found to be favorable for osteoblast proliferation. Diatomite and POSS incorporation showed promising effects with enhancing ALP activity on hFob cells. Therefore, these composite scaffolds could be used for bone tissue engineering applications.

ÖZET

KEMİK DOKU MÜHENDİSLİĞİ UYGULAMALARINA YÖNELİK DOĞAL VE SENTETİK SİLİKA KATKILI KİTOSAN KOMPOZİT DOKU İSKELELERİ

Son dönemde kemik doku mühendisliği çalışmaları uygun poroziteye ve güçlendirilmiş yapıya sahip, doku rejenerasyonunu organize eden üç boyutlu yapı iskeleleri üzerinde yoğunlaşmıştır. Kemik doku mühendisliği uygulamalarında doğal polimer bazlı kompozitler biyouyumlu ve biyobozunur özellikleri yüzünden sentetik kompozitlere göre daha çok ilgi çekmektedir. Bu çalışmada amaç, kitosan ve silikanın faydalı biyomalzeme özelliklerini biaraya getirerek kemik doku mühendisliği uygulamalarına yönelik inorganik/organik biyokompozit biyomalzeme tasarlamaktır. Kompozit yapı iskeleleri iki farklı silika kaynağı; doğal silika, diatom ve sentetik silika okta-tetrametilamonyum polihedral oligomerik silseskioksan (OctaTMA-POSS) kullanılarak dondurarak kurutma yöntemi ile üretilmiştir. Silika türü ve katkısının, kompozitlerin mekanik, morfolojik, kimyasal ve yüzey özellikleri, ıslanırlık ve biyouyumluluğu üzerine etkisi incelenmiş ve temas açısı analizi, su absorpsiyon çalışmaları, biyobozunurluk ve biyomineralizasyon testleri ile karakterize edilmiştir. Kompozit yapı iskelelerinin biyolojik aktivitesi WST-1 sitotoksisite testi, rezasurin ile hücre proliferasyonu ve alkalen fosfataz aktivite testi ile belirlenmiştir. Kompozitler üzerindeki *in vitro* biyomineralizasyon von Kossa ve Alizarin red boyama yapılarak belirlenmiştir. Kitosan-silika kompozitler 82-90% gözeneklilik oranı sergilemiştir. Islak kitosan-diatom ve kitosan-POSS kompozit yapı iskelelerinde saf kitosana kıyasla, 67.3-81.4kPa ve 78.1-107.6kPa aralığında daha yüksek basma modulusu elde edilmiştir. Kitosan-diatom ve kitosan-POSS kompozitlerin ortalama gözenek çapı sırayla 15-180μm ve 220-300μm olarak ölçülmüştür. POSS ve diatom katkıları yüzet pürüzlülüğünü arttırmıştır. Kitosan-silika kompozitler 3T3, MG-63 ve Saos-2 hücreleri üzerinde sitotoksik etki göstermemiştir, hücre proliferasyonu için uygun bulunmuştur. Diatom and POSS katkıları, hFob hücrelerinin ALP aktivitesini arttırarak gelecek vaad eden bir etki göstermiştir.

TABLE OF CONTENTS

LIST OF FIGURES

LIST OF TABLES

CHAPTER 1

INTRODUCTION

Recently, clinical procedures are performed to replace or repair tissues in the human body that have been damaged by disease or trauma. Current techniques are focused on the replacement of the damaged tissue by using donor graft tissues (autografts, allografts or xenografts). However, these conventional grafting techniques have limitations of shortage of donors, harmful immune responses and rejection, possible disease transmission, donor site pain and morbidity. Tissue engineering applications aim to regenerate tissue damage by designing biological substitutes that can renovate, sustain and improve tissue at the defect site.

Bone tissue engineering has focused on the development of 3D scaffolds with required and appropriate porosity that can serve as a support, reinforce and in some cases organize the tissue regeneration or replacement in natural way. An ideal scaffold for bone tissue engineering should have interconnected porous structure. Under favour of this structure, scaffold may guide new tissue in-growth and regeneration. Recently, natural polymer-based composites have been focused with more attention than synthetic polymer composites for bone tissue engineering applications because of their biocompatibility and biodegradability. Biopolymers are natural materials which include polysaccharides (starch, alginate, chitin/chitosan, hylauronic acid derivatives) or proteins (soy, collagen, fibrin gels, silk) and a variety of biofibers, such as lignocelluloses (Sasidharan, 2011).

Chitosan is a promising natural polymer for tissue engineering due to its favorable properties such as being non toxic, non allergenic, mucoadhesive, biocompatible and biodegradable, and also accelerating cell proliferation. Furthermore, it has structural similarity to glycosaminoglycans which are the major component of the extracellular matrix. The porous structure of chitosan is a promising characteristic for the development and optimization of a variety of tissue scaffolds and regeneration aids (Kim et. al., 2008; Arca and Şenel, 2008). However, it has some limitations such as low tensile strength and modulus range when compared with natural bone. One approach to overcome this mechanical incompatibility with bone is to reinforced chitosan by an inorganic compound (Di Martino et al., 2005; Arca and Şenel, 2008; Chew et al., 2011).

Among those inorganic compounds, silica has been widely used in medicine and nanotechnology in various forms. In recent studies, composites consisting biopolymers and silica particles show potential in biomedical applications. Silica, hydrated silicon dioxide, the second most abundant biogenic mineral is produced by various plants and animals (Narayanan et al., 2011). Silica particles can improve mechanical properties of polymers by providing enhancement in the structure. Besides, silica content supports bone cell adhesion and bone tissue formation by increasing the bioactivity of composites. Many studies investigating implants containing bioactive silicate found that the implants induce bone formation, stimulate osteogenic proliferation and activate bone-related gene expression. In addition, studies showed that silica induced CaO accumulation on the surface and nucleation of the apatite layer which is an essential step in the formation and mineralization of hard tissues. (Madhumathi et al., 2009; Puchol et al., 2009; Wu et al., 2010).

Recent reports by Lee *et al*. used a sol-gel method to fabricate chitosan–silicate nanocomposite membranes for bone regeneration. The addition of silicate resulted in improved mechanical properties of the nanocomposite when compared to pure chitosan (Wu et al., 2010). In a study, chitosan-silicate nanocomposites found to initiate calcium phosphate deposition which is an important factor for *in vitro* bioactivity of bone cells. Results indicated significant increase in osteoblast adhesion, proliferation and alkaline phosphatase activity with silica incorporation (Wu et al., 2010).

Polyhedral oligomeric silsesquioxanes (POSS), new class of synthetic silica nanoparticles with 3-dimensional nanophase material, are well-defined cage structures, which contain a silicon/oxygen cage (inorganic portion) and hydrocarbon functional groups (organic portions) as hybrid chemical composition intermediate between that of silica (SiO_2) and silicone (R_2SiO). This unique structure makes POSS one of the most promising nanomaterials to be used in the structure of different polymers for biomedical applications due to stimulation of biological responses at nanoscale. As a natural and abundant silica mineral, Diatomite, known as diatomaceous earth (SiO_2-nH_2O), is composed of microscopic skeletal remains of unicellular algae-like plants called diatoms (Şan et al., 2009). Diatoms have been used in several areas such as filtration (pool water ,beer and wine filtration, absorption, gel filtration), photonics, , sound and heat insulation, chemical reactions (catalyst, sensor components, dynamites, filler material, abrasive) and drug delivery (Bakr, 2010; Cai, et al. 2005, Lopez-Alvarez et al., 2008; Hadjar et al., 2008; Parkinson & Gordon 1999, Scala & Bowler 2001, Stoermer et

al., 2004; Şan et al., 2009; We et al., 2005) due to its abundance, inexpensive cost, unique morphology and porous structure. But up to date, diatomite incorporated silica based scaffolds have not been used for bone tissue engineering applications.

In the present study, the goal was to combine the useful biomaterial properties of both chitosan and silica as biocomposite organic/inorganic biomaterials for bone tissue engineering applications. A number of articles and reviews are available in the literature on the promising properties of chitosan-silica composites. However, there is no literature regarding bone tissue engineering studies on composites composed of natural silica source diatomite and synthetic silica nanocage structure POSS. This study is proposed to design a novel chitosan-silica composites that can be used as scaffolds for bone tissue engineering applications and optimize the silica content of the composites in order to obtain optimum morphological structure, high mechanical properties, enlarged surface area and enhanced cell proliferation. The effect of silica loading on the mechanical, chemical, and swelling properties, as well as morphological and surface wettability of composite membranes were evaluated. In addition, *in vitro* cytotoxicity and cellular activities including cell proliferation and cell differentiation were investigated using MG-63, Saos-2 and hFob cells.

The organization of the dissertation is as follows: Chapter 1 gives a brief information about this dissertation. Chapter 2 gives background on literature regarding biomaterials for bone tissue engineering, natural polymer chitosan and effect of silica reinforcement on bone regeneration. Chapter 3 makes mention of fabrication, characterization methods and *in vitro* studies used in experiments is presented. In Chapter 4 the characterization and *in vitro* results of the study are discussed. Finally, Chapter 5 offers the conclusions of this work and the suggestions for future works.

CHAPTER 2

LITERATURE REVIEW

2.1. Bone Tissue Engineering

One of the major health problems is tissue and organ loss resulting from an injury or damage and such health problems are solved with tissue or organ transplantation which is a standard therapy for treatment. But there are some limitations of this technique such as donor shortage, donor site morbidity, immune rejection, infection and disease transfection. These limitations have elicited the development of an alternative approach, tissue engineering (Chen et al., 2002; Zohora and Azim, 2014).

The term of tissue engineering was initially defined as 'application of the principles and methods of engineering and life sciences toward fundamental understanding of structure–function relationship in normal and pathological mammalian tissues and the development of biological substitutes for the repair or regeneration of tissue or organ function' by first NSF (National Science Foundation, USA) attendees in 1988. Langer and Vacanti reported a comprehensive review and defined the tissue engineering term as "a multidisciplinary field formed with combination of life sciences and engineering principles in order to describe structure-function relationships in mammalian tissues and the development of biological substitutes to restore, maintain or improve tissue function". Tissue engineering methods have been applied to different types of tissue, including skin, bone, liver, muscle, cartilage and nerve tissue (Weigel et al., 2006; Arca and Şenel, 2008; Cheung et al., 2007).

Tissue engineering generally focuses on fabricating living replacement parts for the body by using synthetic or naturally derived materials. The most common approach which is defined as tissue engineering triad (Figure 2.1.), is composed of biological substitutes is based on living cells, signal molecules and scaffolds. This triad is also known as tissue engineering construct (TEC). The cells synthesize new tissue matrice at the diseased or damaged site and the scaffold provides temporary three dimensional frameworks as a suitable environment for the cell adhesion proliferation and differentiation. The signal molecules facilitate and promote the cells for new tissue

regeneration at the defect site. This 3D living construct is structurally, mechanically and functionally similar with the replaced tissue (Hutmacher et al., 2007; Kim et al., 2008; Armentano et al., 2010; Zohora and Azim, 2014).
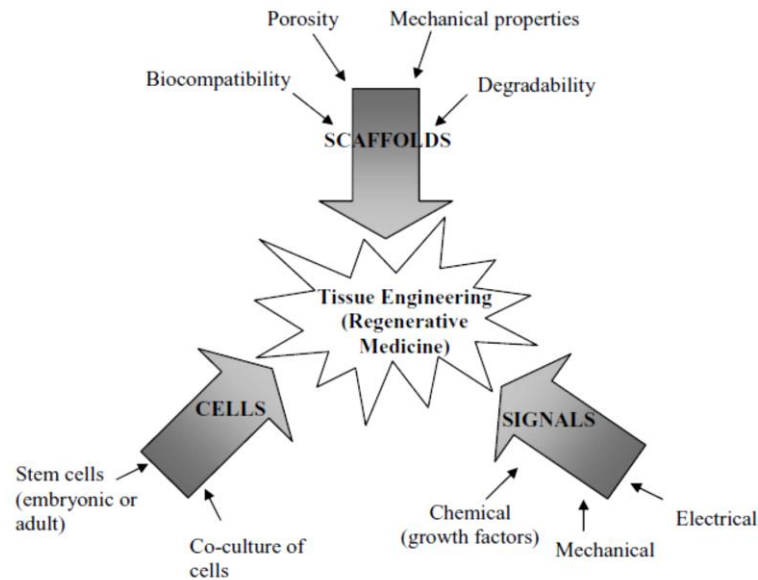
Figure 2.1. The tissue engineering triad
(Source:Lyons et al., 2008).

Bone tissue degeneration and inflammatory problems affect millions of people worldwide and these diseases often require surgery. In addition, numerous bone fractures, osteoporosis, scoliosis and other musculoskeletal problems need to be solved by using permanent or temporary devices (Navarro et al., 2008). Generally traditional methods are used in orthopaedic procedures that require associated space filling known as bone grafting. In this method, bone-defect management include autografting and allografting cancellous bone. In particular, bone grafting is significant in spinal fusion, revision arthroplasty, fracture repair and bone cysts. Bone allograft (dead bone from another patient) and autografts (viable bone from a different site in the same patient) are the current solutions for bone grafting applications. But, these grafting procedures have some limitations: bone from another part of the body is harvested in the autograft technique and this material fills the gap, provides optimal osteoinductivity and osteoconductivity. However, autografting often leads to complications in wound healing, additional surgery, donor pain and an inadequate bone supply for filling. Cadaver bone is used in the allograft technique but this can cause immunogenic

reactions and the risk of transfection of diseases. These bone grafts are avascular and dependent on diffusion, so defect size and the host bed viability can limit their application. In addition to that, unpredictable bone resorption may occur at the large defect sites and the grafts can be resorbed by the body before osteogenesis is complete. Bone cement is another material that is used in the bone defect. However, bone cements can be susceptible to infection due to being prepared in the operating room. These limitations and concerns have conduced to the development of artificial materials as bone graft substitutes (Burg et al., 2000; Bonfield, 2006; Venkatesan and Kim, 2010).

Bone tissue engineering has focused on the development of 3D scaffolds with appropriate porosity that can serve as a support, reinforce and organize the tissue regeneration in natural way. Enhanced bone regeneration is usually obtained with biomimetic scaffolds that provide a suitable microenvironment to promote osteoblast proliferation and osteogenesis. These 3D scaffolds exhibit tailored porosity, pore size and interconnectivity. Cells and signalling molecules (i.e. growth factors) are seeded into highly porous biodegradable scaffolds and cultured, subsequently implanted into bone defect (Figure 2.2.). Cells can be obtained from calvarine, trabecular bone, human embryonic stem (*h*ES) cells and bovine osteoblasts (*b*OB) (Roether and Boccaccini, 2008; Sasidharan, 2011; Razak et al., 2012).
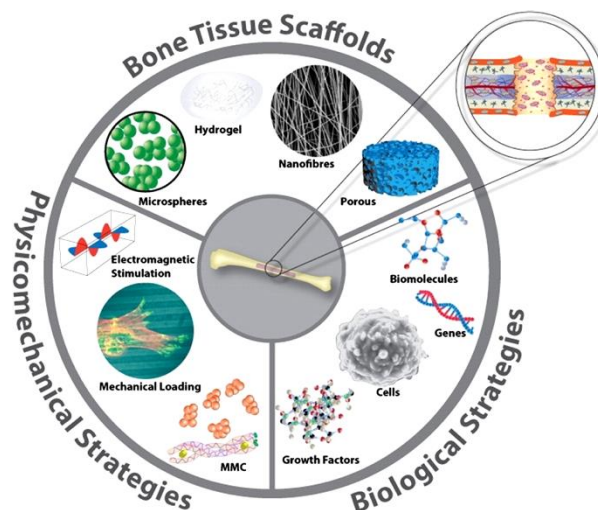
Figure 2.2. Bone Tissue Scaffolds
(Source:Fernandez-Yague et al., 2015).

Bioactive ceramics show chemical similarity to natural bone and allow osteogenesis by providing bond with host bone. However, they have limitations such as brittleness and low biodegradability restricting their use in clinical applications. Natural

and synthetic polymers have been used as bone substitutes to overcome these disadvantages (Kim et al, 2008). Recently, natural polymer-based composites have been focused with more attention than synthetic polymer composites for bone tissue engineering applications due to their biocompatible and biodegradable behavior. Biopolymers which include polysaccharides (starch, alginate, gelatin, chitin/chitosan, cellulose, hylauronic acid derivatives) and proteins (soy, collagen, fibrin gels, silk) are suitable natural-based materials because of their low cost, non toxicity, biocompatibility, and multifunctional properties (Sasidharan, 2011). However, they have limitations in mechanical properties. Therefore, they need to be reinforced with other biocompatible substances to enhance properties (Razak et al., 2012). Natural polymer composite materials which combine biodegradable polymers and bioactive ceramics in order to mimic the natural function of bone, are becoming increasingly important biomaterials for bone tissue engineering. (Venkatesan and Kim, 2010; Sasidharan, 2011). Table 2.1. shows the general bone tissue engineering approaches with their advantages and limitations.

Table 2.1. Bone Tissue Engineering Approaches: Advantages and Limitations (Source:Bueno and Glowacki, 2009).

Approach	Advantages	Limitations
Bone Grafts		
Autograft	Immunocompatible; osteoconductive	Need for harvesting surgery; graft site morbidity
Allograft	Off-the-shelf; osteoconductive	Concerns about disease transmission and immunogenecity; variable efficacy
Scaffolds		
Biodegradable	Maintaining mechanical stability while being replaced with new bone; remodeling bone lls entire site	By-products of degradation can be harmful; degradation rate must be synchronized with new bone growth to preserve mechanical stability

Table 2.1. cont.

Permanent	Immediate mechanical stability	Nidus for infection; immunological response; material fatigue or erosion.
Preformed	Mechanical stability; control over structural properties	Does not conform to shape
Injectable	Conforms to shape; minimally invasive	Limited porosity; limited mechanical strength
Traditional fabrication techniques (e.g. textile processing)	Cost-effective	Limited control over structural properties
CAD/CAM fabrication techniques (computer aided design and manufacturing e.g. rapid prototyping)	Advanced control over structural properties	Complex fabrication
Demineralized bone matrix	Biocompatible; osteoinductive; off-the-shelf; inexpensive	Concerns about immunogenicity and infection; variable ef cacy
Natural polymers	Biocompatible	Limited mechanical strength
Synthetic polymers	Tunable structural, mechanical, and degradation properties	Concerns about biocompatibility and immunogenecity
Ceramics	Biocompatible; good drug delivery; FDA-approved for use in bone regeneration	Brittle; limited to non-weight-bearing sites; injectable formulations present low porosity
Bioactive glasses	Bone binding; osteoconductive	Brittle
Composites	Take advantage of the parent materials' qualities, while mitigating their limitations	Complex fabrication

Table 2.1. cont.

Bioactive Factors		
Growth factors	Enhance cellular activities such as proliferation, migration, bone formation, and angiogenesis	Complicated delivery; leakage; expensive
Platelet rich plasma	Autologous; inexpensive	Mixed reports on efficacy; complex logistics to prepare
Enamel matrix derivative	Available for periodontal use	Available products are porcine
Cell Based Approach		
Autologous marrow	Immunocompatible; readily available	Does not provide mechanical stability
Autologous MSCs(marrow stromal cells) /scaffold constructs	Immunocompatible cells; mechanical stability	Limited numbers of cells; limited clinical data available
Allogeneic cells	Some currently available products do not require FDA-approval	Limited clinical data available

2.1.1. Key Factors of Scaffold Design for Bone Tissue Engineering Applications

Scaffolds are artificial structures on which cells proliferate and three dimensional tissue formation occurs until adequate extracellular matrix (ECM) is formed to support the structure mechanically. Figure 2.3. respresents the important factors involved in the design of optimal scaffolds for bone tissue engineering.

An ideal scaffold design has some key factors;

➢ **Architecture and Structural requirements:** Scaffold should have anatomic shape and void volume for vascularization. Minimum pore size of 100 µm is required critical for the diffusion of nutrients and oxygen for cell survival. Besides, cell migration is determined by degree of porosity and pore

interconnectivity/tortuosity. Recent studies have demonstrated that multi-scale porous scaffolds (combining micro- and macro-porosities) are superior to macro-porous scaffolds in enabling cell attachment and invasion. Scaffold should have interconnected open porous structure for *in vivo* tisssue in-growth where optimum macro (pore size >100 μm) and micro porosity (pore size < 20 μm) increase the surface area for cell attachment, obtain cell migration and diffusion of gases, nutrients and metabolic wastes in and out of the scaffold without significantly compromising the mechanical stability of the scaffold. Generally smooth surfaces exhibit less cell adhesion than rough surfaces. Therefore, scaffold should have the favorable surface properties for cell attachment and differentiation.

➢ **Mechanical Properties:** The mechanical properties of the scaffold should be designed to meet the specific requirements of the tissue at the defect site. Scaffold should provide temporary mechanical support at the site of implantation and exhibit mechanical properties similar to that of the host bone. The mechanical strength of the scaffold should be sufficient to provide mechanical stability to constructs in load bearing sites prior to synthesis of new extracellular matrix by cells. Also initial mechanical strength is crucial for safe handling during sterilizing and packaging as well as in vivo survival of material through physical forces. Furthermore, the scaffold should have sufficient mechanical integrity to allow for handling during implantation procedure and to survive under physiological conditions. After implantation, it should provide biomechanical function until normal tissue function has been restored.

➢ **Biocompatibility:** Biocompatibility of a scaffold is described as its ability to support normal cellular activity including molecular signaling systems without any local and systematic toxic effects to the host tissue. Scaffold must be non-toxic and non-inflammatory with its degradation products. It should be compatible with the surrounding biological fluids and tissues, in order to minimize the immunological response, must not interfere with wound healing and induce fibrosis or a foreign body response. If the scaffold is non-toxic and degradable, new tissue will replace it; if it is non-toxic and biologically active then it will integrate with the surrounding tissue. However, when the scaffold is biologically inactive, fibrous tissue may be formed around the scaffold. In the worst case, if the scaffold is toxic, it will be rejected by the body and localised

death of the surrounding tissue wil ocur.

➢ **Biodegradability:** Scaffold should have an adequate degradation rate in the physiological environment: If the degradation is faster than the cell proliferation, the scaffold might degrade before the tissue construction. Otherwise, cell death can be observed. The breakdown products of degradation should be non-toxic and easily excreted from the body via metabolic pathways or the renal filtration system.

➢ **Osteoconductivity:** An ideal bone scaffold must be osteoconductive by providing bone cells to adhere, proliferate, and form extracellular matrix on its surface and pores. Osteoconduction between the material and host bone eliminates the fibrous tissue formation at the defect site. Besides provides strong bond between host tissue and scaffold during regeneration process.

➢ **Manufacturing technology:** scaffold should have a fabrication process which allows it to be shaped to match defect geometries. It should be sterilisable, readily implanted or delivered through a user-friendly device consequently meet the requirements for clinical use (Arca and Şenel, 2008; Lyons et al., 2008; Roether and Boccaccini, 2008; Jones, 2009; Bhatia 2010; Bose et al., 2012; Zohora and Azim, 2014; Tang et al., 2016).
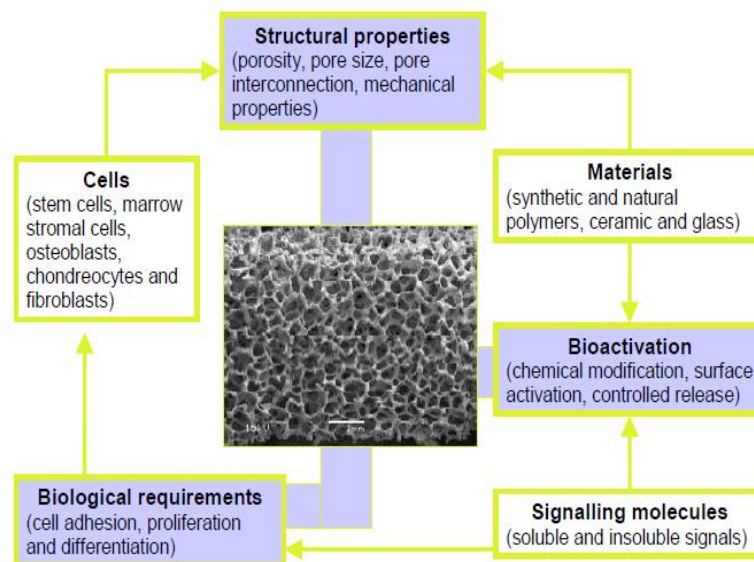
Figure 2.3. Important factors involved in the design of optimal scaffolds for bone tissue engineering (Source:Chen et al., 2008).

2.1.2. Biomaterials for Bone Tissue Engineering

The evolution of biomaterials research has revealed three different generations (Hench & Polak 2002): bioinert materials (first generation), bioactive and biodegradable materials (second generation), and materials designed to stimulate specific cellular responses at the molecular level (third generation) (Navarro et al., 2008).

2.1.2.1. First Generation Biomaterials

During the twentieth century, the availability of materials for implant fabrication was the same as for other industrial applications (Navarro et al., 2008). First generation biomaterials were developed during the 1960s and 1970s. When synthetic materials were first used in biomedical applications, the only requirement was to achieve a suitable combination of physical properties to match with the replaced tissue with a minimal toxic response since the human body consists of a highly corrosive environment (Henkel and Polak, 2002; Navarro et al., 2008). In 1980, there were more than 50 implanted devices in clinical use which were fabricated from 40 different materials. Biological inertness is the most common part of these materials. The principle of the design and development of biomaterials was to minimize the immune host response (Henkel and Polak, 2002).

Consequently, the first generation of biomaterials were easily available materials that are used in industrial applications, but they were required to be inert in order to reduce corrosion and release of particles after implantation (Navarro et al., 2008).

2.1.2.2. Second Generation Biomaterials

The second generation biomaterials are considered to have developed between 1980 and 2000 (Navarro et al., 2008). Biomaterial design began to shift from achieving exclusively a bioinert tissue response to instead producing bioactive components that could interact with the biological environment to enhance the biological response and the tissue/surface bonding (Navarro et al., 2008). Another advance in this second

generation biomaterials was the development of resorbable biomaterials (Henkel and Polak, 2002). During this period, bioactive biomaterials designed for bone regeneration led to the in vivo deposition of hydroxyapatite (HAp) layer at the material surface. The soluble HAp coatings led to a tissue response (osteoconduction) in which bone tissue growth occured along the coating and formed a mechanically strong interface. Bioactive glasses and glass-ceramics were used for conductive hearing loss treatment (middle-ear prostheses) and as oral implants. By the mid-1980s, bioactive glasses (BGs), ceramics, glass–ceramics and composites had reached clinical use in bone tissue and dental applications as bioactive materials (Henkel and Polak, 2002; Navarro et al., 2008).

2.1.2.3. Third Generation Biomaterials

Improvements of first and second generation biomaterials are limited in part. Because synthetic materials can not respond to changing physiological loads or biochemical stimuli as living tissues can. This limitation affects the lifetime of biomaterials as artificial body parts (Henkel and Polak, 2002). The third generation of biomaterials emerged approximately at the same time as scaffolds for tissue engineering applications started to be developed. These biomaterials are improved to be able to stimulate specific cellular responses at the molecular level and perform signaling and stimulation of specific cellular activity by mimicking the ECM components to promote specific cell responses. Thus, cell behaviour including adhesion, migration, proliferation and differentiation is influenced by the biomolecules which are attached to the material surface (Navarro et al., 2008).

2.2. Bone Structure

Bone provides mechanical support for muscles and facilitates movement, while protecting vital organs. Bone is a highly dynamic and complex tissue, concerning structural and functional properties, evolving and adapting to various stimuli. It plays crucial roles in both mechanical support and mineral homeostasis (Costa-Pinto et al., 2011). There are different morphologies of bone. At the macrostructure level, bone is principally separated into the cortical (compact) and cancellous (trabecular) types

depending on the structural organization, porosity and mechanical properties. In cross-section, a dense cortical bone layer (compact) forms the outer region of long bones which contains ~80-90% mineralized tissue providing the mechanical strength, while trabecular bone (cancellous) fills the interior which contain 5-25% mineralised tissue showing metabolic functions as a calcium and phosphate ion. Cortical bone consists of close packets of osteons, cylindrical (Haversian) systems with a central channel that consists of a blood vessel surrounded by concentric rings (lamellae) of bone matrix. The mechanical properties of this system are anisotropic, being a function of the di- rection of applied force. In contrast, cancellous bone is less dense and structured in plates (trabeculae) offering a larger surface area to mass ratio, making it an effective structure for ion exchange (homeostasis), hematopoiesis, and imparting flexibility in load-bearing bones (Pielichowska and Blazewicz, 2010; Costa-Pinto et al., 2011; Vaz et al., 2011; Amini et al., 2012; Fernandez-Yague et al., 2015). Trabecular bone has a porosity around 50-90% filled with bone marrow, while cortical bone is denser and has a maximum porosity of 10-20%. Compact bone and trabecular bone have almost the same elemental composition (Costa-Pinto et al., 2011; Vaz et al., 2011). Although they are composed of similar materials, the maturation of the cortical bone material may alter the mechanical properties at the microstructural level (Hutmacher et al., 2007).

Specifically, bone is a natural composite material, which contains about 60% mineral, 30% matrix and 10% water (w/w %) (Razak et al., 2012). Bone extracellular tissues can be defined as a three dimensional nanocomposite of nano-HAp particles and type-I collagen polymer matrix. This nanocomposite structure is formed by collagen fibers reinforced by hydroxyapatite crystals. In human bone tissue, bone extracellular matrix (ECM) is composed of a non-mineralized organic component collagen matrix (90% of organic component) reinforced with a mineralized inorganic component (40–50 v/v %) apatite crystals. Organic part is predominantly type-1 collagen and inorganic part is composed of 4-nm-thick plate-like carbonated apatite mineralites. Collagen matrix as an organic component of bone is predominantly responsible for the tensile strength and it is related to the capacity of bone to absorb energy (toughness). Other noncollagenous macromolecules in organic part (10%) consists mainly of extremely acidic proteins which are believed to play crucial roles in the formation and function of bone tissue. The inorganic phase is composed essentially by small carbonated apatite ($Ca_5(PO_4,CO_3)_3(OH)$) crystals. The mineral component of bone, calcium phosphate in the form of HAp gives rise to the compressive strength and plays an important role on

the stiffness (Feng, 2009; Pielichowska and Blazewicz, 2010; Beniash, 2011; Vaz et al., 2011; Amini et al., 2012; Fernandez-Yague et al., 2015).

The bone architecture is under continuous modulation by cell activity in response to mechanical loading and resistance (Fernandez-Yague et al., 2015). Bone is a vascularized, dense, supporting skeletal tissue consisting of cells and mineralized ECM. The majority of bones are covered by a highly vascularized fibrous connective tissue known as "periosteum" (Costa-Pinto et al., 2011). Trabecular struts and dense cortical bone are composed of mineralized collagen fibres stacked parallel to form layers, known as "lamellae". These lamellae wrap in concentric layers around a central part named "Haversian canal" containing nerve and blood vessels to form an Osteon (Haversian system) (Henkel et al., 2013). The major component of compact bone is an osteon which creates cylindrical conduits known as Haversian canals, provides access for the circulatory and nervous system. Figure 2.4. illustrates the structure of bone with its main components. Bone is deposited by bone-forming cells (osteoblasts) and by osteocytes. Bone is moulded, remoulded and/or removed by mono- or multinucleated osteclasts (sometimes by osteocytes). The first bone matrix deposited is unmineralized and known as osteoid consisting of collagen fibrils and noncollagenous macromolecules. Subsequently, osteoid mineralizes a few microns away from the cells. Some osteoblasts become entrapped in the mineralizing matrix and differentiate into osteocytes. Osteocytes form a network connecting with each other and the osteoblasts outside of the bone matrix. It is thought that they play an important role in the regulation of bone homeostasis (Pielichowska and Blazewicz, 2010; Beniash, 2011; Costa-Pinto et al., 2011).
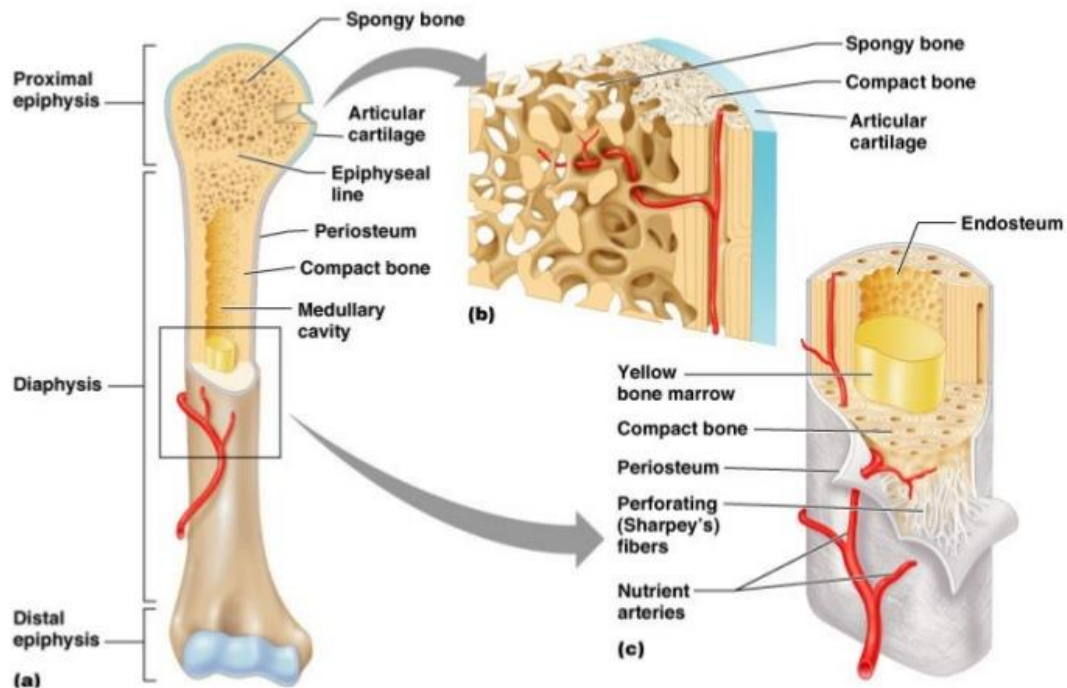
Figure 2.4. Structure of bone
(Source:http://classes.midlandstech.edu/carterp/Courses/bio210/chap06/lecture1)

Five different cell types are involved in bone maintenance and remodeling: MSCs, bone-lining cells, osteoblasts, osteocytes, and osteoclasts. Osteoblasts can be derived from MSCs (Costa-Pinto et al., 2011). The osteoblast manufactures bone, being responsible for the synthesis of collagen and the non-collagenous proteins of bone (osteocalcin, osteopontin, bone sialoproteins, and bone morphogenetic proteins), the organization of collagen fibrils, the synthesis and mineralization of osteoid (Freemont, 1993; Costa-Pinto et al., 2011). Besides, osteoblasts also have active role in the vascularization process. They secrete morphogens that activate angiogenesis by signaling endothelial cells (Costa-Pinto et al., 2011). The typical osteoblast arrayed on bone surface works as part of a consortium with other neighbouring osteoblasts. Thus, they form seams of osteoid. Osteoblasts deposit osteoid only on a pre-existing mineralized surface. Therefore, mineralization occurs only if there are adequate calcium and phosphate ions in the extracellular fluid (Freemont, 1993). Osteocytes are terminally differentiated osteoblasts and they are entrapped within the bone extracellular matrix. Osteocytes are responsible for maintaining ECM and calcium homeostasis. They also sense mechanical stress and communicate signals for bone remodeling. Osteoclast are responsible for bone resorption, which is the first stage of the bone remodeling process, followed by bone homeostasis. Osteoclasts are large

multinucleated cells which are differentiated from monocytes found in peripheral blood (Costa-Pinto et al., 2011). Figure 2.5. represents the location of the osteocytes, osteoblasts and osteoclasts within the trabecular structure.
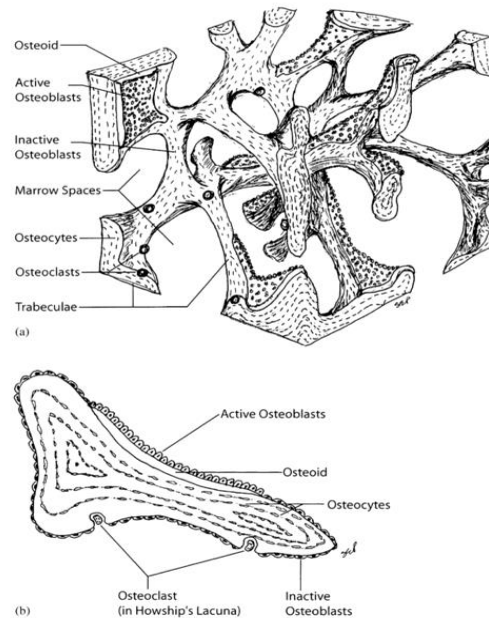
Figure 2.5. Bone Cells
(Source:Seal et al., 2001)

Bone shows both elastic and semi-brittle behavior. Compact bone has a compressive strength in the range of 131 - 224 MPa, and a Young's modulus around 17-20 GPa, while compressive strength and Young's modulus for trabecular bones are 5-10 MPa and 50-100 MPa, respectively (Razak et al., 2012). The mechanical properties of bone generally depend on its structure and orientation. The specific organization of tissue microstructure results in strong anisotropy in mechanical properties. Due to different structural features, macroscopically the cortical bone has much higher compressive strength (100-230 MPa) than the cancellous bone (2-12 MPa) (Hench et al., 1993).

Osteoinduction, osteoconduction, and osseointegration are major interrelated phenomena in bone regeneration. Osteoinduction term is defined as induction of osteogenesis (new bone formation). This phenomenon takes part in most bone healing processes. The process of bony ingrowth from local osseous tissue onto surfaces is defined as osteoconduction. Osseointegration is the process of stable direct anchorage and contact formation between bone and implant. At the light microscope level,

osseointegration states the direct contact, between living bone and implant. At the histological level it is the direct anchorage of an implant by bone tissue formation without fibrous tissue formation at the bone–implant interface (Jayakumar and Silvia, 2010).

2.2.1. *In vitro* Osteoblast Cell Models for Bone Tissue Engineering

2.2.1.1. Osteoblast Cell in Bone Tissue Formation

The osteoblasts are the major bone cells responsible for generating, secreting, depositing, and mineralizing bone matrix. Osteoblasts are derived from osteoprogenitor cells which are formed by undifferentiated mesenchymal stem cells (MSCs) and located in bone marrow and connective tissues. Osteoblast differentiation is illustrated in Figure 2.6. They fundemantally synthesize and secrete organic matrix, predominantly collagen type I and trace quantities of collagen type V. In addition, they secrete various factors, glycoproteins (octeocalcin, osteonectin, osteopontin, proteoglycans and growth factors) and express genetic markers (osterix, collagen type 1(col1), bone sialoprotein (BSP)) (Jayakumar and Silvio, 2010).

In bone tissue formation, osteoblasts facilitate the mineralization process of bone matrix. The mineralization process involves supersaturation of extracellular fluids at local zones and increased osteoblastic alkaline phophatase (ALP) activity, which promotes local calcium and phosphate concentrations. Furthermore, osteoblasts produce osteocalcin, which binds calcium and this leads to calcium deposition in bone matrix (Jayakumar and Silvio, 2010).
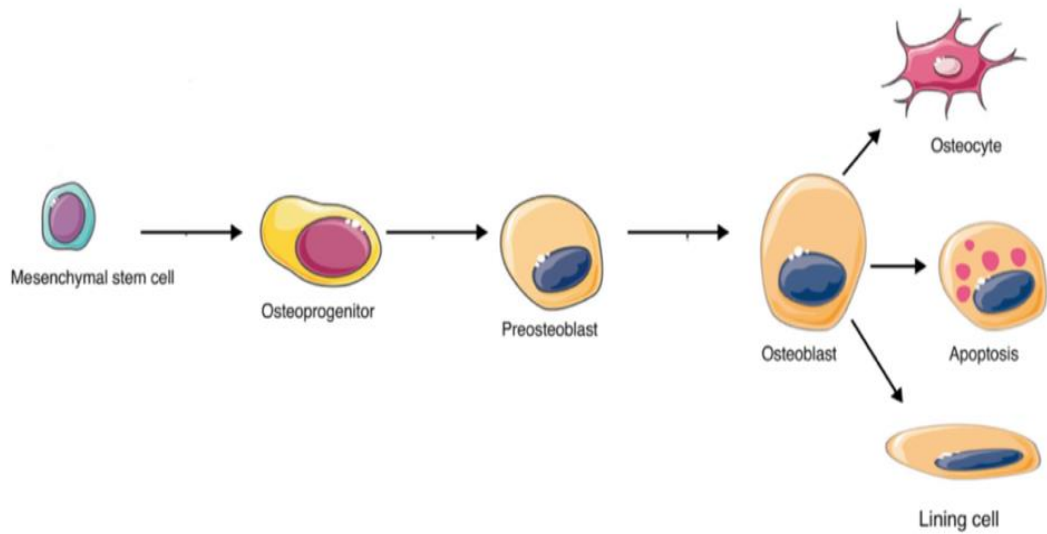
Figure 2.6. Osteoblast differentiation
(Source: Arboleya and Castaneda, 2013)

Generally, *in vitro* cell culture studies are performed with stabilised osteoblastic cell lines which have been developed as models for *in vitro* investigation of cell differentiation, cytokine and hormonal regulation, synthesis and secretion of matrix proteins etc. Recently osteoblast cell culture has been developed to determine the cytocompatibility and osteogenicity of novel biomaterials for bone tissue engineering applications (Czekanska et al., 2012).

Diverse cell culture models have been employed for investigation of osteoblast cell biology comprising induced osteoblasts from pluripotent stem cells, primary cells from different species and immortalised cell lines. These osteoblast models, present advantages and disadvantages for *in vitro* studies (Table 2.2.) (Czekanska et al., 2012).

Table 2.2. Advantages and disadvantages of primary osteoblast cells and osteoblastic cell line models (Source:Czekanska et al., 2012).

Cell Type	Advantages	Disadvantages	References
Primary Human cells	No interspecies differences relevant for clinical studies	Heterogeneous phenotype Long isolation procedure Limited accessibility Cell phenotype Sensitive to donor-related factors	Kasperk et al., 1995 Martinez et al., 1999 Evans et al., 1990 Voegele et al., 2000 Gallager, 2003 Jonsson et al., 1999 Fedarko et al., 1992 Battmann et al., 1997 Siggelkow et al., 1999
Primary Mouse/rat cells	Easily available Possibility to control the selection of donor- animals Cell extraction from all bones in the skeleton	Interspecies differences Genomic differences Cell phenotype sensitive to age and site of isolation factors	Bakker & Klein-Nulend, 2003 Soejima et al., 2001 Carpenter et al., 1998 Declercq et al., 2004 Lian and Stein, 1992 Manduca et al., 1997 Stringa et al., 1995

(Cont.on next page)

Table 2.2. cont.

Primary Bovine/ovine/rabbit cells	Potential for improved in vitro extrapolation of bone remodelling and healing process to current in vivo models. potential formation of trabecular structures (bovine osteoblasts)	Inconsistent results regarding cell mineralisation Need for optimising culture conditions Lack of extensive characterisation of cells.Limitations for molecular biology methods	Ibaraki et al., 1992 Newman et al., 1995 Neyt et al., 1998 Cao et al., 2006 Whitson et al., 1992
SaOs-2	No interspecies differences Unlimited number of cells Homogenous Cytokine and growth factor expression profile similar to human Ob cells sensitive to hormonal administration matrix mineralisation	Do not mirror the whole range of osteoblast phenotypic changes Sensitive to Pi substrates	Masuda et al.,1987 Murray et al., 1987 Bilbe et al., 1996 Rodan et al., 1987 Fernandes et al., 2007 Rao et al., 1996

Table 2.2. cont.

MG-63	No interspecies differences Unlimited number of cells Hormonal administration response similar to human Ob cells Similarity to human integrin subunits	Arrested in pre-osteoblast state Inconsistent regarding cell mineralisation	Heremans et al., 1978 Clover et al., 1992 Olivares-Navarrete et al., 2008 Kumarasuriyar et al., 2009 Saldana et al., 2011 Pierschbacher et al., 1988
MC3T3-E1	Unlimited number of cells Homogenous character Phenotypic differentiation from pre- osteoblasts to mature osteoblasts	Interspecies differences Some signs of cellular replicative senescence	Wang et al., 1999 Sudo et al., 1983 Quarles et al., 1992 Grigoriadis et al., 1985

2.2.1.2. Human Isolated Cells

The main advantage to use primary human cells for *in vitro* studies, is their clinical applicability and ability to maintain their differentiated phenotype in vitro. However, human isolated cells represent a heterogeneous cell population, exhibit phenotypic differences relating to the site they were isolated, gender difference and donor age. ALP activity, the expression of genes and protein synthesis associated with osteoblast phenotype can be influenced by donor age (Czekanska et al., 2012). *In vitro* studies indicated that cells from donors younger than 65 years old were shown to have shorter population doubling times than osteoblasts from older donors (Voegele et al., 2000).

2.2.1.3. Animal Primary Cells

Cells isolated from other species can provide an alternative *in vitro* research model due to the limited accessibility of human osteoblast cells and their phenotypic heterogeneity. Major advantage of primary animal cells is their availability compared to human cell sources. Cell isolation sites are limited in human soruces. However, cells can be obtained more easily from animal sources. Also, donor animal selection can be executed in a more controlled way in relation to age and gender. The distinct disadvantage of animal cells is the interspecies differences. Furthermore, bone structure is different among animals. Rat osteoblast cells are an attractive model for *in vivo* and *in vitro* research focused on the osteoinductivity and cytotoxicity of polymer or implant biomaterials due to the availability and known genome. Also mice can be used for osteoblast cell isolation. Bovine and ovine derived osteoblast cells are less often used for *in vitro* studies compared to rodents although these animals are frequently used as large animal *in vivo* models (Czekanska et al., 2012).

2.2.1.4. Cell Lines

Immortalised osteoblast cell lines have advantages including ease of maintenance, unlimited number of cells without isolation, homogenous population of cells and relative phenotypic stability. However, both transformed and non-transformed cell lines do not reflect the whole phenotypic features of normal osteoblast cells because of being arrested in a particular stage (Czekanska et al., 2012). Despite these disadvantages, osteoblast cell lines are extensively used for *in vitro* studies. The most commonly used cell lines are MC3T3- E1(Quarles et al., 1992), hFOB (Harris et al., 1995), MG- 63 (Billiau et al., 1977), SaOs-2 (Rodan et al., 1987) and U2OS (Ponten and Saksela, 1967).

Rodan et al. characterised osteoblastic properties of the SaOs-2 human osteosarcoma cell line, which was isolated from an 11-year old Caucasian female in 1975 (Rodan et al., 1987). SaOs-2 cells have a mature osteoblast phenotype, possessing a high matrix mineralisation capacity and showing much higher levels of ALP activity than other osteosarcoma cell lines, such as MG-63 and SaOs-1 (Murray et al., 1987).

Saldana et al. indicated that the ALP activity of SaOs-2 cells was similar at the early time points when compared to human primary osteoblast cells, but 120-fold higher after 14 days under the same conditions (Saldana et al., 2011). In addition, Rodan et al. reported that SaOs-2 cells formed a calcified matrix typical of woven bone (Rodan et al., 1987). Cytokine and growth factor expression of SaOs-2 cells have been shown to be similar to primary normal human osteoblast cells (Bilbe *et al.*, 1996). SaOs-2 cells have been shown to express receptors specifically for parathyroid hormone (PTH) and calcitrol (1,25(OH)$_2$D$_3$) similar when compared to osteoblasts *in vitro* and *in vivo* (Rao *et al.*, 1996). As a consequence, SaOs-2 cells show responses resembling HOb cells more closely, regarding the expression of osteoblastic factors. Therefore, they can be used as a model for some osteoblast function studies, such as synthesis of some osteoblast-specific proteins (Czekanska et al., 2012).

The MG-63 cell line is derived from a juxtacortical osteosarcoma diagnosed in a 14year old male femur (Billiau et al., 1977). These cells showed rapid cell growth without exhibiting contact inhibition, resulting in the formation of aggregates (Heremans et al., 1978). MG-63 cells attracted much attention as they produce interferon with high yields (Billiau et al., 1977). MG-63 cells represent an immature osteoblast phenotype and undergo temporal development in long term culture (Czekanska et al., 2012). In a recent study, Kumarasuriyar et al. reported changes in MG-63 phenotype. In this study, ALP activity increased on 15th day, then declined to basal levels, whereas expression of type I collagen increased during the second week of the culture. Osteocalcin and osteonectin expression were observed at 15th and 29th day of incubation, while calcium accumulation was initiated after 28 day of incubation (Kumarasuriyar et al., 2009). Furthermore, different studies reported that MG-63 cells had low ALP enzyme activity and did not mineralise (Pierschbacher et al., 1988; Saldana et al., 2011). MG-63 cells were identified as expressing a similar integrin subunit profile to HOb cells Therefore, MG-63 may provide a good alternative for studies interested in initial attachment to various materials. MG-63 cells were also found to be appropriate for studying the regulation and production of osteocalcin. Contrary to this, MG-63 cells were not very representative regarding proliferation and alkaline phosphatase activities (Clover and Owen, 1994). Consequently, MG-63 cells have been used in long-term *in vitro* biomaterial studies regardless of their limitations (Czekanska et al., 2012).

2.3. Scaffold Fabrication Techniques

In the body, cells and tissues are organized into three-dimensional architecture. Thus, scaffolds have to be fabricated by different methodology to facilitate and guide the cell distribution and growth into three-dimensional structure. Many conventional techniques have been developed in order to engineer to fabricate three-dimensional porous architectures. Table 2.3. shows the most commonly used scaffold fabrication technologies for potential tissue engineering applications indicating their merits and demerits of each technique.

Table 2.3. Advantages and disadvantages of scaffold fabrication techniques (Source:Subia et al., 2010)

Methods	Advantages	Disadvantages	References
Solvent casting/	Control over Porosity, pore size and crystallinity	Limited mechanical property, residual solvents and porogen material	Ma, 2007; Xiang et al., 2006
Particulate Leaching (Porogen leaching)	Controlled over porosity and pore geometry	Inadequate pore size and pore interconnectivity	Mano et al., 2007
Gas Foaming	Free of harsh organic solvents, control over porosity and pore size	Limited mechanical property, inadequate pore interconnectivity	Ikada., 2006
Electrospinning	Control over porosity, pore size and fiber diameter	Limited mechanical property, pore size decrease with fiber thickness	Liang et al., 2007
RapidPrototyping	Excellent control over geometry, porosity, no supporting material required	Limited polymer type, highly expensive equipment	Hutmacher et al., 2000; 2001
Freeze Drying	High temperature and separate leaching step not required	Small pore size and long processing time	Boland et al.,2004; Mandal Kundu, 2008

2.3.1. Solvent casting

Solvent casting is a very simple, easy and inexpensive method which does not require any large equipment and it is totally based upon the evaporation of some solvent in order to form scaffolds. There are two solvent casting methods: 1.Dipping the mold into polymeric solution and creating a layer of polymeric membrane. 2. Adding the polymeric solution into a mold and providing the sufficient time to evaporate the solvent in order to create a layer of polymeric membrane in mould (Figure 2.7). The scaffolds fabricated by this method may have toxic affect because of solvent residuals. Scaffolds are fully dried by vacuum process to remove toxic solvent (Subia et al., 2010).
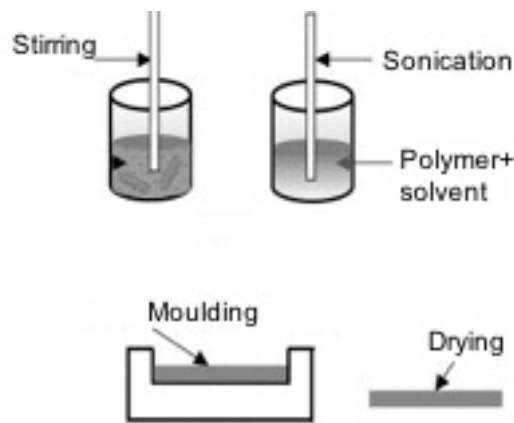
Figure 2.7. Solvent Casting method
(Source: Subia et al., 2010)

2.3.2. Particulate-leaching (Porogen-leaching)

Particulate leaching is one of the popular techniques that is widely used to fabricate scaffolds for tissue engineering applications. Porogen leaching is a common method used for preparation of scaffolds with controlled porosity. It is totally based upon the dispersion of porogen (salt, sugar and wax) in liquid particulates or powdered materials by evaporation process. Porogen act as place holder for pores and interconnections. Porogen leaching is a simple and versatile method for pore size and geometry control. Pore size can be controlled by controlling the amount of porogen added, the size and shape of the porogen. In this method, porogen particles with desired

size are poured into a mould and polymer solution is cast into the mold. Solvent is evaporated and the salt crystals are leached away using water to form the pores of the scaffold (Figure 2.8.) (Subia et al., 2010).
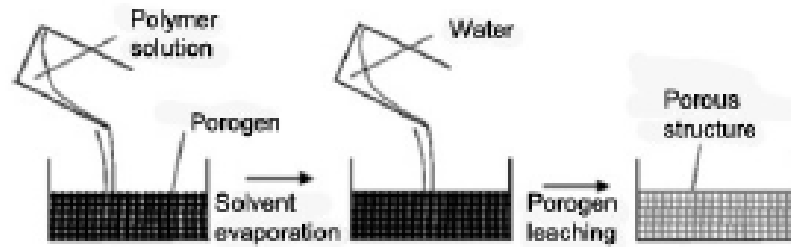
Figure 2.8. Particulate-leaching method
(Source: Zhu and Chen, 2013)

2.3.3. Freeze-drying

Freeze drying technique is based upon the sublimation principle. Polymer is first dissolved in a solvent to form a solution and it is frozen. In the freezing stage, the polymer solution is cooled down to a certain temperature at which all materials are in a frozen state and the solvent forms ice crystals. Finally, solvent is removed by lyophilization under the high vacuum which causes controlled solidification in a single direction. When the solvent is completely sublimated, a dry polymer scaffold with an interconnected porous microstructure is obtained. Figure 2.9 shows the schematic illustration of steps in freeze drying method. Scaffold is fabricated with high porosity and interconnectivity by freeze-drying method. The pore size can be controlled by freezing rate, polymer solution concentration and pH (Subia et al., 2010; Zhu and Chen, 2013).
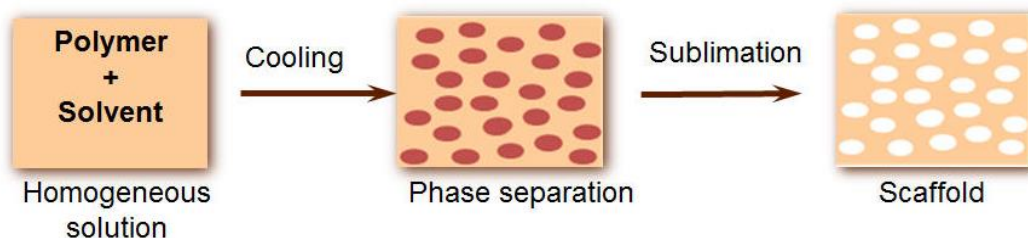
Figure 2.9. Schematic illustration of freeze-drying method
(Source:http://madihally.okstate.edu/project_scaff.html)

2.3.4. Gas Foaming

Gas foaming technique generally uses high pressure carbon dioxide (CO_2) gas to obtain highly porous scaffolds. The porosity and porous structure depend on the amount of gas dissolved in the polymer. Under high pressure, dissolved CO_2 becomes unstable and phase separates from the polymer (Figure 2.10.). This results in nucleation and growth of gas bubbles in the polymer. After foaming process, porogen is removed and a highly interconnected porous scaffold is formed (Subia et al., 2010; Zhu and Chen, 2013)
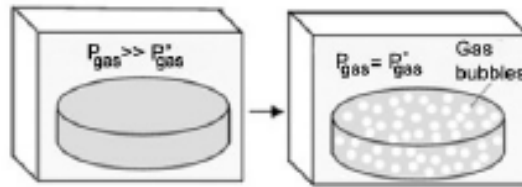
Figure 2.10. Gas foaming method
(Source: Zhu and Chen, 2013).

2.3.5. Electrospinning

The electrospinning technique utilizes the electrostatic force for the production of polymeric fiber ranging from nanoscale to microscale. The process is controlled by electric field between two electrodes having electric charges of opposite polarity (Subia et al., 2010). Fibers are generated with diameters ranging from 2 nm to several micrometers with small pore sizes and high surface area (Zhu and Chen, 2013).

Electrospinning setup includes a syringe pump, a high voltage source and a collector (Zhu and Chen, 2013). Polymer solution is pumped to form a drop and electric field is generated, intending to produce a force. The solution droplets overcome the surface tension of the solution by this force. Polymer jet is ejected from syringe pump and formed fibers are deposited at the collector (Subia et al., 2010). Figure 2.11. illustrates the electrospinning setup. Electrospinning parameters (solvent concentration, applied voltage, distance between tip and collector, flow rate) effect the morphology and size of fibers (Zhu and Chen, 2013).
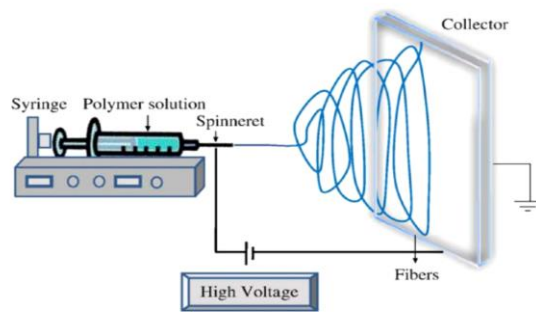
Figure 2.11. Schematic illustration of elctrospinning method
(Source: Zhu and Chen, 2013)

2.3.6. Rapid prototyping (RP)

Rapid prototyping (RP) is an advanced alternative method to conventional scaffold fabrication methods. RP is also called as solid free-form technique (SFF). RP technique provides controlled internal microstructure and external macroshape compared to conventional techniques. The primary RP techniques for tissue scaffold fabrication are stereolithography (SLA), selective laser sintering (SLS), fused deposition modeling (FDM), three dimensional (3D) printing, and 3D plotting (Zhu and Chen, 2013).

This technique generally designs the scaffold model by using the computer aided design (CAD) software. The computer reduces the model to layers and designed microarchitecture is fabricated layer by layer. RP has advantage of ability to control matrix architecture yielding biomimetic structure (Subia et al., 2010).

2.4. Biomedical Polymer Composites for Bone Tissue Engineering

Biomaterial design and development which will replace the form and function of native tissue while promoting regeneration without necrosis is a challenging area of biomedical research. Various biomaterial scaffolds have been explored as suitable constructs for bone regeneration by identifying the most appropriate physical, chemical and biological properties to encourage *in vitro* bone regeneration.

There are two distinct biomaterial based approaches that have demonstrated potential to support bone regeneration; (1) the use of soft polymer-based scaffolds (natural and synthetic polymers), and (2) the use of stiff mineralized scaffolds that mimic the *in vivo* environment of mature bone. In addition, another approach is presented as the use of a combinational approach of these materials (Fernandez-Yague et al.,2015).

Composites are generally two or more closely interacting materials which are in intimate (at molecular level) contact with each other. According to the International Organization for Standardization, composite materials are solid ones with multiple phases, which is a combination of two or more materials with different physical and chemical properties. One continuous phase is called the matrix, while the other dispersed phase is a reinforcing material in a composite. Organic-inorganic composite materials consist of two phases with organic molecules or polymers and inorganic molecules in each phase. Organic-inorganic nanocomposites refer to composite structures in which the inorganic phase has nanoscale morphology such as particles, fibers and tubes (Ke and Stroeve, 2005; Chen et al., 2008; Sarker et al., 2015). These materials are considered to be a new generation of high-performance materials by combining the advantages of inorganic materials (eg, rigidity and high stability) with the advantages of organic polymers (eg, exibility, ductility, and processability) (Wang et al., 2014).

Naturally derived polymers, such as collagen, glycosaminoglycans, gelatin, chitosan, silk fibrin, and elastin, have been widely used in tissue engineering applications. As being the components of the extracellular matrix of many biological tissues, they demonstrate appropriate biocompatibility for in vivo applications. Besides, they present a range of ligands that facilitate bone cell adhesion and osteospecific function (Fernandez-Yague et al., 2015).

Naturally derived polymers theoretically should not cause foreign material response when implanted in body. They also provide a natural substrate for cellular attachment, proliferation and differentiation and are considered favorable materials for bone tissue engineering applications. However, their poor mechanical properties and variable physical properties have prevented progress with these materials. Mechanically, bioceramics and glasses are stronger than polymers and play a critical role in providing mechanical stability to constructs prior to synthesis of new bone matrix by cells. However, ceramics and glasses are very fragile and prone to catastrophic failure due to their intrinsic brittleness and flaw sensitivity. The formation of composites thus capitalises on the advantages of both material types and minimise their shortcomings (Roether and Boccaccini, 2008).

Massive release of acidic degradation from polymers may cause inflammation in body, however presence of calcium phosphate or bioactive glasses with the basic degradation behaviour in polymer matrix could buffer the acidic by-products of polymers. Thus, an unfavourable environment for cells could be prevented. Bioceramics and glasses are mechanically stronger than polymers. So they play a critical role in providing mechanical stability to scaffold during new bone matrix formation (Chen et al., 2008). However, bioceramics and glasses are very fragile due to their intrinsic brittleness and flaw sensitivity. Composites possess advantages of both phases and minimise their limitations (Roether and Boccaccini, 2008).

Combining polymers and bioceramics to fabricate scaffolds for bone tissue engineering makes sense with regard to an estimation of biological perspective. Bone has a composite structure composed of naturally occurring polymer and biological apatite. Generally single material type does not provide adequate mechanical and/or chemical properties required for bone tissue regeneration. Therefore, the properties of two or more materials can be combined in a composite material. Polymers and ceramics that have the ability to degrade *in vivo* are ideal candidates for composite scaffolds (Chen et al., 2008).

Ceramic scaffolds are typically derived from bioactive inorganic materials the most frequent being the calcium phosphates, in particular hydroxyapatite (HA) and tricalcium phosphate (TCP), which are both extremely biocompatible and osteoconductive because of their chemical composition which is close to the inorganic mineral phase crystals found in bone. HA undergoes favorable osteointegration by chemical bonding, induces new bone tissue formation and exhibits a controlled

degradation rate and osteoconductivity. Furthermore, the release of calcium and phosphate ions during HA degradation can induce osteogenic responses (Fernandez-Yague et al.,2015).

The optimized biological and mechanical properties of bioactive polymer/ceramic composites are generally obtained by providing good chemical and/or physical bonding between the polymer and the inorganic phase (Roether and Boccaccini, 2008). Generally, inorganic particles used as reinforcement are in a few microns or larger in size range in conventional hybrid composites Recently, studies have focused on nanocomposites composed of an organic binding matrix and an inorganic nanoparticle (reinforcing filler) (Cho, 2006). Faster deposition or mineralization of tissues such as bone or teeth can be obtained with nanoscale particles, rather than micron-sized particles due to the nanoscale features of the bone structure which consists of a tailored mixture of collagen fibrils and hydroxyapatite nanocrystal (Boccaccini et al., 2010). Inorganic nanoparticles have been incorporated into common polymers to generate nanocomposites that combine the desirable properties of inorganic nanoparticles (e.g. high strength, electrical conductivity, and thermal stability) and polymers (e.g., ease of processing, flexibility, and toughness). These nanocomposites are defined as polymers reinforced with nanoparticles (Cho, 2006). Recently studies focused on using nanomaterials as bone tissue engineering scaffolds in order to mimic the natural bone structure which possesses a nanocomposite structure interwoven in a three dimensional matrix. The inclusion of nanoparticles into the polymer matrix has advantages of improving the mechanical properties as well as incorporating nanotopographic features that mimic the nanostructure of natural tissue (Roether and Boccaccini, 2008; Wu et al., 2010). The particle size of inorganic filler in polymer matrix affects the mechanical properties of the composite. The incorporation of nanosized inorganic particles with desired morphology improves the mechanical properties to a higher extent than microfillers. In addition, nanosized inorganic particles provide a higher specific surface area which enhances the interfacial bonding strength between the polymer matrix and inorganic reinforcement (Sarker et al., 2015).

2.5. Chitosan as a Natural Polymer

Chitosan is a deacetylated derivative of chitin, the most abundant biopolymer in nature after cellulose and found in the exoskeletons of insects, crustaceans and walls of fungi. Several millions tons of chitin are harvested annually in the world. Thus, chitosan represents a cheap and readily available source as a biopolymer. Due to its poor solubility in aqueous solution and organic solvents, chitin is not used in practical applications. Chitosan as a deacetylated derivative of chitin is more suitable for bioapplications (Dash et al., 2011).

It is a linear heterogenic polysaccharide, composed of glucosamine and N-acetyl glucosamine units linked by β (1–4) glycosidic bonds (Figure 2.12). The content of glucosamine/N-acetyl glucosamine ratio is referred as the degree of deacetylation (DD). Content and sequence of these units determine the physico-chemical and the biological properties of chitosan. In its crystalline form, chitosan is normally insoluble in aqueous solution above pH 7 (Prashanth and Tharanathan 2006; Arca and Şenel, 2008; Kim et al., 2008; Dash et al., 2011). Chitosan has three types of reactive functional groups, an amino group as well as both primary and secondary hydroxyl groups at the C (2), C (3), and C (6) positions, respectively. These functional groups allow modification of chitosan (Kim et al., 2008). Chitosan which is the only positively charged, naturally occurring polysaccharide with protonated amino groups becomes a polycation that can subsequently form ionic complexes with a wide variety of natural or synthetic anionic species such as lipids, proteins, DNA and some negatively charged synthetic polymers The presence of the amino groups on glucosamine units of chitosan structure allows the alteration of properties and charged state by pH change. At low pH, these amino groups get protonated and become positively charged. As a result, chitosan turns into a water-soluble cationic polyelectrolyte. Otherwise, as the pH increases (pH>6), amino groups become deprotonated and in crystalline form, chitosan becomes insoluble by losing its charge (Dash et al., 2011). Depending on the source and preparation procedure, its

molecular weight may range from 300 to over 1000 kDa with a degree of deacetylation from 30% to 95% (Martino et al., 2005; Croisier and Jerome, 2013).
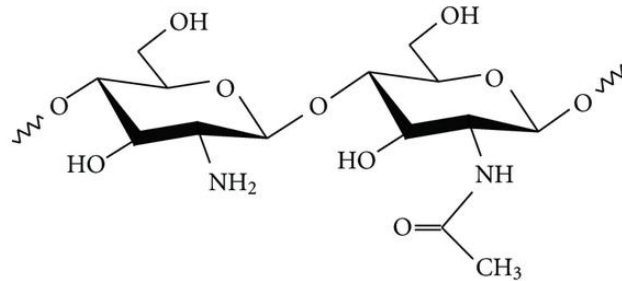
Figure 2.12. Chemical structure of chitosan: N-acetyl-D-glucosamine (right) and
D-glucosamine (left) units (Source:Andrade et al., 2011)

Chitosan has been found an ideal material with its unique biological properties including biocompatibility, biodegradability, nontoxicity, physiological inertness, remarkable affinity to ECM proteins. Chitosan has also antibacterial, non-allergenic, mucoadhesive, haemostatic, fungistatic, antitumoral and anticholesteremic properties. Furthermore, it has structural similarity to glycosaminoglycans which are the major component of the extracellular matrix (Arca and Şenel, 2008; Kim et al., 2008). The choice of chitosan as a tissue support material is governed among others by multiple ways by which its biological, physical and chemical properties can be controlled and engineered under mild conditions (Kim et al., 2008).

The polycationic nature of chitosan also allows explaining its analgesic effects. The amino groups of the D-glucosamine residues can protonate with proton ions that are released in the inflammatory area. This results in an analgesic effect (Croisier and Jerome, 2013)

Degree of deacetylation (DD) of chitosan is an important factor for matrix-cell interaction. As the DD increases, cell adhesion and proliferation increase due to the presence of free amino groups. In addition, DD affects the degradation rate of chitosan, higher degradation rates are obtained with the lower DD. This fact causes an accumulation of monosaccharide that can produce an acute inflammatory response. On the other hand, the higher DD chitosan with the lower degradation rate produces a minimal response (Dash et al., 2011). The cationic nature of chitosan is primarily responsible for electrostatic interactions with anionic GAGs, proteoglycans and other

negatively charged molecules. This property is one of the important factors for tissue engineering applications Cytokines/growth factors are bound and modulated glycosaminoglycans (GAGs) (including heparin and heparan sulphate) in the body. For this reason, chitosan is presented as a favorable carrier for growth factors (Martino et al., 2005; Arca and Şenel, 2008; Kim et al., 2008).

One of the properties of chitosan is considerable antibacterial activity against a broad spectrum of bacteria. Amino groups of chitosan which cause cationic properties, are related to anions on the bacterial cell wall. Positively charged chitosan and negatively charged microbial cell wall interacts, this leads to the leakage of intracellular constituents of bacteria (Martino et al., 2005).

Chitosan is degraded *in vivo* via enzymatic hydrolysis. Lysozyme is the primary enzyme responsible for degradation of chitosan which is normally produced by macrophages and targets acetylated residues. Chitosan contains breakable glycosidic bonds. The final degradation products of chitosan are biocompatible oligosaccharides of variable length. These oligosaccharides can be incorporated in metabolic pathways or be further excreted. The degradation rate is inversely related to the DD. Highly deacetylated forms of chitosan (i.e.85%) exhibit a low degradation rate and may last several months *in vivo*, while chitosan forms with lower DD degrade more rapidly on the contrary (Kim et al., 2008, Croisier and Jerome, 2013).

Chitosan possesses some special properties for tissue engineering applications. Chitosan can easily be formed as interconnected-porous structures by freezing drying method. The porous structure of chitosan is an important characteristic for the development and optimization of a variety of tissue scaffolds and regeneration aids (Arca and Şenel, 2008). Chitosan has been widely used in bone tissue engineering applications.due to its favorable properties as promoting cell growth and mineral rich matrix deposition by osteoblasts. It can be molded into porous structures to allow osteoconduction (Dash et al., 2011). As well as being a promising material for tissue engineering applications, chitosan has some limitations as poor solubility and mechanical strength. Bioceramics, polymers and inorganic materials can be used with chitosan in order to achieve the desired mechanical properties (Arca and Şenel, 2008).

The most common methodology for producing chitosan scaffolds utilizes freeze-drying. This process consists of the lyophilization of a frozen chitosan solution, where the chitosan acetate salt is induced by the freezing conditions to phase-separate from the ice crystal phase. The ice phase is further sublimated, producing a porous structure. In

most cases, the scaffolds can still have chitosan acetate that will cause fast swelling and subsequently dissolution in a neutral aqueous medium. This can be overcome by cross-linking upon immersion in sodium hydroxide, sodium sulfate, tripolypho- sphate, ethanol series, or with a combination of cross- linking with rehydration (Costa-Pinto et al., 2011).

2.5.1. Chitosan Based Biomaterials for Bone Tissue Engineering Applications

Bone and tooth are mineralized tissues consisting of inorganic minerals combined with organic polymers (Silva et al., 2003). Natural bone mineral consists of nanocrystals of carbonated hydroxyapatite. Therefore, a composite of a bone mineral-like phase with a biodegradable polymer should be favorable as a bone substitution material. The mineral phase would be responsible for the mechanical strength (hardness) and the polymer phase for the elasticity of the biomaterial (Neumann and Epple, 2006). Recent studies focused on development of nanomaterials for bone tissue engineering applications due to the fact that the inclusion of nanoparticles into the biopolymer matrix both improves the mechanical properties and mimics the nanostructure of natural bone by incorporating nanotopographic features (Swetha et al., 2010).

Over the past two decades, chitosan has been developed considerably in a wide range of biomedical applications due to its high biocompatibility, biodegradability, porous structure, suitability for cell ingrowth, osteoconduction and intrinsic antibacterial nature (Venkatesan and Kim, 2010). It can promote adhesion and functional expression of osteoblast because of its similarity to glycosaminoglycan in structure (Bao et al. ,2010).

Chitosan and its derivatives are also very challenging candidates for composite biomaterials due to their degradation behaviour without inflammatory reactions or toxic products (Swetha et al., 2010). In addition, chitosan can be easily fabricated in various forms like films, fibers, beads, sponges, and more complex shapes for orthopedic applications. Generally, porous chitosan biomaterials can be fabricated by freze-drying method. Chitosan scaffolds as a polymer matrix, can not imitate all the properties of

natural bone. The significant developments concerning the design of composite materials with chitosan mimics all the properties of bone (Martino et al., 2005; Venkatesan and Kim, 2010). Several materials based on chitosan and its derivatives have been used as osteogenic bone substitutes (Table 2.4.).

Table 2.4. *In vitro* studies with chitosan-based scaffolds proposed in the literature for bone tissue engineering applications (Source:Costa-Pinto et al., 2011)

Scaffold Structure	Processing Method	Cell Type
Chitosan scaffolds	Freeze-drying	-
Chitosan/TCP sponges	Freeze-drying	Fetal rat calvaria cells
Chitosan/gelatin scaffolds	Freeze-drying	-
Chitosan/TCP sponges	Freeze-drying	MG63 human cell line
Chiton/HAp scaffolds	Rapid prototyping &Freeze-drying	-
Chitosan/calcium phosphate scaffolds	Freeze-drying	MG63 human cell line
Chitosan scaffolds	Freeze gelation	Rat Osteosarcoma (ROS) 17/2.8 cells
Chitosan sponges	Freeze-drying	Rat calvaria cells
Chitosan fiber mesh scaffolds	Wet spinning	Human SAOS-2 cell line
Chitosan scaffolds	Freeze-drying	MG63 human cell line
Chitosan/silk scaffold	Freeze-drying	-
Chitosan scaffolds	Rapid prototyping	Porcine BMSCs
Chitosan scaffolds	Electrospinning	-
Chitosan/gelatin scaffolds	Freeze-drying	Huma umbilical vein endothelial cells (HUVECs)
Chitosan scaffolds	Precipitation/Particle aggregation	Adipose-derived stem cells (ADAS)

(Cont. on next page)

Table 2.4. cont.

Chitosan sponges	**Freeze-drying**	**MG63 human cell line**
CPC/chitosan scaffold	Cement/Particle leaching	MG63 human cell line
Chitosan scaffolds with HAp formation	Freeze-drying	Human SAOS-2 cell line
Chitosan/nanoHAp scaffolds	Freeze-drying	MC3T3-E1 cell line
Chitosan/coralline scaffolds	Freeze-drying	CRL-12424 cell line
HAp/chitosan scaffold	Freeze-drying	Goat bone marrow cells
Chitosan/gelatin scaffolds	Freeze gelation	Human bone marrow mesenchymal stem cells. (BMSCs)
BCP/chitosan scaffolds	Freeze-drying	MC3T3-E1 cell line
Chitosan/PLAGA scaffolds	Particle aggregation	MC3T3-E1 cell line
Chitosan/gelatin/ montmorillonite scaffolds	Freeze-drying	Rat stromal cells TC1
Chitosan scaffolds	Freeze gelation	-
Chitosan/collagen sponges	Freeze-drying	Rat bone marrow mesenchymal stem cells (BMSCs)
Chitosan-PBS/PBTA/PCL	Compression molding/salt leaching	Mouse BMC-9 cell line
Chitosan scaffolds	Wet spinning	Mouse osteoblast 7F2 cell line
Chitosan/PBS scaffolds	Melt spinning/fiber bonding	Human bone marrow mesenchymal stem cells (BMSCs)
Chitosan-PBS/PCL/PBTA/PBSA	Compression molding/salt leaching	-

(Cont. on next page)

Chitosan/PCL scaffolds	**Electrospinning**	**MC3T3-E1 cell line**
Chitosan scaffolds	Freeze-drying	MC3T3-E1 cell line
PLGA/chitosan scaffolds	Freeze-drying	Human bone marrow mesenchymal stem cells (BMSCs)
Chitosan sponges	Freeze-drying	Chicken embryo chondrocyte
Chitosan/starch/lysozyme scaffolds	Freeze gelation	Rat BMSCs
PCL/chitosan	Solvent-casting/salt leaching/ freeze drying	Rat osteoblasts

Hydroxyapatite (HAp); tricalcium phosphate (TCP); poly (l-lactic acid) (PLLA); calcium phosphate cement (CPC); biphasic calcium phosphate (BCP); poly (lactic-co-acid-glycolic acid) (PLAGA); poly (butylene succinate) (PBS); polycaprolactone (PCL); poly (butylene terephtalate adipate) (PBTA); poly(butylene succinate adipate) (PBSA); poly(l-glycolic acid) (PLGA).

Numerous studies have focused on the use of chitosan–calcium phosphate composites for bone tissue engineering applications (Martino et al., 2005). Zang et al. developed a three dimensional macroporous calcium phosphate bioceramic embedded with porous chitosan sponges. Results indicated that nested chitosan sponge enhanced the mechanical strength of the ceramic phase via matrix reinforcement and preserved the osteoblast cells (Zhang and Zhang, 2002). The compressive modulus and yield strength are greatly improved and a reinforced microstructure is achieved by incorporating calcium phosphate into chitosan scaffolds (Puppi et al., 2010). In a study, b-tricalcium phosphate (b-TCP) and a calcium phosphate invert glass were used as powder fillers to reinforce the chitosan scaffold. Both compressive modulus and yield strength of the scaffolds were greatly improved by incorporating powder fillers, and reinforced microstructures were achieved (Zhang and Zhang, 2002). Liao et al developed a freeze-dried porous tricalcium phosphate-chitosan composite with 120 μm pore size and 91.07% porosity which showed higher proliferation rate than the pure chitosan, and up-regulated the gene expression of bone sialoprotein and cementum attachment protein as well as the alkaline phosphatase and osteopontin expressions were up-regulated in the composite. *In vivo* results showed that human periodontal ligament

cells in the composite not only proliferated but also recruited vascular tissue ingrowth. (Liao et al., 2010).

The loading of natural coralline into chitosan microporous scaffolds was also found to cause an increase in compressive modulus, and to have a positive impact on the adhesion of MSCs. Chitosan/HAp composites have been reported to promote the formation of bone-like apatite on their surfaces after soaking in SBF and to enhance the attachment, proliferation and differentiation of osteoblast-like cells. Recently, chitosan hydrogel–HAp composite membranes were prepared through deposition of Hap on the surface of the hydrogel by a wet chemical synthesis method. A novel biomimetic nanocomposite chitosan/Hap was recently developed by Zhang et al. by combining an in situ co-precipitation synthetic approach by means of electrospinning (Puppi et al., 2010). Pourhaghgouy et al. developed a chitosan based nanocomposite scaffold with unidirectional aligned pore channels by freeze casting method through blending chitosan with different portions of synthesized bioactive glass nanoparticles (BGNPs). XRD and FT-IR analysis results detected strong interfacial bonding between chitosan polymers and BGNPs. Results showed that BGNP incorporation enhanced the mechanical properties and degradation behavior of scaffolds. The chitosan/BGNP nanocomposite represented the more acceptable absorption capacity and bioactivity (Pourhaghgouy et al., 2015). Shirosaki et al. synthesized chitosan/silicate hybrids with glycidoxypropyltrimethoxy silane whose epoxy group react with the amino groups of chitosan. Results indicated that significant stiffening was obtained by incorporation of silane in chitosan matrix. Moreover, full flexibility was retained by the increasing Young's modulus with higher silane content. The adhesion and proliferation of the MG63 osteoblast cells cultured on the hybrid surface were improved when compared to those on the pure chitosan membrane (Shirosaki et al., 2009).

The mechanical properties of the chitosan/HAp composites play a significant role in bone tissue engineering. The intermolecular hydrogen bond and chelate interaction between the chitosan and HAp contribute to good mechanical properties. There is a possible interaction between the NH_2 group and primary and secondary –OH group of chitosan with Ca_{2+} of HAp. This interaction might be responsible for the higher mechanical strength of the composite scaffolds as compared to chitosan and HAp alone (Venkatesan and Kim, 2010). The mechanical resistance of chitosan–HAp multilayer nanocomposites was reported by Hu et al. with high strength and bending modulus as a suitable material for internal fixation of long bone fractures (Hu et al.,

2004). Oliveira et al. fabricated composites of hydroxyapatite forms with chitosan derivatives as well and obtained regular, interconnected pore structures with 20–500µm size range and 58.9% ± 6% porosity. The composite scaffolds were found to be degradable and bioactive (Oliveira et al., 2009). The chitosan–nHAp composite scaffolds exhibit greater compression modulus, slower degradation rate and reduced water uptake (similar to that of pure chitosan) with favorable cell responses by improving cell adhesion and proliferation (Thein-Han and Misra, 2009).

The chitosan/HAp composite scaffolds possess a pore size of 100–200 µm, providing a spatial arrangement of cells (10–30 µm) and thus cells are able to migrate towards the composite. It was observed that when the osteoblast cells were cultured in the medium of phosphorylated chitosan/HAp, the cell morphology changed within 30 min of seeding and later became triangular at 24 h, polygonal at 48 h, and finally, aggregated to be indistinct at 5 days. Apart from HAp, other calcium phosphate minerals also provide adhesion and cell proliferation when combined with chitosan. The cell proliferation and adhesion has been found with osteoblast mouse cells MC3T3-E1 and L929 cells in chitosan/calcium phosphate specimens. The chitosan/HAp composite scaffolds possess higher ALP activity compared to the chitosan scaffold whereas the highest ALP activity has been achieved in the composite containing 30–40% of HAp with good cell proliferation; however, cell proliferation decreases with an increase in the HAp concentration. The modified chitosan and its composites are found to have good cell proliferation and higher ALP activity then compared to non modified chitosan (Venkatesan and Kim, 2010; Zhang and Zhang, 2013).

Tang et al. showed that the natural hydroxyapatite and chitosan composites have a good hard tissue biocompatibility and an excellent osteoconductivity. They also suggested that this compositemaybesuitable for artificial bone implants and frame materials of tissue engineering (Tang et al., 2008). Zhang et al. prepared electrospun HAp/chitosan nanofibers with compositional and structural features close to the natural mineralized nanofibril and they reported that these HAp incorporated nanocomposite fibers are found to have potential by significantly stimulating the bone forming ability (Zhang et al., 2010). Liuyun et al. prepared the composite scaffold composed of nano-hydroxyapatite, chitosan and carboxymethyl cellulose by freeze-drying method. *In vitro* cell culture studies were evaluated by MG-63 cells and Mesenchymal stem cells (MSCs) The results indicated that the composite scaffold has good cell biocompatibility (Liuyun et al., 2009). Kashiwazaki et al. fabricated novel chitosan/hydroxyapatite

nanocomposites with porous structure by the co-precipitation and porogen leaching method. These composites were found to have biocompatibility and biodegradation (Swetha et al., 2010). In a study, chitosan–gelatin/nanophase hydroxyapatite composite scaffolds were prepared by blending chitosan and gelatin with nanophase hydroxyapatite (nHA). Composite scaffolds showed a decreased degradation rate and increased mineralization in SBF with nHA incorporation. MG-63 cells on nanocomposite scaffolds were higher in terms of improved cell attachment, proliferation, and spreading compared to chitosan–gelatin (CG) scaffold (Peter et al., 2010). A biopolymer-based novel nanocomposite chitosan/montmorillonite (MMT) /hydroxyapatite (HAp) has been reported for biomedical applications. This nanocomposite showed improved mechanical properties suggesting its potential applications in bone tissue engineering (Katti et al., 2008). Porous chitosan/brushite composite scaffolds were produced by a freeze-drying technique. Results showed that obtained chitosan/brushite composite scaffolds are promising candidates for bone tissue engineering applications and the brushite content may be used to improve the yield strength of the composite scaffolds (Araujo et al., 2006).

2.6. Polymer-Silica Composites Studies for Bone Tissue Engineering

Bioactive silicate glasses were first developed by Hench and co-workers in 1969 and represented a group of surface reactive materials consisting of high SiO_2 content which are able to bond to bone in physiological environment (Boccaccini et al., 2010). They are based on a random network of silica tetrahedra containing Si-O-Si bonds. The network can be modified by the addition of network modifiers such as Ca, Na and P, which are bonded to the network via non-bridging oxygen bonds. Bioactive glasses are resorbable, osteoproductive, and stimulate new bone growth on their surface (Jones et al., 2006).

Class A bioactive materials are osteogenetic and osteoconductive materials while Class B bioactive materials (such as hydroxyapatite) exhibit only osteoconductivity. Bioglass nanoparticles offer remarkable advantages due to their high bioactivity index (Class A), and ability to bond to both soft and hard connective tissues. In other respects, reactions on bioactive glass surfaces release critical concentrations of soluble Si, Ca, P and Na ions, which induce intracellular and extracellular responses

(Roether and Boccaccini, 2008). Therefore, polymer/bioactive glass composites are of great interest for bone tissue engineering applications. Bioactive glasses consisting of a silicate network incorporating sodium, calcium and phosphorus, are widely used in biomedical applications (Boccaccini et al., 2010).

Tsigkou et al. investigated the cellular response of fetal osteoblasts on bioactive resorbable composite films consisting of a poly-D, L-lactide (PDLLA) matrix and bioactive glass 45S5 Bioglass[®] (BG) particles. Differentiation and maturation of fetal osteoblasts was examined, incorporation of 45S5 BG within the PDLLA matrix was found to significantly enhance alkaline phosphatase enzymatic activity and osteocalcin protein synthesis (Tsigkou et al., 2006).

The chemical reactions and processes that occur at the surface of silicate-based bioactive glasses regarding the SiO_2, or silicon content can be summarized as: breaking of Si-O-Si bonds with the related loss of soluble silica; formation of Si-OH bonds and the condensation and repolymerization of a SiO_2-rich layer on the glass surface; and the calcium phosphate layer formation on SiO_2-rich layer. In consequence of these processes, subsequent crystallization of apatite crystals, cell adhesion and collagen formation occurs (Gibson et al., 1999).

There is a distinct difference between the chemical structure of HAp particles and bioactive glasses and glass–ceramics arised from the high SiO_2 levels. Bioglass contains approximately 45 wt % SiO_2. It has been proposed that the SiO_2, or silicon, in these silicate-based bioactive glasses plays an important role in surface reactions and therefore *in vitro* and *in vivo* bioactivity (Gibson et al., 1999). Bioglass 45S5 which is a bioactive glass containing 45% silicon dioxide (by weight) has stimulated osteogenesis *in vitro* by inducing the proliferation and osteogenic differentiation of human osteoblasts (Xynos et al., 2000). Hensch et al. investigated the interactions of living tissue with bioactive glasses. Vogel et al. further investigated how the solubility of bioactive glass affects bond formation between bone and implants. Implantation studies of bioactive glasses in rabbits found these materials to be nontoxic and non inflammatory (Wu et al., 2010).

A recent study indicated that the ionic products of dissolution which contains Ca, P, and Si ions had a direct effect on the gene-expression profile of human osteoblasts (Xynos et al., 2000). Sun et al. investigated the Bioglass®and its ionic products on human osteoblasts growth cycle *in vitro* and reported that Bioglass®

promoted osteoblast proliferation, reducing the human osteoblast growth cycle to pass through G_1 and S phase and then enter G_2 phase quickly (Sun et al., 2007).

Silicate nanoparticles have been extensively used to improve the mechanical properties of synthetic and natural polymers. These polymer nanocomposites often show significant improvements in structure, modulus, strength and toughness that cannot be achieved by using the polymer alone. Thus, silicate nanoparticles are commonly used for biomedical applications as reinforcements (Wu et al., 2010). Besides, there have been a number of studies that revealed the biological functions of silica and it was found that silica has an important role in biomineralization of bone tissue. Silicon is one of the trace elements known to be essential in biological processes. There are various substitutions that exist in the actual human bone mineral including Na, Mg, K, Sr, Zn, Ba, Cu, Al, Fe, F, Cl and Si. The importance of Si on bone formation and calcification has been demonstrated through *in vitro* and *in vivo* studies. High Si contents have been detected in early stages of bone matrix calcification, and aqueous Si induced precipitation of hydroxyapatite in bone tissue. Silicon enhances the bone in growth as a calcifying agent and its incorporation in the HAp is considered to be a potential method for improving the bioactivity of HAp (Yacoubi et al., 2014).
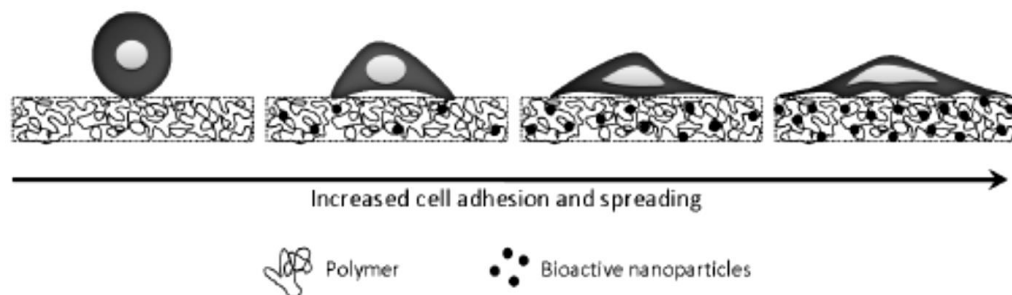
Figure 2.13. Effect of bioactive nanoparticle incorporation on cell adhesion and spreading (Source:Wu et al., 2010).

Shirosaki et al. fabricated porous chitosan–silicate composite scaffolds and investigated the effect of glycidoxypropyltrimethoxysilane (GPTMS) on *in vitro* osteoblast attachment and proliferation. *In vitro* results indicated that increasing silicate concentration favored cell proliferation. Osteoblasts migrated deep into the pores, attached, and proliferated on the pore walls (Shirosaki et al. 2008). Madhumathia et al. prepared chitin composite scaffolds containing nanosilica using chitin hydrogel and

analyzed their bioactivity, swelling ability and cytotoxicity *in vitro*. These scaffolds were found to be bioactive in simulated body fluid and biocompatible when tested with MG 63 cell line. The results suggest that chitin/nanosilica composite scaffolds can be useful for bone tissue engineering applications (Madhumathia et al., 2009). Studies by Schwarz et al. suggested that silica may act as a cross-linking agent in connective tissue (Wu et al., 2010).

Many other studies investigating implants containing bioactive silicate found that the implants induce bone formation, stimulate osteogenic proliferation and activate bone-related gene expression Recent reports by Lee et al. used a sol-gel method to fabricate chitosan–silicate nanocomposite membranes for bone regeneration. The addition of silicate resulted in improved mechanical properties of the nanocomposite when compared to pure chitosan. When immersed in simulated body fluid, the chitosan-silicate nanocomposites induced deposition of calcium phosphate minerals, suggesting *in vitro* bioactivity. A significant increase in osteoblast adhesion, proliferation and alkaline phosphatase activity was enhanced by the presence of silicate. Histological results of polymer nanocomposite implantation in a rat calvarium model showed a significant increase in bone regeneration when compared to the pure chitosan (Wu et al., 2010).

Nano-silica fused whiskers combined with calcium phosphate cements act as fillers in a composite, the role of nano-silica being to strengthen the phosphate-based composite: the mechanical properties of the phosphate-silica-whisker composites nearly matched those of cortical and trabecular bone (Muzzarelli, 2011). In a study, hydroxyapatite/chitosan–silica (HApCSi) nanocomposites were synthesized by co-precipitated method and their potential application as filler materials for bone regeneration were investigated in simulated body fluid (SBF). *In vitro* biocompatibility, cell morphology, proliferation, and cell adhesion tests confirmed the osteoblast attachment and growth on the $HApCSiO_2$ surface (Jongwattanapisan et al., 2011).

Lehmann et al. fabricated silicon-substituted hydroxyapatite (Si-HAp, 1.4% wt) porous cylinders studied the effect of silicon particles on osteblast proliferation and differentiation. In particular, porous Si-HAp appeared to enhance cell proliferation at early stages of culture, whereas both materials showed adequate support for bone apposition, but with different gene expression patterns and cell morphology. In addition, *in vitro* bioresorption capability of both materials was revealed, but the osteoclast activity seemed to be better performed on Si-HAp disks (Lehmann et al., 2012). Zhou et

al. studied the feasibility of silica/HACC/zein composite scaffold applied in bone tissue engineering. The current results suggest that the zein-HACC-S20 scaffold graft is particularly suitable to in bone regeneration due to effective pre- vention of implant-associated infection and effective promotion of osteogenesis (Zhou et al., 2014). Nair et al. fabricated chitosan–gelatin–siloxane scaffold and studied the effect of siloxane on bone regeneration. *In vitro* evaluation of the hybrid scaffolds using rabbit adipose mesenchymal stem cells revealed that osteogenic cell-clusters formed on polymer-siloxane scaffold, siloxane enhanced alkaline phosphatase activity and the expression of bone-specific genes, whereas the control scaffold supported more of cell-proliferation than differentiation (Nair et al., 2015).

2.7. Diatomite as a Natural Silica Source (Diatomaceous earth)

Diatoms are microscobic (~1-500 µm), non-motile, unicellular eukaryotic photosynthetic microalgae that belong to the class Bacilariophyceae of the phylum Bacilariophyta. They are encased within a unique cell wall composed of silica (hydrated silicon dioxide) which is the second most abundant biogenic mineral produced by various plants and animals (Wee et. al., 2005; Narayanan et al., 2011).

These single celled microalgae develop biomineralised external cell walls known as frustules. The frustule is composed of amorphous silica skeletons and organic materials. It is estimated that more than 100,000 different species have been discovered and classified by their unique frustule morphologies. Such morphological specificity is a strong indication that the frustule assembly process is under genetic control (Parkinson and Gordon 1999, Gaddis and Sandhage 2004; Wee, et al. 2005).

Diatoms are classified in two major groups based on the frustules symmetry: pennate and centric (Goldberg, et al. 1998). Pennate types of diatoms tend to be elongated and are usually bilateral symmetrical. Centric types of diatoms are radial symmetric (Parkinson and Gordon, 1999). The centric type is of primary interest as having nanoengineering potential because of its uniform pore structure, well-aligned pores and wide ranges of heights and diameters (Wee et.al.,2005).

Each diatom cell consists of two halves known as the thecae, which can be divided into a valve and one or more girdle bands. The thecae overlap like a petri dish

and separate during cell division. The inner part of diatom frustule is known as the hypotheca and the outer part is called the epitheca. Each half (theca) consists of a valve which forms the larger outer surface and several ring-like silica structures known as girdle bands. Each diatom species forms uniquely-shaped frustules with fine features such as pores, ridges and protuberances arrayed in intricate and species-specific patterns. The dimensions of amorphous silica skeletons range from ~1-500 μm, whereas the regular features distributed on the frustules show dimensions in a range of 10-200 nm (Fuhrmann, et al. 2004, Gaddis and Sandhage 2004).

The cell division does not occur unless there is sufficient bio-available silica for frustules formation and the silica necessity for frustules formation causes the growth of silica-dependent control points in diatom mitosis. The silica transport vesicles accumulate silica at intracellular concentrations up to 250 times higher than in the surrounding media. Diatom frustule formation process is thought to be formed by diffusion limited precipitation of silica particles. Cell-wall formation occurs primarily in silica deposition vesicles (SDVs), intracellular organelles in which an unpolymerized, soluble form of silicate. Amorphous silica particles of relatively low molecular weight and ~1−10 nm in diameter are thought to be transported to the perimeter of the SDV by silica transport vesicles (Parkinson & Gordon, 1999).

They have almost 110,000 species which have thousands of different morphologies and size ranging from 2 μm to 2 mm in size. (Figure 2.14.). Diatoms have well-arranged pores on the outer or inner surfaces and a numerous sieve pores being approximately 40 nm for exchanging nutrients and gases. The porous structure of frustules also increases their surface area possibly reaching 200 m^2/g (Wang et al.,2013). Hamm and co workers reported that the surface area of diatomaceous earth was relatively high with 22 m^2/g (Hamm et al., 2003). The BET specific surface area of diatomaceous earth was reported to be 3.6 m^2/g (Strzelczyk, et al. 1998). In another study, Tsai and co wrokers found that the BET surface area of diatomaceous earth as 3.81±0.01 m^2/g (Tsai, et al. 2006).
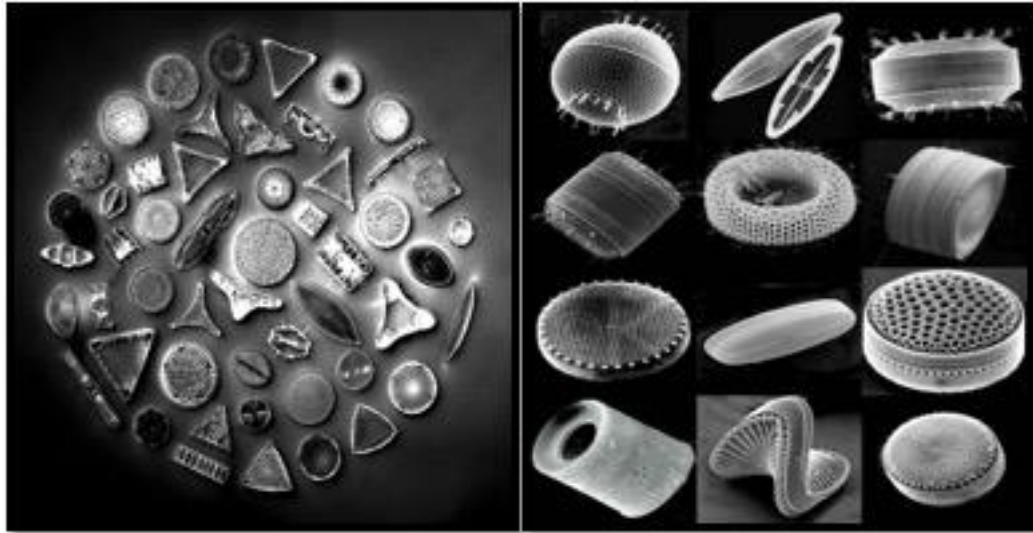
Figure 2.14. Diatom frustule morphologies of different species
(Source:www.nextnature.net/2012/12/nanotech-diatoms)

Gulturk and Guden studied the chemical and microscopic properties of natural and calcined diatom frustules. Both frustules are found to be composed of high silica mineral (88-90%) and small amount of other oxide components. (Gulturk and Guden, 2011).

When diatom cells die, the remnant silica cell wall is collected at the floor of the ocean and form fossils. These fossilized cell walls are called diatomite or Diatomaceous earth (Şan et al., 2009). Diatomaceous earth (SiO_2-nH_2O) is a natural occurring mineral compound from microscopic skeletal remains of unicellular algae-like plants called diatoms. This mineralised exoskeleton is termed as "frustule". In respect to the biogenic sources, the diatomaceous earth (diatomite) constitutes biogenic amorphous silica source and the most abundant form of silica on earth (Şan et al, 2009). Frustules are primarily amorphous agglomerations of very small silica particles in the order of a few ten nanometers. The amorphous silica (opal-A) is mainly in the form of diatom frustules, and secondarily in the form of sponge spicules, silicone-flagellate skeletons or radiolarian cells. This type of SiO_2 can react with $Ca(OH)_2$ and produce calcium silicate hydrates (CSH). The diatomite also contains carbonate and clay minerals, quartz and feldspars. Pure diatomite ($SiO_2 > 95\%$) particles are widely used as filtering agents and supplementary cementing materials. In addition, calcareous diatomites are used as abrasives, special fillers, absorbents and insulation products (Kastis et al., 2005).

Diatomite has unique physical characteristics, such as high permeability (0.1-10 mD) and porosity (35-65%), small particle size, large specific surface area, low thermal

conductivity, density and high absorption capacity. It has intrinsic properties such as relatively high melting-point, chemical inertness and small grain size. Diatomite particles as a biogenic source has a great potential because of its abundance, inexpensive cost and extensive application area in sound, heat insulation, chemical reactions (catalyst, sensor components, dynamites, pool water ,beer and wine filtration, absorption and gel filtration, filler material, abrasive) (Bakr, 2010; Cai, et al. 2005, Lopez-Alvarez et al., 2008; Hadjar et al., 2008; Parkinson&Gordon 1999, Scala& Bowler 2001, Stoermer et al., 2004; Şan et al., 2009; We et al., 2005).

The studies demonstrated the importance of the various functional groups, available on the surface of diatomite, which are responsible adsorption mechanism. Diatomite surface is terminated by OH groups and oxygen bridges (Figure 2.10.). These groups act as adsorption sites on the surface (Khraisheh et al., 2004).
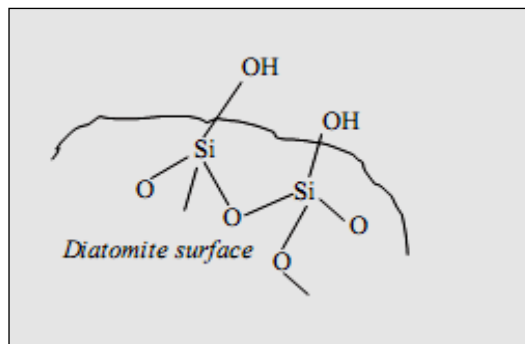
Figure 2.15. Functional groups on diatomite surface
(Source: Khraisheh et al., 2005)

Frustules, the silica shells of diatoms, have unique porous architectures with good mechanical strength. In recent years, biologists have learned more about the mechanism of biosilica shells formation; meanwhile, physicists have revealed their optical and microfluidic properties, and chemists have identified ways to modify them into various materials while maintaining their hierarchical structures. These efforts have provided more opportunities to use biosilica structures in microsystems and other commercial products (Wang et al., 2013).

The potential engineering and medical applications of diatom frustules have recently proposed, including metal film membrane, pinpoint drug delivery and nano powder silica. In metal film membrane fabrication, a continuous membrane can be created using a unique process of casting amorphous silica diatom frustules in a continuous metal film. In the second application, diatoms can be cultured in an iron-rich environment for magnetization and these magnetized frustules can be used in micron-

scale electrical motors in order to move the drug for the treatment of a disease such as cancer. The last application mentioned above involves the processing SiO_2 nano powders from diatom frustules. These frustules or purified silica powders obtained from frustules can be used to reinforce composites(We et al.,2005).

A few studies exist regarding the use of diatoms for biomedical applications. Lopez-Alvarez et al. investigated the influence of silicon substituted hydroxyapatite coatings on osteoblast-like SaOs-2 cell line. Diatomaceous earth and synthetic silica with commercial hydroxyapatite were used to produce the Si–HAp coatings. *In vitro* cell culture results indicated that Si–HAp coating from diatomaceous earth significantly favoured osteoblast proliferation and activity in comparison to the Si-HAp coating from synthetic silica (Lopez-Alvarez et al., 2008).

Hertz et al. prepared porous SiO_2 and SiO_2/ TiO_2 monoliths from Flux calcined diatomaceous earth and found that samples containing only SiO_2 were proved to be biocompatible for bone tissue engineering (Herzt et al., 2012). In a study, raw diatomite (RD) and calcined diatomite (CD) powders were purified by acid treatments, and diatom microparticles (MPs) and nanoparticles (NPs) were produced. *In vitro* cytotoxic effect of diatom-derived particles was investigated. Results indicated that diatom particles had no cytotoxic effect on 3T3 cells and purification route could impact the cytotoxicity, especially in the case of microparticles (Le et al., 2016).

2.8. Polyhedral oligomeric silsesquioxane (POSS)

The silsesquioxane family is among the most commonly used nanofillers or monomers for developing composite materials. (Ghanbari et al.,2011). Organosilicate molecules with the basic formula (R_n Si_n $O_{1.5n}$) with R groups (hydrogen, alkyl, alkylene, arylene, etc.) are defined as silsesquioxanes (Xu et al., 2011). The molecular architecture of silsesquioxanes vary from random, ladder, partial-cage, to cage structure. Among them, polyhedral oligomeric silsesquioxanes (POSS) are those classes with well-defined cage structures, which contain a silicon/oxygen cage (inorganic portion) and hydrocarbon functional groups (organic portions) attached to corner Si molecules (Cho, 2006; Xu et al., 2011).

Polyhedral oligomeric silsesquioxanes (POSS) are excellent examples of a three dimensional nanophase where all these dimensions are in the nanometer range. The

name silsesquioxane comes from the "sesqui", which refers to one and a half. This definition is derived from the general formula, (RSiO1.5) n where 1.5 oxygens are present for each silicon. The suffix "ane" represents a hydrocarbon group "R". POSS has two unique characteristics: First, its chemical composition is a hybrid, intermediate $(RSiO_{1.5})$ between that of silica (SiO_2) and silicone (R_2SiO) (Cho, 2006). This family posseess a regular three-dimensional (3D) shape and a structure consisting of an inner inorganic framework of silicon atoms (n=8) linked with oxygen atoms (n=12), and an outer shell of organic groups (n=8) which merge together to form a three dimensional nanocaged structure (Figure 2.15.). In POSS structure each silicon atom is bonded to three oxygen atoms by siloxane bonds (Si-O-Si), and one carbon silicon bond (Si-C) (inert or reactive). These are highly symmetrical molecules with a nanoscopic feature size of approximately 1.5nm in diameter (including the R side chain groups) (Ghanbari et al., 2011). POSS nanocages with different R groups have silicon/oxygen cage structure in a range of 32-100 wt%. Octa methyl POSS molecules posses 78 wt% weight cage structure (DeArmitt, 2010).
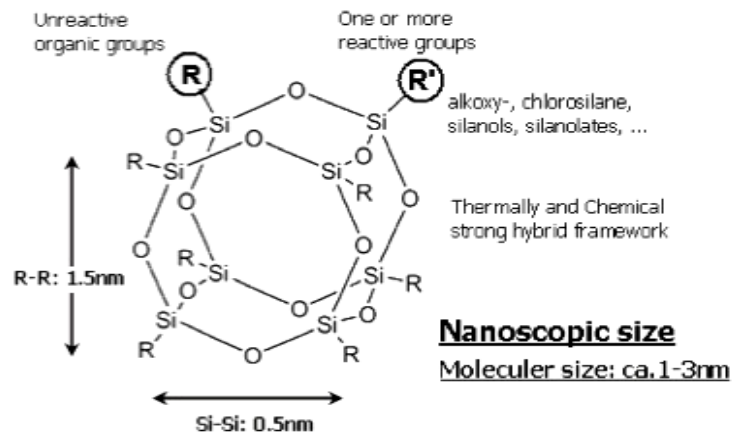
Figure 2.16. Structure of POSS nanocage with R groups
(Source:www.sigmaaldrich.com/japan/materialscience/nanomaterials/silsesquioxanes)

Generally, silsesquioxanes can be classified into two main categories based on their molecular architecture: Non-caged silsesquioxanes that form ladder, random, and partial-caged molecular structures which show enhanced insulating properties, gas permeability, play host to a range of applications from surface coatings and gas separation membranes to binding agents for carcinostatic drugs. (Ghanbari et al., 2011).

POSS, regarded as the smallest possible particles of silica, are widely used as nanofillers in polymers and can be incorporated into polymers through

copolymerization, grafting or blending (Xu et al., 2011). POSS nanophases have been utilized for preparing lightweight, high-performance hybrid nanocomposites. The performance region of POSS-reinforced nanocomposites is thought to be between polymers and ceramics. POSS-reinforced nanocomposites have been reported with higher use temperatures, oxidation resistance, surface hardening, mechanical properties, decreased flammability, reduced heat evolution and lower processing viscosities. POSS incorporation to polymers can enhance thermal and mechanical properties (Cho, 2006). POSS nanocomposites can be easily prepared by blending with polymers. Copolymerizing POSS into polymer systems has been an alternative method to ensure molecular-level dispersion and covalent attachment of nanoparticle in polymer matrix (Cai et al., 2012; Reno et al., 2012). The inorganic silica core of POSS is thermally and chemically robust and the different R groups make them compatible with various polymer systems (Ghanbari et al., 2011).

The modifications of POSS nanofillers on the material properties predominantly depend on the interactions between POSS nanoparticles and the polymer matrix. The same POSS molecule can serve as a reinforcing agent or a plasticizer when introduced into different polymer systems. For the same polymer system, POSS with different R groups can have very different effects on the glass transition temperature, rheological and mechanical properties. Therefore, it is possible to tailor the structure and bulk properties of POSS/polymer composites by varying the R groups of POSS (Xu et al., 2011). Increase in glass transition temperature at higher concentrations of POSS loading is obtained due to the reduced distances between these nanofillers, in consequence of aggregating. This effect prevents molecular rotation with regard to the polymer and makes it stronger (Kannan et al., 2005). The incorporation of POSS also influences the surface properties such as surface chemistry (wettability), energy, and topography (Ghanbari et al., 2011). Fernandez and co workers prepared poly (L-lactic acid)/polyhedral oligomeric silsesquioxane derivatives nanocomposite (PLLA/POSS) with solution casting method. Three different POSS molecules, two amino-POSS derivatives with different nonreactive organic substituents were used in order to investigate the effect of POSS type and concentration on the morphology and properties of PLLA/POSS nanocomposites. TEM results showed self-assembled POSS molecules of sub- micrometer size homogeneously dispersed in the polymer matrix, the shape and size of which depended on the POSS type and concentration. POSS derivatives acted as plasticizers by lowering the glass transition temperature of PLLAs. In addition, the

incorporation of POSS nanoparticles to PLLA led to an increase in the material stiffness and brittleness (Fernandez et al., 2016).

POSS nanocages differ in structure and chemistry to silica (SiO_2). Inorganic SiO_2, both colloidal and amorphous, have a defined three dimensional spherical morphology composed of cross-linked Si-O-Si with surface silanol (Si-OH) groups (instead of Si-C), and range in size from 5 to 100 nm in diameter (leading to micrometer scale dimensions for amorphous SiO_2), while the number of silicon atoms increase within the POSS structure (were n=4, 10 or 12) and the nanocages are larger than 1.5 nm, but usually smaller than 5nm in diameter. When acting as a nanofiller, POSS aggregation occurs naturally in polymeric systems despite their small size. These aggregations form dispersions of nanoparticulate materials ranging from 10–100nm in diameter (Ghanbari et al., 2011). Unlike silicas, silicones, or other nanofillers, each POSS molecule contains either unreactive organic functional groups, which help POSS molecules become soluble in, and compatible with, polymers or reactive organic functional groups, making POSS molecules more suitable for polymerization or grafting (Wang et al., 2014).

POSS-based nanocomposites have been shown as potential novel materials for biomedical applications due to the enhanced biocompatibility, and physicochemical properties.These highly biocompatible materials can be designed with tunable biodegradation rates and intricate chemistries that provide superior scaffolds for tissue engineering with many different cell types, tissues, and organ systems (Ghanbari et al., 2011).

A wet-spinning approach was used by Chew and co-workers to extrude ribbon-like micrometer-thick fibres comprising chitosan with polyhedral oligomeric silsesquioxanes (POSS). In this study, effect of POSS loading on the mechanical properties was only studied. Tensile testing results reveal that POSS incorporation influenced positively the maximum stress, toguhness and elastic energy of fibres. However, on further increase in the POSS concentration, it is observed that mechanical properties were affected negatively (Chew et al., 2011).

Cai et al. synthesized novel organic-inorganic nanohybrid injectable polymers to reinforce PPF with covalently grafted POSS. *In vitro* MC3T3-E1 cell studies have been performed to assess the corresponding cell responses to this series of nanohybrid polymer networks. Decreases in these mechanical properties are observed at higher

POSS % because of decreased crosslinking density and larger POSS aggregate formation. MC3T3-E1 cell functions including cell attachment, spreading, proliferation, differentiation, and gene expression maximized at 10% POSS (Cai et al., 2012).

Ha and coworkers have fabricated novel porous silicificated pristine (PVAc)/POSS composite nanofibers by facile electrospinning technique and studied the interaction of nanofibers with simulated body fluid (SBF) in order to determine bioactivity. They demonstrated that the silicificated PVAc/POSS composite had excellent ability to form apatite structures on its surface after soaking in SBF solution and showed favorable effects on the adhesion and propagation of myoblast cells (Ha et al., 2013).

In a another study, nanocomposites composed of methacryl isobutyl POSS (MI-POSS, one methacrylate functional group) and methacryl POSS (MA-POSS, eight methacrylate functional groups) were studied to determine the effect of functional group in the POSS structure on the properties of dental resin. It was found that mechanical properties and wear resistance decreased with increasing amounts of MI-POSS and agglomerates of MI-POSS act as the mechanical weak point in the dental resins. The addition of small amounts of MA-POSS improved the mechanical and shrinkage properties. However, lower flexural strength and flexural modulus were obtained at higher MA-POSS concentrations. Results indicated that the concentration dependence is attributed to phase separation at higher concentrations of POSS affecting the structural integrity and the mechanical properties of the dental resin (Wang et al., 2014).

Du et al. developed a series of poly (octanediol citrate)-polyhedral oligomeric silsesquioxanes (POC−POSS) hybrids with highly tunable elastomeric behavior (hydrated state), biodegradation and osteoblasts biocompatibility through a facile one-pot thermal polymerization strategy. POC−POSS hybrids show significantly improved stiffness and ductility in either dry or hydrated conditions, as well as good antibiodegradation ability as 20−50% weight loss in 3 months. *In vitro* results indicated that POC−POSS hybrids exhibit enhanced osteogenic differentiation through upregulating alkaline phosphatase (ALP) activity, calcium deposition, and expression of osteogenic markers (ALPL, BGLAP, and Runx2) (Du et al., 2016).

CHAPTER 3

MATERIALS AND METHODS

3.1 Materials

Chitosan (Low molecular weight, Sigma-Aldrich) powder was used for preparation of composite scaffolds. Diatomite (Sigma-Aldrich) and POSS Octa TMA® (Hybrid Plastics TM) were used as silica based reinforcements. Acetic acid (analytical grade, Sigma-Aldrich) was used as solvent for preparation of composites. Sodium hydroxide (NaOH- Sigma-Aldrich) was used for neutralization. BCA protein kit (Pierce Thermo) and BSA (Bovine Serum Albumin-ALDldrich, Sigma) were used for protein adsorption. Lysozyme (Aldrich, Sigma; from chicken egg white), sodium azide (Sigma-Aldrich) and phosphate buffer solution (10X) (PBS tablets, Sigma-Aldrich) were used for biodegradation studies. Simulated body fluid (SBF) was prepared for biomineralization tests. PBS (10X) solution (Lonza) was used for swelling studies. NIH/3T3, MG 63 and Saos-2 cell lines (ATCC®, CCL-92™, CRL-1427™, HTB-85™) with cell culture supplements; Dulbecco's modified Eagle's medium (DMEM, Sigma-Aldrich) and Minimum essential medium (MEM, Sigma-Aldrich), fetal bovine serum (FBS-Lonza) penicillin-streptomycin solution (streptomycin and penicilin) and L-glutamine (Lonza) were used for cell culture studies. WST-1 assay was used for *in vitro* cytotoxicity and proliferation (Biovision Inc.). Rezasurin cell viability kit (Cell Signaling Technology Inc.) was used for determination of *in vitro* cell proliferation. STEMTAG™ Alkaline Phosphatase Activity Assay Kit (Fluorometric) was used to determine the alkaline phosphatase activity of cells on scaffolds. L-ascorbic acid (Sigma, Aldrich) and β-glicerophosphate (Sigma, Aldrich) were used for osteogenic medium preparation. Silver nitrate (Sigma, Aldrich) and sodium thiosulfate (Sigma, Aldirch) were used for Von kossa staining. Paraformaldehyde (PFA, Merck), DAPI (4′,6-diamidino-2-phenylindole, Molecular Probes™, Thermo Fisher Scientific) and Alexa Four 488 Phalloidin (Molecular Probes™, Thermo Fisher Scientific) stains were used for fluorescence imaging.

3.2 Methods

3.2.1. Preparation of Chitosan/Diatomite and Chitosan/POSS Composites

Chitosan/diatomite and chitosan/POSS composite scaffolds were prepared by freeze drying method. A freeze drying process consists of three stages: freezing, primary drying and secondary drying. The freezing process is realized by contacting a liquid sample with or placing it in a cold bath. The frozen sample is then placed in a freeze dryer to remove the frozen solvent by sublimation. During the freeze drying process, the frozen sample should be kept below the glass transition temperature or melting point and the frozen solvent is removed under vacuum. Porous structures are formed from the voids left by the removal of the solvent. Thus, the frozen solvent acts as porogen to produce porous materials.

Before use, diatomite and POSS particles were dried at 80°C for 24h in order to remove moisture and prevent agglomeration. Chitosan-silica composite dispersions were prepared by using separately prepared chitosan solutions and silica dispersion in acetic acid (1% v/v), separately. Before dispersion of silica in acetic acid; diatomite and POSS particles were dried at 80°C for 24h in order to remove moisture and prevent agglomeration. First, chitosan was dissolved and silica particles were dispersed in acetic acid separately for 24 h . Then they were mixed and sonicated with Misonix Ultrasonic Liquid Processor for 30 min at 15 °C and 35 Amplitude for homogenization. They were poured into 24 and 48 well-plates for moulding.Then prefreezed at -20°C for 24 h. After prefreezing, samples were lyophilizied at -46°C and 0.01 mBar vacuum. Freeze dried scaffolds were then stored in dessicator for further use.

Chitosan/diatomite and chitosan/POSS composite membranes were prepared by solvent casting method. Composite dispersions were prepared as the same procedure described for scaffold preparation before freeze drying protocol. Membrane forms of these composites were used for AFM and contact angle analysis.

3.2.2. Neutralization of Scaffolds

Sodium hydroxide solution was used in order to neutralize remaining acetic acid residues. Prepared chitosan-silica composites were immersed in 1M NaOH (sodium hydroxide) aqueous solution and washed with distilled water to remove remaining NaOH.

3.2.3. Characterization Tests

3.2.3.1. Mechanical Analysis (Compression Test)

Mechanical strength of chitosan/silica composite scaffolds were measured by compression test according to the ASTM-D 5024-95a standard. TA XT Plus Texture Analyzer (Stable Micro Systems) was used for compression test. Dry samples and hdrated samples (immersed in PBS- pH 7.4) were tested. Scaffolds were hydrated in PBS (pH = 7.4, at 37 °C) for 1 h prior to testing and were kept immersed in PBS throughout the test. Compressive stress-strain curves were plotted and compressive elastic modulus (E*) and compressive strength (r*) were determined for all scaffolds Mechanical compression data are described as an average of five test specimens with standard error. The diameter and length of specimens were measured prior to compression test and the areas were calculated. Tests were performed with a cross-head speed of 5 mm/min at room temperature and compressed up to 75% of original height. Compression mold and test set up is shown in Figure 3.1.

Figure 3.1. Compression test set up
(Source:http://www.stablemicrosystems.com)

3.2.3.2. Static Air-water Contact Angle Analysis

The wettability term is known as the ease of a fluid spreads across a solid surface. The surface tension of the solid, the liquid, and the interfacial tension are three factors that affect the wettability of a solid (Menzies and Jones, 2010). Surface wettability is one of the most important parameters for biomaterial design that affects protein adsorption, platelet adhesion/activation, blood coagulation and cell and bacterial adhesion at the defect site. Therefore, it is an important factor for the biological response of body to the implanted biomaterial. It is considered that hydrophobic surfaces are generally more protein-adsorbent than hydrophilic surfaces due to strong hydrophobic interactions occurring at material surface. Contrary to this fact, water molecules strongly bound to hydrophilic surfaces form the repulsive solvation forces. However, studies concerning relationship of surface wettability with protein adhesion have not been consistent (Xu and Siedlecki, 2007). Measuring wettability of biomaterials is evaluated by measuring the contact angle at the liquid-solid interface. There are three major techniques for measuring in vitro wettability: sessile drop, captive bubble, and the Wilhelmy balance method, Sessile drop is the most commonly used technique among them (Menzies and Jones, 2010). The contact angle term is defined as the angle formed by the intersection of the liquid-solid interface and the liquid-vapor interface. The contact angle less than 90° indicates favorable wetting property on the surface, while contact angle greater than 90° indicates unfavorable wetting on the surface (Yuan and Lee, 2013). As the contact angle increases, the wetting decreases. Low contact angle indicates good wettability (Mekayarajjananonth and Winkler, 1999).

Static contact angle analysis was performed with composite films and compressed scaffolds. The specimens (1cm width-5cm length) were prepared before the measurement. Ultrapure water was used as liquid phase and drop size was set to 6 μL. Contact angle was measured from five different points of each sample and the average value was reported. Figure 3.2. illustrates the behaviour of hydrophobic and hydrophilic surfaces.
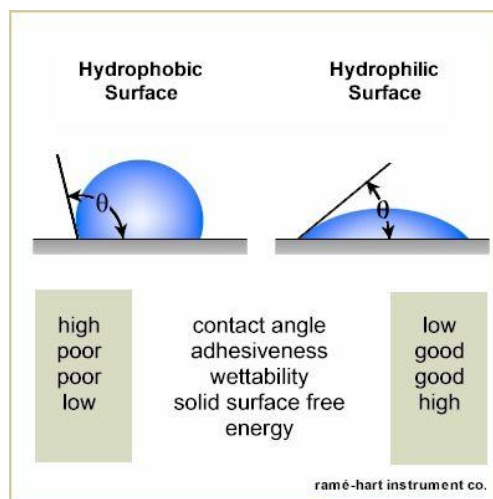
Figure 3.2. Contact Angle of Hydrophobic/ Hydrophilic Surface
(Source:Ramehart, 2012).

3.2.3.3. AFM Analysis

Atomic force microscopy (AFM) is a very high-resolution type of scanning probe microscopy. In AFM imaging modes, the cantilever is usually scanned over the surface to produce a three dimensonal image of the surface. The cantilever and tip are in contact the surface and the interaction between the tip and the sample is measured. There are different AFM imaging modes providing a range of different information about surface of the sample being examined. The most common imaging modes are contact and tapping modes (Figure 3.3). The AFM probe remains in contact with the sample at all times in contact mode imaging. It is often used for imaging of hard surfaces. The cantilever is allowed to oscillate at a value close to its resonant frequency in tapping mode. The oscillatory amplitude of the cantilever changes as it encounters differing topography (Johnson et al., 2006).

Atomic force microscopy measurements (Digital Instruments-MMSPM Nanoscope IV, Brucker Inc.) was performed with point probe cantilever tip in contact mode for chitosan/diatomite membrane samples and tapping mode was used for chitosan/POSS membrane samples by the accompanying Nanoscope (Digital Instruments Inc., USA) software to determine the surface morphology and roughness of investigated film surfaces. The roughness parameters of each sample were evaluated on three scanned areas of 100μm x 100μm each.
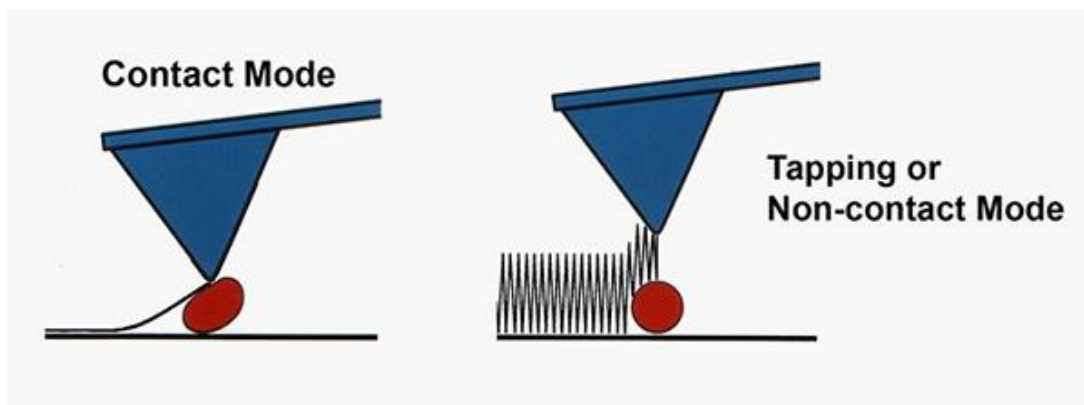
Figure 3.3. Contact mode and tapping mode in AFM
(Source:https://www.deakin.edu.au/research/facilities)

3.2.3.4. SEM Analysis

Chitosan/diatomite and chitosan/POSS composite scaffolds were analysed by SEM in order to observe surface morphology, pore size and distribution of diatomite and POSS particles in chitosan matrix. Before the analysis, samples were coated with thin gold layer under argon gas by using Emitech K550X. Then SEM analysis was performed with Quanta FEG 250 (at $7x10^{-2}$ mbar and 15 mA). Image J software was used to evaluate average pore size by using SEM images.

3.2.3.5. Porosity Analysis

The mechanical and biological properties of a scaffold are primarily influenced by its architectural characteristics including porosity, pore size, surface area to volume ratio, interconnectivity and permeability. Molecular transport which includes oxygen, nutrient, metabolic waste, molecular signaling and cell survival, is dependent on vascularization at the defect site, while diffusion would be the main factor for *in vitro* culturing. This process is carried out by optimum pore size and porosity. When molecular transport is inhibited with poor diffusion, peripheral cellular growth occurs and necrosis happens at the interior part of the scaffold (Ho and Hutmacher, 2006). In a study by Langer et al., optimum porosity was found 90% for *in vitro* diffusion and transport (Ho and Hutmacher, 2006). Biomaterials are generally characterised in terms

of mean porosity, pore size diameter and total pore surface in porosity analysis. Three different type of pores can be observed in the structure: through pores, blind pores and closed pores (Giesche, 2006). Schematic representation of pore types is depicted in Figure 3.4.
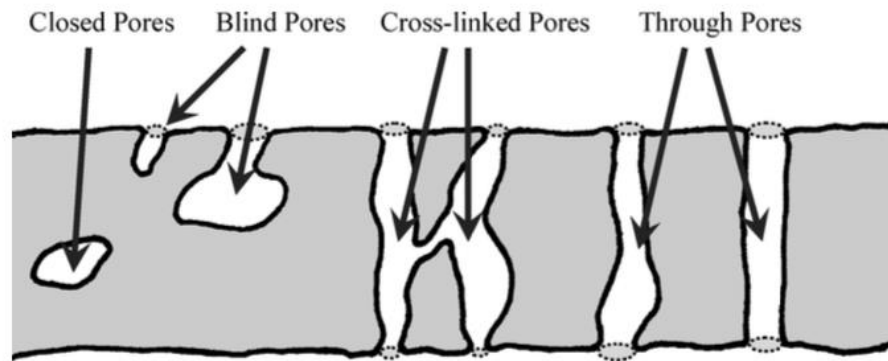
Figure 3.4. Schematic representation of pore types
(Source:Giesche, 2006).

Porosity of scaffolds was evaluated by mercury intrusion porosimeter and Micro Ct analysis.

3.2.3.5.1. Mercury Intrusion Porosimeter

Porosity of composite scaffolds was determined by mercury intrusion porosimeter (Micromeritics, AutoPore IV). Mercury intrusion porosimeter is a well known method which characterizes a material's porosity by applying various levels of pressure to a sample immersed in mercury. Mercury is used in this technique because it is a non-wetting liquid that does not intrude into pore spaces except under sufficient pressure. The pressure required to intrude mercury into the sample's pores is inversely proportional to the size of the pores. R_1, R_2 and R_3 represent the radius of pores (Figure 3.5). Pore diameter-pressure relationship was evaluated by Washburn equation

[$D= (-4\gamma \cos\theta)/P$,where D: pore diameter; P: pressure] (Webb, 2001; Giesche, 2006; Ho and Hutmacher, 2006).
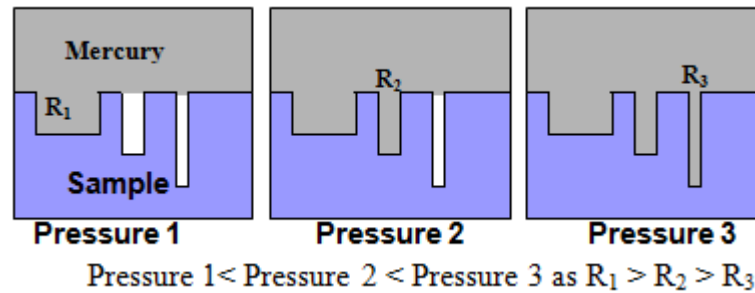
Figure 3.5. Mercury intrusion into pores with different sizes.
(Source:http://nptel.ac.in/courses/ 103103026/module2/lec11/4.html)

3.2.3.5.2. Micro Computed Tomography (micro CT)

Micro computed tomography (micro CT) provides precise quantitative and qualitative information about the 3D morphology of the material. The specimen can be examined in great detail without physical sectioning or using toxic chemicals. In micro CT scanning, the specimen is divided into a series of 2D slices which are irradiated from the edges with X-rays (Ho and Hutmacher, 2006). Micro-CT has been used to evaluate the morphology and topology of various scaffolds. It allows to obtain the actual pore size distribution by using 3D thickness maps which are conventionally used for quantifying trabecular bone thickness (Peyrin, 2011).

Porosity and 3D architecture of composite scaffolds were obtained by microtomography imaging using Scanco-µCT 50 (Scanco Medicals, Switzerland) with penetrative X-rays of 45 kVp-88uA. Scaffolds were scanned at a native resoliton with air filter. 500 slices was used for each specimen with 3µm voxel size in order to investigate the 3D structure of scaffolds.

3.2.3.6. Protein Adsorption Assay

Protein adsorption assay predicts the amount of protein adsorbed to a surface as a function of time. Generally, protein/surface interactions result in adsorption. In this study, the bicinchoninic acid (BCA) assay was used to determine the protein adsorbed on the scaffold surfaces. BCA assay is a colorimetric method that is commonly employed to estimate the concentration of protein in a sample. In this assay, protein

levels are measured via reduction of Cu^{+2} to Cu^{+1} by protein in an alkaline medium (the biuret reaction) with the highly sensitive and selective colorimetric detection of the cuprous cation (Cu^{+1}) using a unique reagent containing bicinchoninic acid. The purple-colored reaction product which is formed by the chelation of two molecules of BCA with one cuprous ion exhibits a strong absorbance at 562nm. The relationship between protein concentration and absorbance is nearly linear over a wide working range (20-2,000 µg/ml). Protein concentrations generally are determined and reported with reference to standards of a common protein such as bovine serum alb umin (BSA) (Smith et al., 1985; Bainor et al., 2011).

In this study, first, composite scaffolds were incubated with 0.1 % Bovine serum albumin (BSA) solution in order to determine the protein quantity adsorbed on surface. Experiment was carried out in 24 well plates. The sample specimens were incubated at $37^{o}C$ for 24h and 48h. The amount of adsorbed proteins on scaffolds was determined by BCA (Pierce, Rockford, IL) protein assay kit, using bovine serum albumin (BSA) as standard. The microplate procedure was used for protein determination adsorbed on samples.

3.2.3.7. Swelling Study

Swelling test was performed in order to obtain water uptake capacity of scaffolds in implanted tissue. Dry samples were weighed before test (W_d), immersed in PBS (Phosphate Buffered Saline) solution and incubated at $37^{0}C$ for 1 h, 24 h and 48 h. Then, wet samples were removed from plate and weighed (W_w). Extra solution on the surface was removed with filter paper before weighing. Swelling ratio (SR) was determined with the following equation:

$$SR = \frac{(Ww - Wd)}{Wd} \qquad (Eq\ 3.1.)$$

3.2.3.8. Enzymatic Degradation Study

Enzymatic degradation of composite scaffolds was tested by incubating samples in enzymatic solution composed of lysozyime and PBS solution (pH 7.4). Lysozyme is one of enzymes present in the human body that can hydrolyze the β(1-4) linkages between N-acetylglucosamine and glucosamine units in chitosan (Han et al., 2011). 1.5 µg/ml lysozyme from chicken egg white was used in order to mimic human serum (Freier et al., 2005). The enzymatic degradation of chitosan-silica composite scaffolds was performed in centrifuge tubes at 37°C. Phosphate-buffered solution (PBS, pH 7.4) containing 1.5 µg/mL lysozyme was used as degradation medium. 0.01% sodium azide was used in order to prevent bacterial contamination. The lysozyme solution was refreshed every 48h periods to ensure continuous enzyme activity. Weight loss % of samples were investigated for 7, 14, 21 and 28day incubation periods. The extent of enzymatic degradation was expressed as percentage of weight loss of the dried scaffolds after lysozyme treatment. Three specimens were used for each group.

Enzymatic Biodegradation was indicated by weight loss % calculated using Equation 3.2. as shown below;

$$\text{Weight loss \%} = \frac{W0 - W1}{W0} \qquad (\text{Eq. 3.2.})$$

3.2.3.9. Mineralization Study

Bone is a mineralized structural tissue and mainly composed of phosphorus, magnesium and calcium. In order to simulate bone tissue, biomaterial designed must include or secrete these mineral components. Minerals add structural integrity to the scaffold and also make it actively osteoconductive (Holzwarth et al., 2011). Mineralization is an important factor in biomaterial design used in bone tissue regeneration. It has been concluded that biomaterials having hydroxyapatite (HAP, $Ca_{10}(PO_4)_6(OH)_2$) layer formed at the surface, enhanced the binding with living bone layer in consequence of its similarity with bone mineral. SBF has been used widely for

in vitro assessment of the bioactivity of artificial materials by examining their apatite-forming ability in the fluid.

Integration of biomaterial with bone tissue can be evaluated by immersing in simulated body fluid (SBF) test in order to determine *in vitro* Ca-P phase formation at the material surface. The SBF is a solution that has similar ion concentration to human blood plasma. Mineralization test with SBF is carried out by maintaining pH and temperature of solution to match the required for formation of an apatite mineral. During mineralization test, free calcium and phosphate ion concentrations decrease as mineralization progresses. Therefore, the SBF solution is periodically replaced (typically every 3–4 days) to ensure maintenance of these concentrations closest to the original SBF solution. Mineral formation is evaluated by characterizing the calcium phosphate mineral formed on the material surface. Alternatively, changes in calcium and phosphate ion concentration with time can be evaluated in order to determine the mineralization capacity of a biomaterial (Oyane et al., 2003; Kepa et al., 2015). SBF was first produced and used by Kokubo et al. in 1990. Simulated body fluid (SBF) is a solution having ion concentrations similar to that of human blood plasma. SBF is used as a biomimetic surface modification technique to form apatite layer on biomaterial surface. There are many different types of SBF, which are all different modifications of the Kokubo's first SBF recipe (Katsanevakis et al 2010).

In this study, mineralization process on composite scaffolds was tested in modified SBF solution (m-SBF (1X)). The contents of the prepared solution were given in Table 3.1. Three replicates were prepared for each scaffold group. Scaffolds were immersed in a solution containing SBF with 0,01% sodium azide in order to prevent bacterial contamination and incubated at 37°C for 7, 14, and 21days. After removing from SBF solution, samples were washed with distilled water thrice and dried for 24 hours at 37°C. Ca and P minerals deposited on scaffold surface were evaluated by EDX analysis. Modified simulated body fluid (m-SBF) was used in order to mimic the in vivo condition. Ion concentrations either equal to those of blood plasma than the ion concentrations of a conventional SBF. Also, m-SBF shows no change in ion concentrations and it is more stable under storage conditions (Oyane et al., 2003). Scaffolds were incubated in. SBF medium was refreshed for 48h periods to provide the circulation. SEM analysis was performed with backscatter mode to investigate mineralisation on scaffold surface. EDX analysis was used to determine Ca and P ion

accumulation on surface. EDX is semi quantitative method. Therefore, Ca and P percentages on the surfaces couldn't be determined effectively.

Table 3.1. Contents of m-SBF
(Source:Oyane et al., 2003)

Order	Reagents	Amount
1	Distilled Water	1000mL
2	NaCl	5.403g
3	$NaHCO_3$	0.504g
4	Na_2CO_3	0.426g
5	KCl	0.225g
6	$K_2HPO_4.3H_2O$	0.230g
7	$MgCl_2.6H_2O$	0.311g
8	HEPES in 0.2M NaOH	17.892g
9	$CaCl_2$	0.293g
10	Na_2SO_4	0.072g
11	NaOH	15mL

3.2.4. *In vitro* Cell Culture Studies

3.2.4.1. *In vitro* Cytotoxicity Determination

Cytotoxicity of composite films and scaffolds were evaluated by the WST 1 assay. Working principle of WST 1 [4-3-(4-Iodophenyl)-2-(4-Nitrophenyl)-2H-5-Tetrazolio]-1,3-Benzene Disulfonate] assay is based on the conversion of stable tetrazolium to a soluble formazan by a complex cellular mechanism that occurs primarily at the cell surface. This bioreduction is largely dependent on the glycolytic production of NAD(P)H in viable cells. Therefore, the amount of formazan dye formed directly correlates to the number of metabolically active cells in the culture (Berridge et al., 1996). Indirect extraction method (ISO 10993; 24h extraction of scaffolds) was used for WST 1 cytotoxicity assays. NIH/3T3, MG 63 and Saos-2 cell lines were used. Cells

were maintained in DMEM supplemented with 2 mM L-glutamine, 10% fetal bovine serum, 100 μg/ml streptomycin and 100 U/ml penicillin in an atmosphere of 5% CO_2 at 37°C. Sub-cultivation of cell lines was performed for every 48 hours. Experiments were performed in triplicate. Optical density was determined in the absorbance of 440nm. Cell viability % was determined by normalizing absorbance data of samples with absorbance data of negative control. Cell viability was calculated by using the equation:

$$\text{Cell viability \%} = \frac{\text{(Average absorbance value of treated cells)}}{\text{(Average absorbance value of control cells)}} \times 100 \qquad (\text{Eq. 3.3.})$$

3.2.4.2. Subcultivation of Different Cell Lines for Cell Proliferation Assays

MG 63 (Human osteosarcoma), Saos-2 (Human osteosarcoma) and hFob (human osteoblast) cell lines were subcultivated for further *in vitro* cell culture studies. MG 63 cell lines were cultived in MEM Eagle's medium with 10% FBS, 100 μg/ml streptomycin and 100 U/ml penicillin in an atmosphere of 5% CO_2 at 37°C. Saos-2 cell line was cultivated in DMEM with 10% FBS, 100 μg/ml streptomycin and 100 U/ml penicillin in an atmosphere of 5% CO_2 at 37°C. hFob cell line was cultivated in DMEM (with high glucose and without sodium pyruvate) with 10% FBS, 100 U/ml gentamicin in an atmosphere of 5% CO_2 at 33°C.

3.2.4.3. Cell Seeding on Composite Scaffolds

Chitosan/diatomite and chitosan/POSS scaffolds were sterilized with ethanol before cell seeding studies. Scaffolds were incubated with 70% ethanol overnight at room temperature in the laminar flow cabinet. Then ethanol was removed and scaffolds were incubated with PBS (1X) solution at room temperature for 30min by changing PBS thrice. After washing with PBS, scaffolds were conditioned with cell culture medium for 2h at 37°C. Finally, medium was discarded and the scaffolds were air dried in the laminar hood before cell seeding. 50000cell/well were seeded on scaffolds

(1x1cm) with 20μl inoculation volume and incubated 4h without medium to obtain cell attachment on scaffold surface. Scaffolds were incubated at 37°C / 5% CO_2 with 500μl cell culture medium in 48 well plates. Cell culture medium was changed twice a week.

3.2.4.4. *In vitro* Cell Proliferation on Composite Scaffolds

The Resazurin Cell Viability Kit is a fluorescent assay that detects cellular metabolic activity. The blue non fluorescent resazurin reagent is reduced to highly fluorescent resorufin by dehydrogenase enzymes in metabolically active cells. This conversion only occurs in viable cells and thus, the amount of resorufin produced is proportional to the number of viable cells in the sample. The resorufin formed in the assay can be quantified by measuring the relative fluorescence units (RFU) using a fluorosecence plate reader (Varioskan Flash) at 530-570 nm excitation and 590-620 nm emission.

3.2.4.5. Cell Attachment and Spreading on Scaffolds

Cell attachment and spreading on composite scaffolds was determined by SEM analysis and fluorescence microscopy. MG 63 cells were seeded on scaffolds and incubated for 3 and 7 days.

3.2.4.5.1. Fluorescence Imaging

Cells incubated on scaffolds for 7 days were stained with Alexa fluor 488 phalloidin and DAPI fluorescence stains. Culture media was removed and scaffolds were gently washed with PBS solution before staining protocols. Dapi stain was used for detecting nuclei, whereas phalloidin was subjected to cell membrane.

The cells on scaffolds were fixed with 3.7% paraformaldehyde (w/v in PBS) solution for 20 min at room temperature before DAPI-Phalloidine staining. Then washed with 1X PBS solution and permeabilized with 0.1% Triton X-100 for 5min. The samples were rinsed with PBS. Non-specific binding sites were blocked by incubation

of scaffolds at 37°C for 30 min with 1% BSA with PBS solution. Cells were stained with Alexa fluor 488 phalloidine (0.5μg/ml) for 1h at 37°C. The stained cells were examined and visualized by fluorescent microscopy with excitation of 350 nm and emission of 470 nm for DAPI FITC excitation filter at 490 emission filter at 525 for phalloidin.

3.2.4.5.2. SEM Analysis

Cells incubated on scaffolds for 3 days were fixed with 3.7 % PFA solution for 20 min at room temperature and washed with 1X PBS solution. The fixed cells on the surfaces were dehydrated in ethanol graded series (50%, 70%, 80%, 90% and 100%) for 5 min. The dried samples were mounted on stubs and coated with gold in vacuum and examined with a SEM.

3.2.4.6. Alkaline Phosphatase (ALP) Activity Determination

Alkaline phosphatase (ALP) is a membrane-bound tetrameric enzyme attached to glycosyl-phosphatidylinositol moieties which are located on the outer cell surface. Bone is synthesized by the osteoblasts and plays an important role in osteoid formation and mineralisation of bone matrix. Alkaline phosphatase (ALP) is the most widely recognized biochemical marker for osteoblast activity (Sabokbar et al., 1994; Seibel, 2005; Roudsari and Mahjoub, 2012). ALP is among the first functional genes expressed in the process of calcification in bone tissue and therefore ALP has a role in the mineralization process occurring at an early step (Golub and Boesze-Battaglia, 2007).

For ALP activity determination firstly, cells were cultured with osteogenic medium on composite scaffolds. ALP activity of cells were quantified by fluorometric StemTAG ™ALP activity kit at 7, 14, 21 and 28day incubation periods. ALP activity detection is based on hydrolysis of p-nitrophenly phosphate (pNNP) to p-nitrophenol, the conversion of p-nitrophenol is directly related proportional to ALP. Cell culture medium was aspirated and scaffolds were washed with cold PBS solution. Cells were incubated with cell lysis buffer for 20 min at 4°C and centrifuged at 12000g for 20min. Supernatant was used as cell lysate. 50μl cell lysate and 50 μl 1X substrate solution

(pNNP) were incubated at 37°C for 30min. The absorbance of mixture was measured by fluorescence plate reader (Varioskan Flash) at 480nm excitation and 520nm emission. BCA assay was also performed in order to determine the protein concentration of the cell lysate.

3.2.4.7. Alizarin Red and Von Kossa Staining

In histology alizarin red S and von Kossa staining are common techniques for calcium salt determination. Calcium ions precipitate with alizarin, calcium deposits turn into red immediately when immersed in alizarin stain (Puchtler et al., 1969). The von Kossa reaction remains the routine method for demonstrating calcium deposits in tissue. This technique is a two-step reaction based on tissue calcium substitution, bound to phosphates by silver ions and the subsequent visualization of silver cations reacting with calcium deposit components. Silver is reduced to black metallic silver by organic material with the aid of light or by photographic developers (Meloan and Puchtler, 1985; Rungby et al., 1992). Alizarin red staining is commonly used to detect and quantify calcium, while von Kossa staining is used to visualize phosphate within the deposited mineral (Hoemann et al., 2009).

Von kossa staining protocol was used to detect mineral formation by cells incubated on composite scaffolds. Osteogenic medium was removed and scaffolds were washed with 1X PBS solution thrice. Cells were fixed with 3,7 % paraformaldehyde for 20 min at room temperature and washed with 1X PBS solution and distilled water several times. 1% (w/v) aqueous silver nitrate solution was prepared and each scaffold was incubated with 500 μl silver nitrate solution for 30 min under UV light in laminar flow cabinet. After incubation, silver nitrate solution was aspirated, scaffolds were rinsed with distilled water and incubated with 5% (w/v) sodium thiosulfate solution for 5 min at room temperature to remove unreacted silver. After incubation with sodium thiosulfate, scaffolds were again washed with distilled water and observed under stereomicroscope (SOIF DA 0737) for detecting a yellow-brownish stain.

Alizarin red S staining protocol was used to detect calcium deposits by cells on scaffolds. Osteogenic medium was removed and scaffolds were washed with 1X PBS solution twice. Cells were fixed with 3.7 % paraformaldehyde for 20 min at room

temperature and washed with 1X PBS solution and distilled water several times. 2% (w/v) aqueous alizarin red S solution was prepared, pH was adjusted to 4.1 and filtered in order to remove residuals. Scaffolds were stained with alizarin red S solution by incubating at room temperature in the dark for 30min. After incubation, alizarin red S solution was aspirated, then scaffolds were rinsed with distilled water several times and observed under stereomicroscope (SOIF DA 0737) for red stain detection.

CHAPTER 4

RESULTS AND DISCUSSION

4.1. Characterization of Chitosan/Diatomite and Chitosan/POSS Composites

4.1.1. Mechanical Characterization with Compression Test

Mechanical characterization of chitosan/diatomite and chitosan/POSS composite scaffolds were determined by compression test according to the ASTM-D 5024-95a standard. For this study, two experiment groups were designed including dry and wet conditions. Dry samples and hydrated samples were tested with 5 specimens for each group. Compression modulus and strength of composite scaffolds groups with a range of 1-40% diatomite and POSS incorporation were determined in dry condition. In second experiment, composite scaffolds including 5-40 wt% diatomite and POSS content were subjected to compression test in wet condition in order to mimic the *in vitro* condition. Mechanical properties of dry chitosan/diatomite and chitosan/POSS composite scaffolds were presented in Table 4.1. In dry condition, chitosan-diatomite composite scaffolds exhibited lower modulus and compressive strength when compared to pure chitosan scaffolds (Figure 4.1.). Compression test results indicated that, diatomite reinforcement showed no significant effect on compression modulus and compressive strength. At lower concentrations (1-3%) and higher concentrations (20-40%) diatomite frustules having various non-uniform morphology caused to agglomerations and heterogenic distribution on scaffold structure. This heterogenicity occurring on pore surfaces leads to a decrease in mechanical properties. However, increasing diatomite concentration from 1 wt% up to 10 wt % enhanced the modulus of composite scaffolds. Above 10 wt % diatomite, moduli of composite scaffolds decreased with increasing diatomite concentrations. This decrease may arise from larger and brittle pore wall surfaces coated with diatomite particles. Compression modulus and strength of chitosan-diatomite composite scaffolds changed in a range of 17.4-20.6 and

109-128 kPa respectively. Similarly, dry chitosan-POSS composite scaffolds showed lower modulus and compressive strength when compared to chitosan (Figure 4.2.). On the other hand, increasing POSS content had a positive effect on mechanical properties of composite scaffolds up to 20% incorporation. Above this concentration, mechanical properties of composite decreased. This result indicates that, in higher POSS concentrations, POSS nanoparticles tend to bond with one another through their R groups and agglomerate in polymer structure and this may effect the homogenity of composite structure. Compression modulus and strength of chitosan-POSS composite scaffolds changed in a range of 13.5-20 kPa and 74-114.4 kPa, respectively. Besides, mechanical properties of a biomaterial are strongly related with its porosity and pore morphology (Guarino et al., 2007).. Although porosity is an important factor for bone ingrowth, and permeability, higher pore size and porosity impair the mechanical properties by conducing decrease in compressive strength. The decrease in the pore wall thickness and overall density lead to larger and more interconnected pores with a higher void volume which cause lower mechanical strength (Hutmacher et al., 2007; Levengood and Zhang, 2014). Alternatively, the scaffold mechanical properties can also be adjusted by altering the structure of pores within the scaffold. The spherical pores exhibit higher elastic moduli that the one with cylindrical pores (Wu et al., 2014). In a study, PCL scaffolds were obtained with different pore sizes. Increasing pore size from 125μm to 300 μm decreased the modulus from 10.3 MPa to 3 MPa. In addition, the scaffold with a spherical pore exhibited higher elastic moduli that the one with a cylindrical pore (Wu et al., 2014). Similarly, in our study, in dry condition, increasing diatomite concentrations had a negative effect on mechanical properties of composite scaffolds due to having large pores and high porosity. The difference between chitosan control group and 1,3,10,20 and 40 wt % diatomite and POSS incorporated chitosan groups was found statistically significant at $p<0.0001$ level.

Figure 4.1. Compression modulus of dry chitosan/diatomite composite scaffolds

Figure 4.2. Compression modulus of dry chitosan/POSS composite scaffolds

Table 4.1. Mechanical properties of dry chitosan/diatomite and chitosan/POSS composite scaffolds. Data was reported as mean ±SE of five samples.

Scaffold Groups	Compression Modulus (kPa)	Compressive Strength (kPa)
Chitosan	36.0 ± 0.55	128.8 ± 1.47
Chitosan-1% POSS	13.5 ± 0.67	114.4 ± 1.72
Chitosan-3% POSS	12.6 ± 1.15	108.0 ± 5.12
Chitosan-5% POSS	17.3 ± 0.22	97.1 ± 0.22
Chitosan-10% POSS	17.0 ± 1.26	80.4 ± 1.58
Chitosan-20% POSS	20.0 ± 2.8	90.0 ± 3.88
Chitosan-40% POSS	12.5 ± 0.31	74.0 ± 2.58
Chitosan-1% Diatomite	17.4 ± 1.88	109.0 ± 3.02
Chitosan-3% Diatomite	26.3 ± 1.37	107.0 ± 2.48
Chitosan-5% Diatomite	30.8 ± 1.77	103.2 ± 1.22
Chitosan-10% Diatomite	28.2 ± 1.19	127.8 ± 2.76
Chitosan-20% Diatomite	25.6 ± 0.8	121.0 ± 3.55
Chitosan-40% Diatomite	20.6 ± 1.37	128.0 ± 2.81

In second experiment group, scaffolds were conditioned in PBS (pH 7.4) solution for 1h at room temperature before compression test. Wet scaffolds exhibited a flexible structure during compression. Scaffolds regained their initial shape and size after compression.

In contrary to dry condition results, wet chitosan-diatomite composite scaffold exhibited higher compression moduli in the range of 67.3-81.4 kPa when compared to pure chitosan scaffold (56.3 kPa) (Figure 4.3.) . Similarly, chitosan-POSS composite scaffolds showed higher modulus values compared to pure chitosan. Increasing POSS content from 5 to 40 % showed a positive effect on compression modulus changing from 78.1 to 107.6 kPa (Figure 4.4.). Mechanical properties of wet chitosan/diatomite and chitosan/POSS composite scaffolds are depicted in Table 4.2. Statistically, no significant difference was obtained between wet chitosan and chitosan-diatomite composite groups. However, wet chitosan-POSS composite groups (20% and 40%) showed significant difference compared to control chitosan at $p < 0.05$.

Wang and co workers investigated the mechanical properties of silica-chitosan hybrid porous scaffolds and indicated that high porosity caused low compressive strengths in

the freeze cast hybrid scaffolds in the range of 150–250 kPa along the freezing direction (Wang et al., 2015). In another study, Wang et al studied effect of silica concentration on mechanical properties of chitosan/silica composite scaffolds. Increasing the inorganic 3-Glycidoxypropyl trimethoxysilane (GPTMS: 4060 GC1) quantities resulted in the elastic-brittle deformation behaviour. Increasing the amount of inorganic from 40% to 60% increased the yield strength from 66 kPa to 94 kPa (Wang et al., 2016).
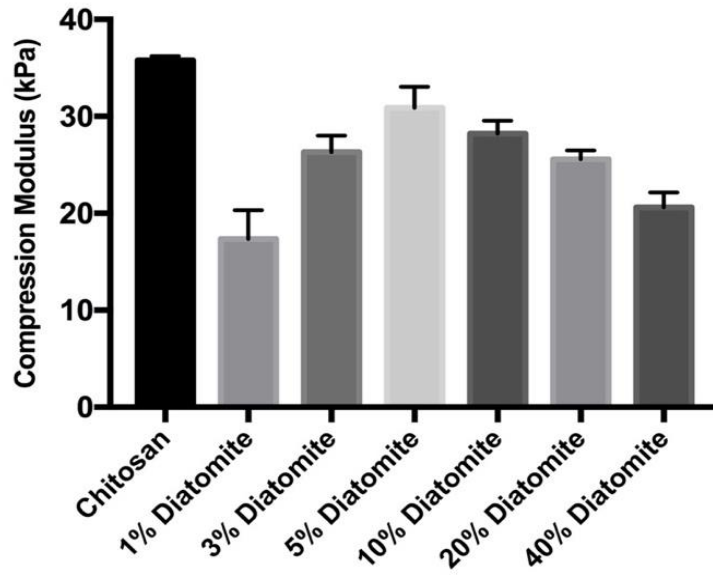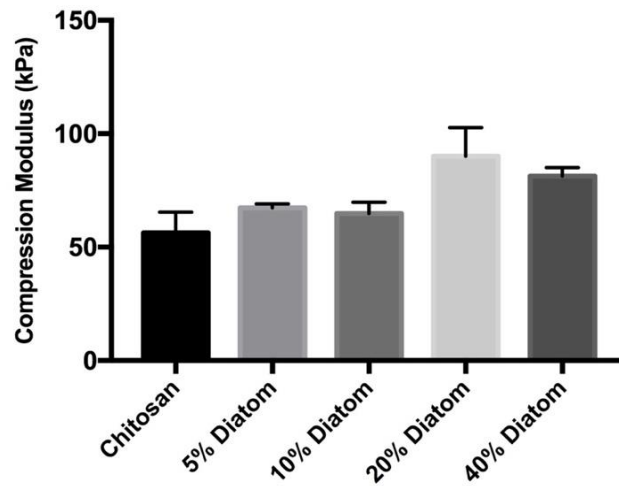

Figure 4.3. Compression modulus of wet chitosan/diatomite composite scaffolds
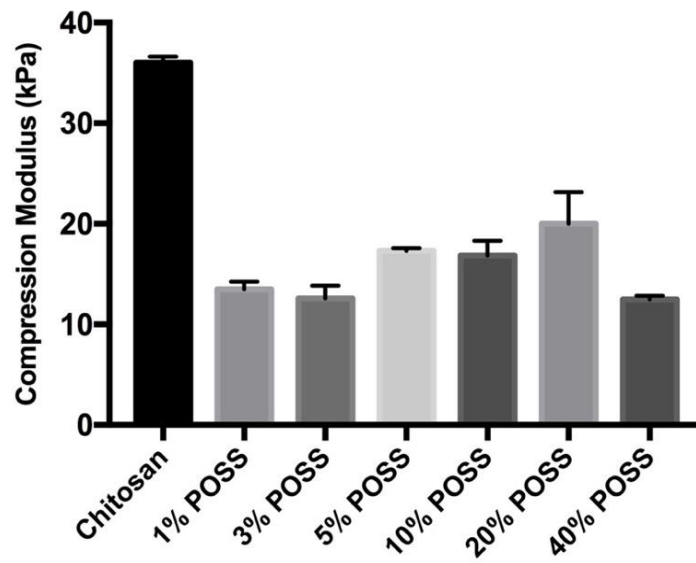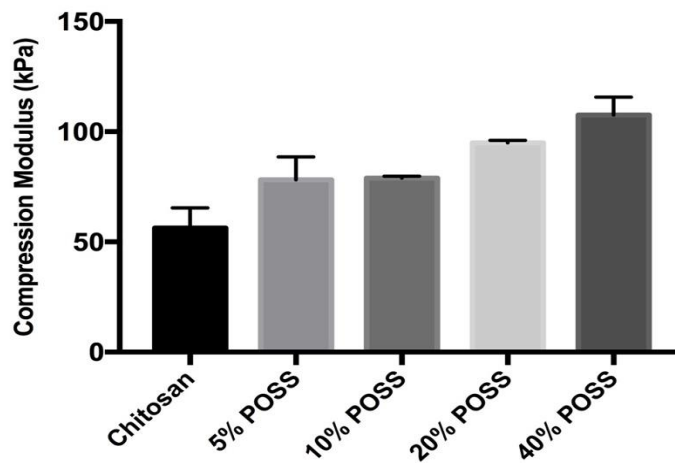

Figure 4.4. Compression modulus of wet chitosan/POSS composite scaffolds

Table 4.2. Mechanical properties of wet chitosan/diatomite and chitosan/POSS composite scaffolds. Data is reported as mean ±SE of five samples.

Scaffold Groups	Compression Modulus (kPa)	Compressive Strength (kPa)
Chitosan	56.3 ± 7.42	72 ± 4.03
Chitosan-5% POSS	78.1 ± 8.5	67.4 ± 2.37
Chitosan-10% POSS	79 ± 0.68	56 ± 3.30
Chitosan-20% POSS	95 ± 0.93	55.7 ± 0.72
Chitosan-40% POSS	107.6 ± 6.57	58 ± 0.82
Chitosan-5% Diatomite	67.3 ±1.41	62 ± 5.10
Chitosan-10% Diatomite	65 ± 4.10	59 ±0.94
Chitosan-20% Diatomite	90.1 ± 10.25	64.3 ± 2.68
Chitosan-40% Diatomite	81.4 ± 3.01	61.7 ± 2.23

4.1.2. Surface Wettability

Surface wettability of chitosan/diatomite and chitosan/POSS composite membranes were determined by static air-water contact angle analysis. The contact angle has been considered to be one of the physical parameters which determine the affinity between cells and the biomaterial surface. The hydrophilicity and hydrophobicity of the scaffold surface regulate protein adsorption, which is an initial factor for cell adhesion and proliferation. Generally, hydrophilic surface is considered to be appropriate for cell proliferation (Costa-Pinto et al., 2011). Studies on the interaction between cells and monolayers indicated that protein adhesion which initiated the cell-surface interaction, was limited on highly hydrophobic and hydrophilic surfaces. Extracellular matrix protein adsorption was better on highly hydrophilic surface. However, cell-cell interaction decreased and this prevented monolayer formation due to the stronger substrate-cell interaction. Results showed that moderately wettable surfaces induced cell adhesion and proliferation (Faucheux et al., 2004; Tzoneva et al., 2007).

Consequently, balanced moderately wettable surface provides strong cell-substrate and subsequent strong cell-cell interactions which lead to required monolayer formation for tissue regeneration (Menzies and Jones, 2010).

Static air-water contact angle data of the prepared composite membranes were measured and tabulated in Tables 4.3 and 4.4. Incorporation of diatomite and POSS particles into chitosan matrix didn't not conduce a significant change on the surface hydrophilicity of membranes. In contact angle measurement, when the water dropped on composite membrane, swelling occurred on the surface due to the hydrophilic properties of chitosan. This slightly effected the measured contact angle on surface. The measured contact angle value for chitosan (77.9$^{°}$) was found be good agreement with the study of Hamilton et. al (2006). They evaluated the contact angle of chitosan materials with different degree of acetylation in a range of 62.1-85.6° (Hamilton et al., 2006). All the membranes prepared in this study showed moderately hydrophilic surface properties with contact angle data below 90°. Thus, surface of the membranes was considered to be suitable for protein and cell adhesion.

Table 4.3. Static air-water contact angle of chitosan and chitosan/POSS composite membranes. The water contact angle data is reported as the mean ±SD for five measurements.

Composite Groups	Contact Angle (º)
Chitosan	77.9 º ± 5.6
Chitosan-1% POSS	77.1 º ± 0.79
Chitosan-3% POSS	77.6 º ± 1.82
Chitosan-5% POSS	77.8 º ± 2.24
Chitosan-10% POSS	80.2 º ± 1.40

Table 4.4. Static air-water contact angle of chitosan and chitosan/Diatomite composite membranes. The water contact angle data is reported as mean ±SD for five measurements.

Composite Groups	Contact Angle (º)
Chitosan	77.9 º ± 5.6
Chitosan-1% Diatomite	73.7 º ± 1.72
Chitosan-3% Diatomite	73.5 º ± 1.71
Chitosan-5% Diatomite	77.0 º ± 2.5
Chitosan-10% Diatomite	79.1 º ± 0.63

4.1.3. Surface Topography and Roughness

Surface characteristics are critical factors that regulate cell function on biomaterial surface. When cells adhesion and growth on a surface is correlated with integration of physicochemical signals such as surface topography, chemistry and wettability. These signals effect the regulatation of cell behavior (Zheng et al., 2008). Nanocomposites represent promising osteomimetic architecture with inherent properties such as increased wettability, roughness, and surface area when compared to microscale biomaterials. The nanometer grain size and high surface fraction of nanophase ceramics (i.e. nanoHAp) and other nanofillers increase osteoblast functions (such as adhesion, proliferation, and differentiation) (Zhang and Webster, 2008; Gong et al., 2015).

Surface topography and roughness of composite membranes were determined by atomic force microscopy analysis (AFM). Chitosan-diatomite composite membranes were analyzed in contact mode due to the microstructure of diatom particles, however, tapping mode was used for chitosan-POSS composites. Atomic force micrographs of chitosan-diatomite composites were scanned with 100µ-100µ scale in order to observe diatom frustules on surface and obtain significant roughness results. Chitosan-POSS composites were scanned with 5µ-5µ scale in order to observe dispersion of POSS particles on chitosan surface. For each group, three samples were subjected to roughness determination.

Figure 4.5 presents the topographic and phase AFM images of pure chitosan membrane with 5μ-5μ scan size. Pure chitosan membranes exhibited essentially smooth surface, showing few topographic features with a roughness of 3.58 nm. In a study surface topography of chitosan and chitosan/ poly-L-lysine films were investigated and similar roughness results were obtained for pure chitosan films as 4.6 nm (Zheng et al., 2008).
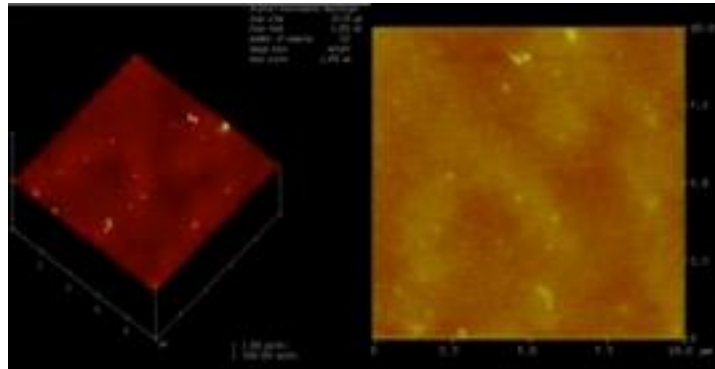
Figure 4.5. AFM images of pure chitosan membrane. Topography (left) and phase (right), the scan size: (5 × 5μm).

It was found that surface roughness of the composites depends on the silica type and its concentration. For chitosan- POSS composites, incorporation of POSS increased the surface roughness which is an outstanding phenomenon for cell adhesion and proliferation in tissue regeneration (Fig 4.6). Surface roughness increased from 3.58 to 9.54 nm with increasing POSS concentration on chitosan membranes (Table 4.5). The surface topography images showed that at low POSS loadings, few small protruding regions were observed, however, at high POSS loadings (5 -10% wt), more concentrated protruding regions were obtained inducing higher roughness on the surface. AFM phase images indicated that POSS nanoparticles tend to agglomerate on surface with increasing concentrations (Figure 4.6 and Figure 4.7).

The POSS incorporation in polymer matrix induces micro- and nanometer-scale topography on the polymer surface enhances cell attachment and proliferation. In a study, AFM analysis of POSS-PCU thermoplastic elastomer composite showed enhanced micro- and nanotopography due to the agglomeration of POSS nanocages on the surface (Ghanbari et al., 2011). Cai et al. investigated the surface morphology and roughness of Poly (propylene fumarate) (PPF)-*co*-(POSS) copolymers with AFM

analysis. Root-mean-square (rms) roughness data of PPF-POSS copolymers were measured between 6.3 ± 1.6 and 7.8 ± 0.8 nm (Cai et al., 2012).
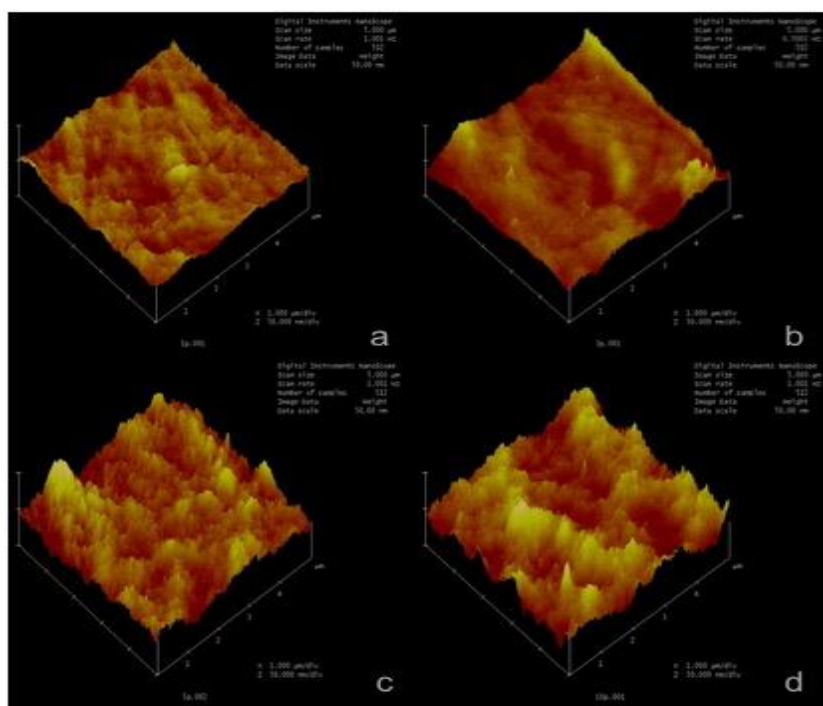
Figure 4.6. Atomic force microscopy (AFM) image of Chitosan-POSS showing surface topography of composite membranes: 1% POSS (a), 3%POSS (b), 5% POSS(c) and 10 % POSS (d) content respectively. Surface roughness is induced by agglomeration of POSS nanocages on the surface.

Table 4.5. Surface roughness of pure chitosan and chitosan/POSS composite membranes. The data was presented as the mean ±SE for three measurements.

Composite Groups	Mean Surface Roughness (Rq) (nm)
Chitosan	3.58 ± 0.06
Chitosan-1 % POSS	3.85 ± 0.37
Chitosan-3 % POSS	6.17 ± 0.80
Chitosan-5 % POSS	6.50 ± 0.18
Chitosan-10 % POSS	9.54 ± 0.60
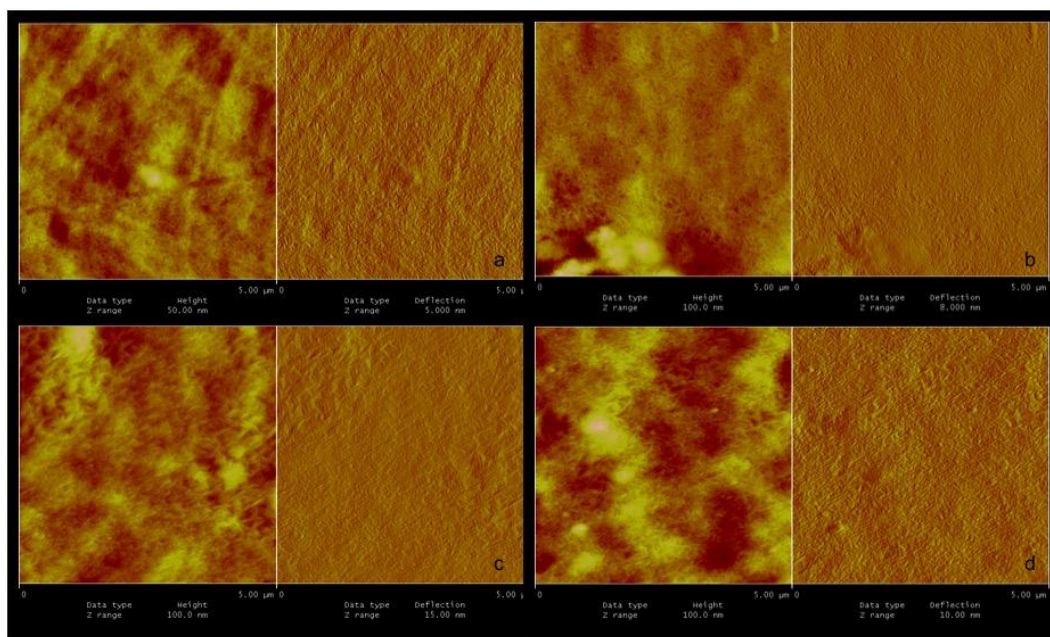
Figure 4.7. AFM phase images of chitosan/POSS composite membranes: 1%POSS (a),3% POSS (b), 5% POSS (c) and 10% wt POSS (d) with (5× 5μm) scan size.

AFM topography images of chitosan/diatomite composite membranes were presented in Figure 4.8. Chitosan-diatomite composite membranes exhibited much higher roughness on the surface due to the porous microstructure of diatomite frustules (Table 4.6.). AFM images indicated that surface topography and roughness were induced by agglomeration of diatomite frustules on the surface.

Table 4.6. Surface roughness of pure chitosan and chitosan/Diatomite composite membranes. The data was represented as the mean ±SE for three measurements.

Composite Groups	Mean Surface Roughness(Rq) (nm)
Chitosan	3.58 ± 0.06
Chitosan-1 % Diatomite	115.00 ± 4.53
Chitosan-3 % Diatomite	265.00 ± 2.66
Chitosan-5 % Diatomite	229.30 ± 6.63
Chitosan-10 %Diatomite	249.8 ± 3.94
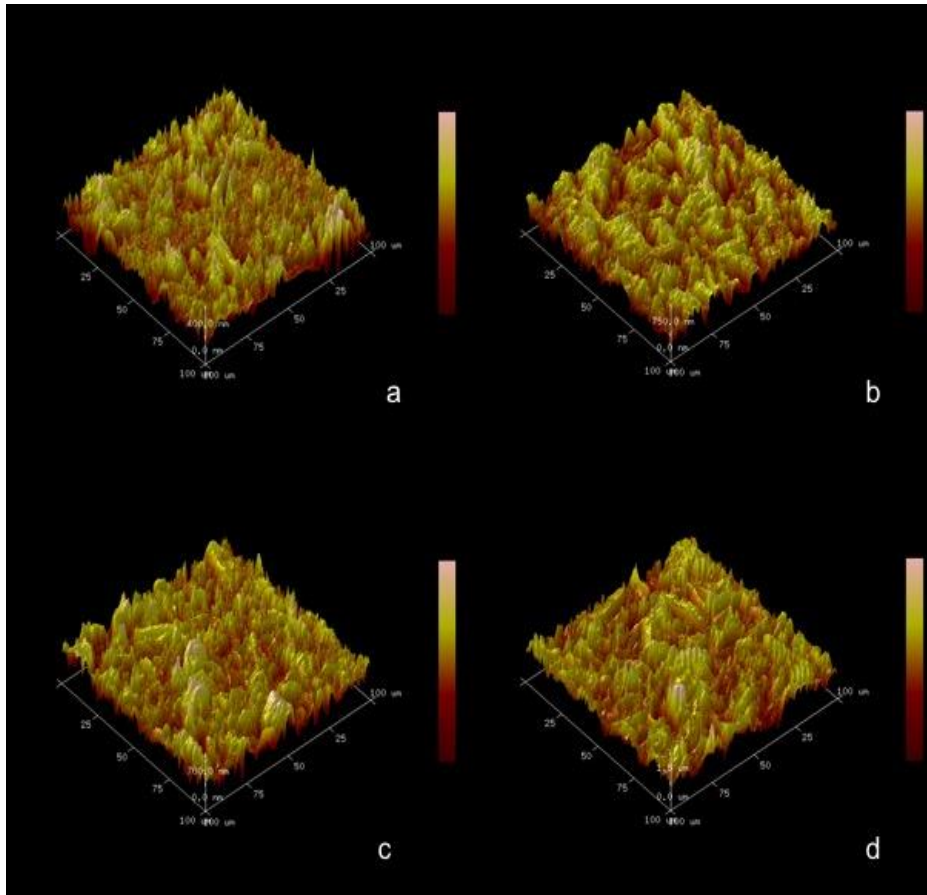
Figure 4.8. Atomic force microscopy (AFM) image of chitosan/diatomite composite membranes. Surface topography 1% diatomite (a), 3% diatomite (b), 5% diatomite (c) and 10 % wt diatomite (d) content, respectively.

AFM phase images of chitosan/diatomite composite membranes (Figure 4.9.) showed that diatomite frustules with various morphology distributed on polymer surface inducing roughness. Besides, uniform distributions were observed on surface with increasing diatomite content (5-10%).
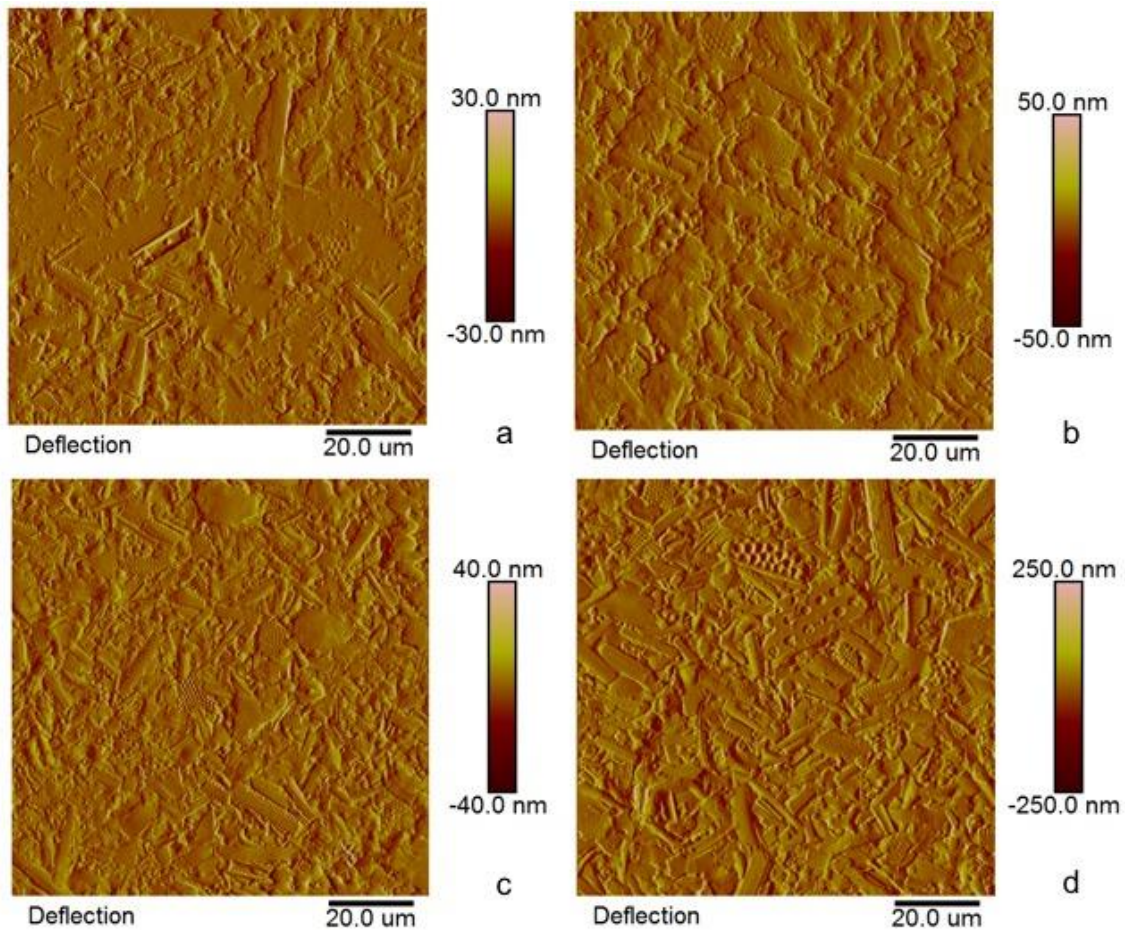
Figure 4.9. AFM phase images of chitosan/diatomite composite membranes with deflection mode: 1% diatomite (a), 3% diatomite (b), 5% diatomite (c) and 10% wt diatomite (d).

AFM analysis of cell skeleton of diatom in the literature showed that outer layer of the skeleton showed a granular nanostructure composed of 100-200 nm spherically shaped fused silica particles and a surface topography with holes with a 200-300nm size range (Noll et al., 2002). Similarly, diatom frustules distributed on composites showed a pore size range of 0.3μm to 5μm in their structure.

A comparison of AFM images of two different composite scaffolds; chitosan-diatomite and chitosan-POSS; prepared in this work presented different surface topographies. (Figure 4.10.). Diatomite frustules with diverse porous structures showed higher roughness on chitosan surface, while POSS nanoparticle distributions on the surface showed a uniform structure on surface with lower roughnesss.
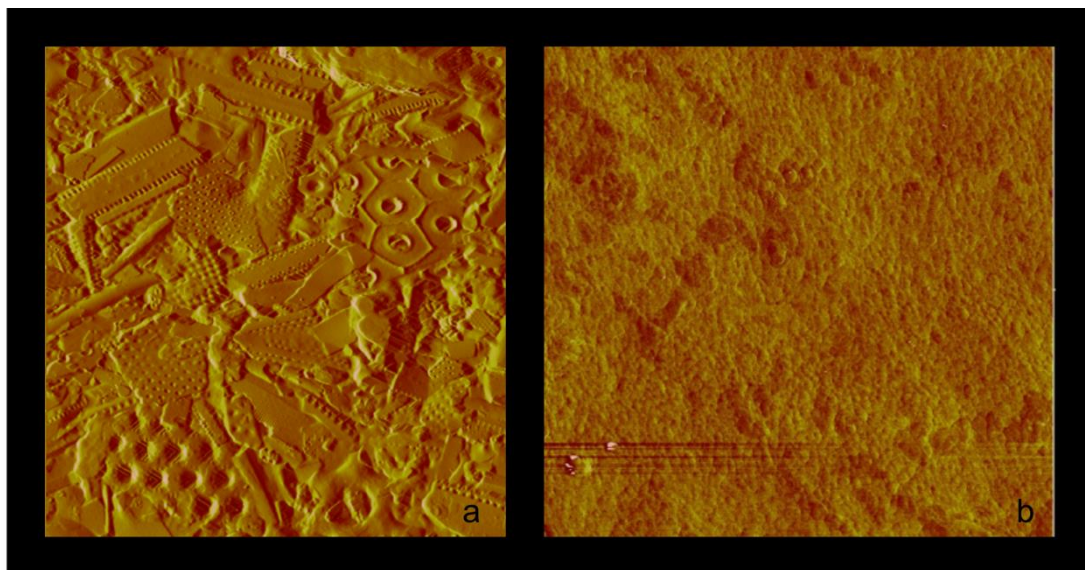
Figure 4.10. Surface topography of chitosan-10% Diatomite (a) and chitosan-10% POSS (b) composite membranes with ($10 \times 10\mu m$) and ($5 \times 5\mu m$) scan size respectively.

4.1.4. Morphology and Structure of Composite Scaffolds

Surface structure, morphology and size distribution of lateral pores of composite scaffolds were determined by scanning electron microscopy (SEM) analysis. Lateral pore sizes were calculated by using Image J software. Chitosan/diatomite and chitosan/POSS composite scaffolds were analysed in order to observe surface structure, pore size and distribution of diatomite and POSS particles in chitosan matrix. The diverse morphology of porous diatomite frustules was depicted in Figure 4.11.
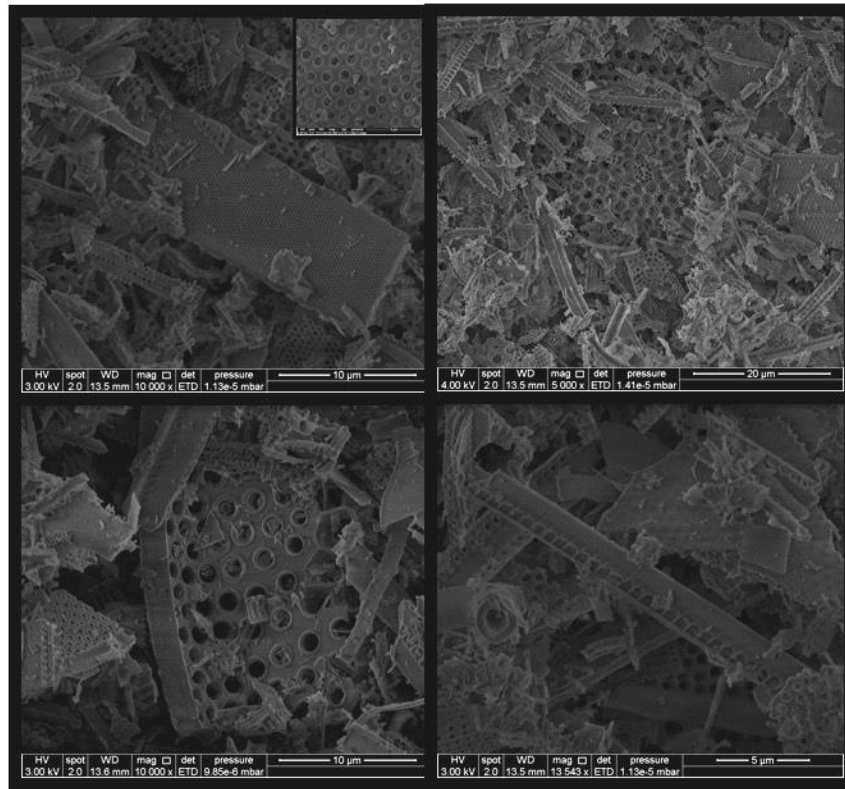
Figure 4.11. Scanning electron micrographs of diatom frustules with different morphologies

SEM images of pure chitosan scaffolds showed that highly porous microstructure was obtained with freeze-drying method. Chitosan scaffolds exhibited uniform interconnected open pores with an average pore size of 213 ± 44 µm (Figure 4.12).
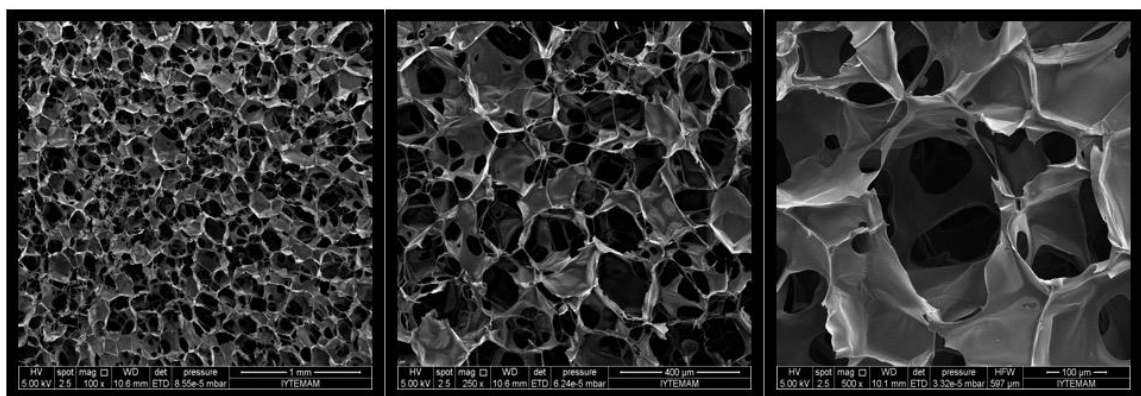
Figure 4.12. Scanning electron micrographs of chitosan scaffold with 100x, 250x and 1000x magnification.

Pore size is an important factor in the progression of osteogenesis due to the fact that it induces vascularization in bone tissue growth. Generally, cancellous bone has a porous structure in a range of 30–90%. Macro pores (pore size >100µm) of scaffold provide favorable vascularization and results in osteogenesis. *In vitro* studies showed that, lower porosity stimulated osteogenesis by enhancing cell proliferation and inducing cell aggregation. On the other hand, higher porosity and pore size result in better bone ingrowth *in vivo*. The minimum requirement for pore size was considered to be approximately 100 µm regarding cell size, migration requirement and transport. Recently, *in vitro* and *in vivo* studies indicated that pore size and interconnection larger than 300 µm are suitable for sufficient vascularization of graft (Hutmacher et al., 2007; Bose et al., 2012). Porosity of scaffold depends on macro- and micropores. Microporosity provides larger surface area inducing protein adsorption and ion exchange for apatite formation. On the other hand, macroporosity (poresize<50 µm) effect the osteogenesis (Karageorgiou and Kaplan 2005). In literature, the optimum pore size of a scaffold is defined as in the range of 75–250 µm for bone tissue formation (Cheung et al., 2007).

Average pore sizes were determined by using cross-section image of scaffolds. SEM images of chitosan-POSS composite scaffolds indicated that POSS incorporation in polymer matrix did not alter the microstructure and overall porosity of chitosan scaffold. (Figure 4.13.). Lateral pore size distributions of chitosan and chitosan/POSS composite scaffolds are depicted in Table 4.7. Chitosan scaffolds exhibited an average pore size of 213 µm. Uniform porous structure with a pore size range 150-190 µm was obtained for chitosan-POSS composites. However, at high POSS concentrations (20-40%) morphology changed and pore wall surfaces enlarged (Figure 4.14).
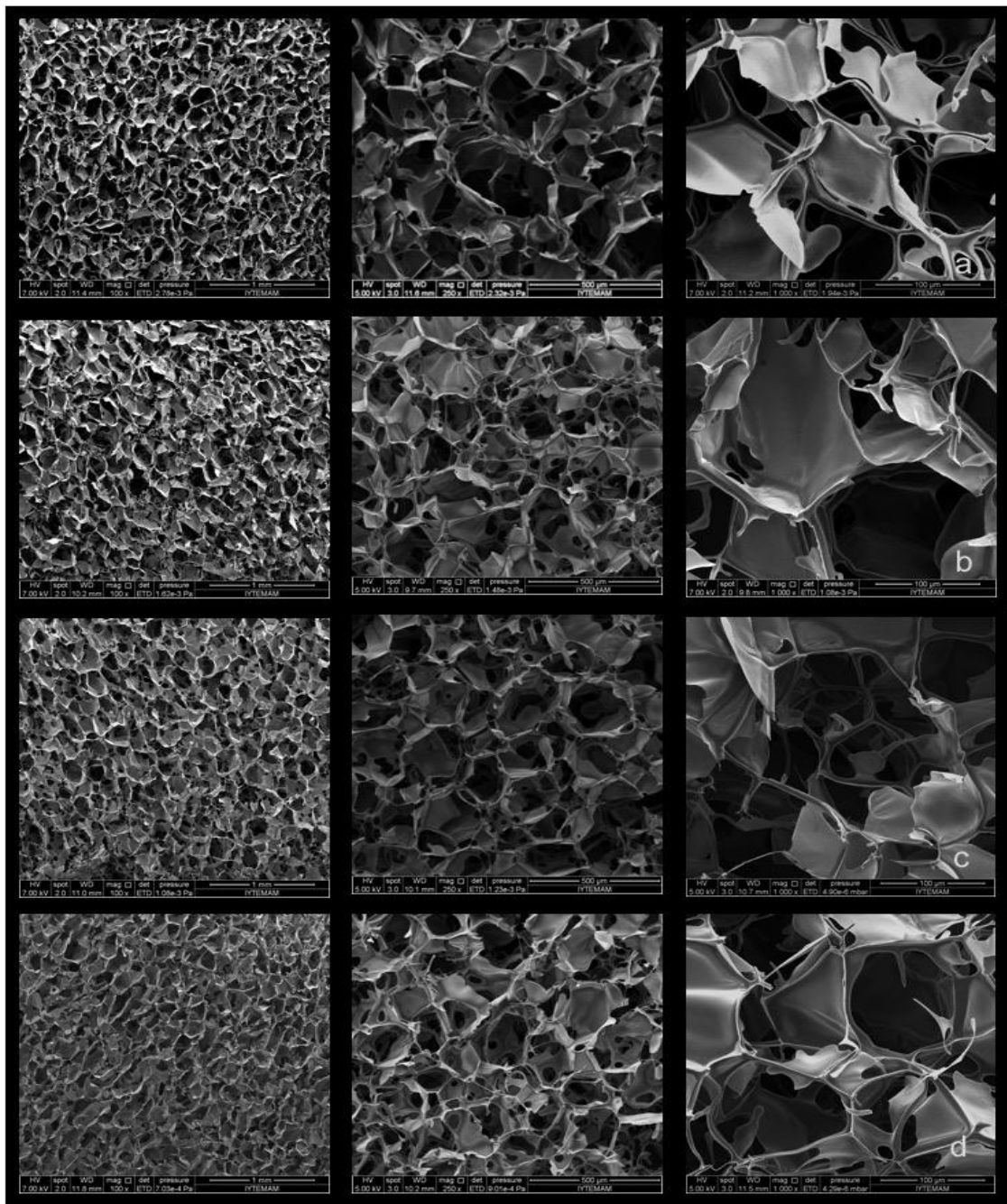
Figure 4.13. Scanning electron micrographs of chitosan/POSS scaffolds with 100x, 250x and 1000x magnifications: 1%POSS (a); 3% POSS (b); 5% POSS (c);10% POSS (d)
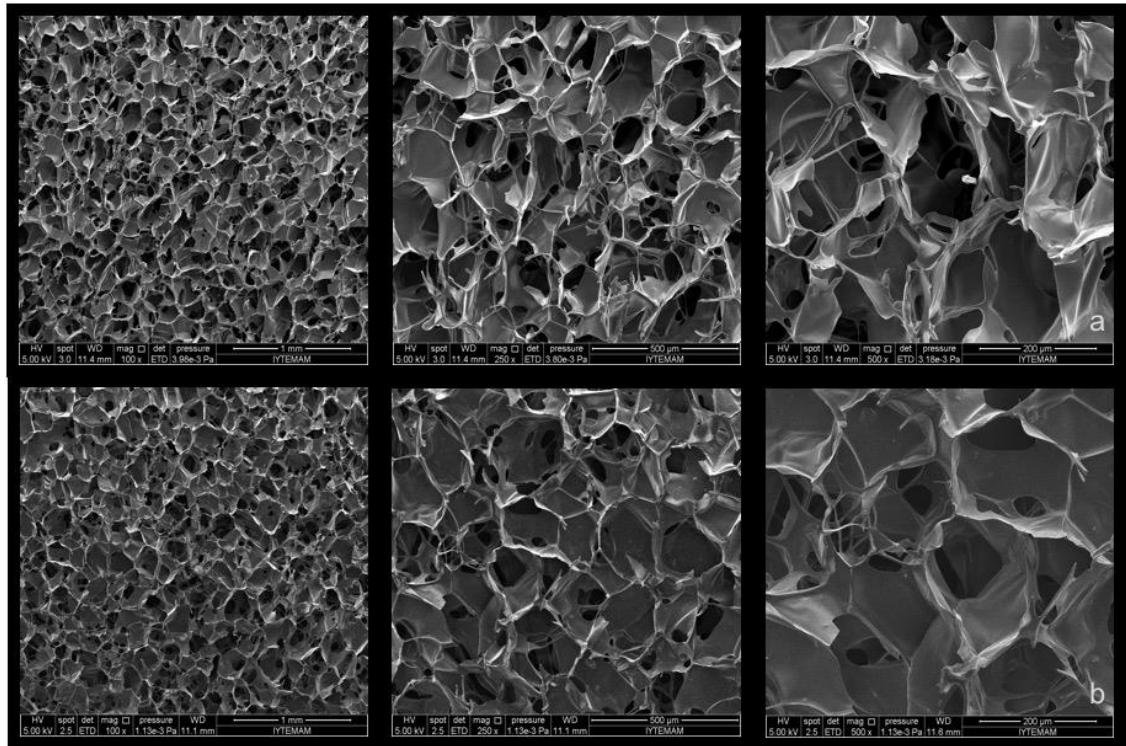
Figure 4.14. Scanning electron micrographs of chitosan/POSS scaffolds with 100x, 250x and 1000x magnifications: 20%POSS (a); 40% POSS (b)

Table 4.7. Lateral pore size distribution of chitosan and chitosan/POSS composite scaffolds

Scaffold Groups	Average Pore Size (µm)
Chitosan	213 ± 44
Chitosan- 1 % POSS	150 ± 28
Chitosan- 3 % POSS	157 ± 18.6
Chitosan- 5 % POSS	180 ± 28.2
Chitosan- 10 % POSS	190 ± 31.2
Chitosan- 20 % POSS	191 ± 36.7
Chitosan- 40 % POSS	180 ± 46.5

SEM images of chitosan-diatomite composite scaffolds also showed uniform highly porous structures as obtained in chitosan/POSS composite scaffolds (Figure 4.13., Figure 4.14.). When compared with pure chitosan scaffold, surface area of pore walls increased and pore morphology of composite scaffolds changed with increasing diatomite content. Average pore size range was obtained between 219-297 μm. An increase in diatomite content increased the pore size when compared to pure chitosan scaffolds. However, pore size increased up to 10 wt % diatomite contents. Above this concentration, pore size of the composite scaffold slightly decreased. In addition, above this concentration, surface morphology of the pores changed with increasing diatom content significantly. 20 wt % and 40 wt % diatomite contents showed uniform distributions of diatom frustules on surface which lead to favorable surface topography for cell adhesion and proliferation (Figure 4.15.). Lateral pore size distributions of chitosan and chitosan/diatomite composite scaffolds are depicted in Table 4.8. It was found that pore size and morphology is affected by diatomite particles concentration and its dispersion level in polymer matrix. Diatom frustules with different microstructural properties on scaffold surface is presented in Figures 4.17 & 4.18 with low and high magnifications. Diatom frustules showed a pore size range of 0.3μm to 5μm in their structure.

In literature, chitosan-silica porous membranes were fabricated by incorporation of synthetic silica particles; TEOS and GPTMS.The morphology studies revealed that the silica phase appeared as a continuous phase covering the walls of the chitosan pores without affecting significantly the porosity of the scaffolds (Pandis et al., 2014). SEM images of chitosan-diatomite and chitosan-POSS composites showed that silica incorporation did not effect porosity and pore structure significantly in a similar manner.
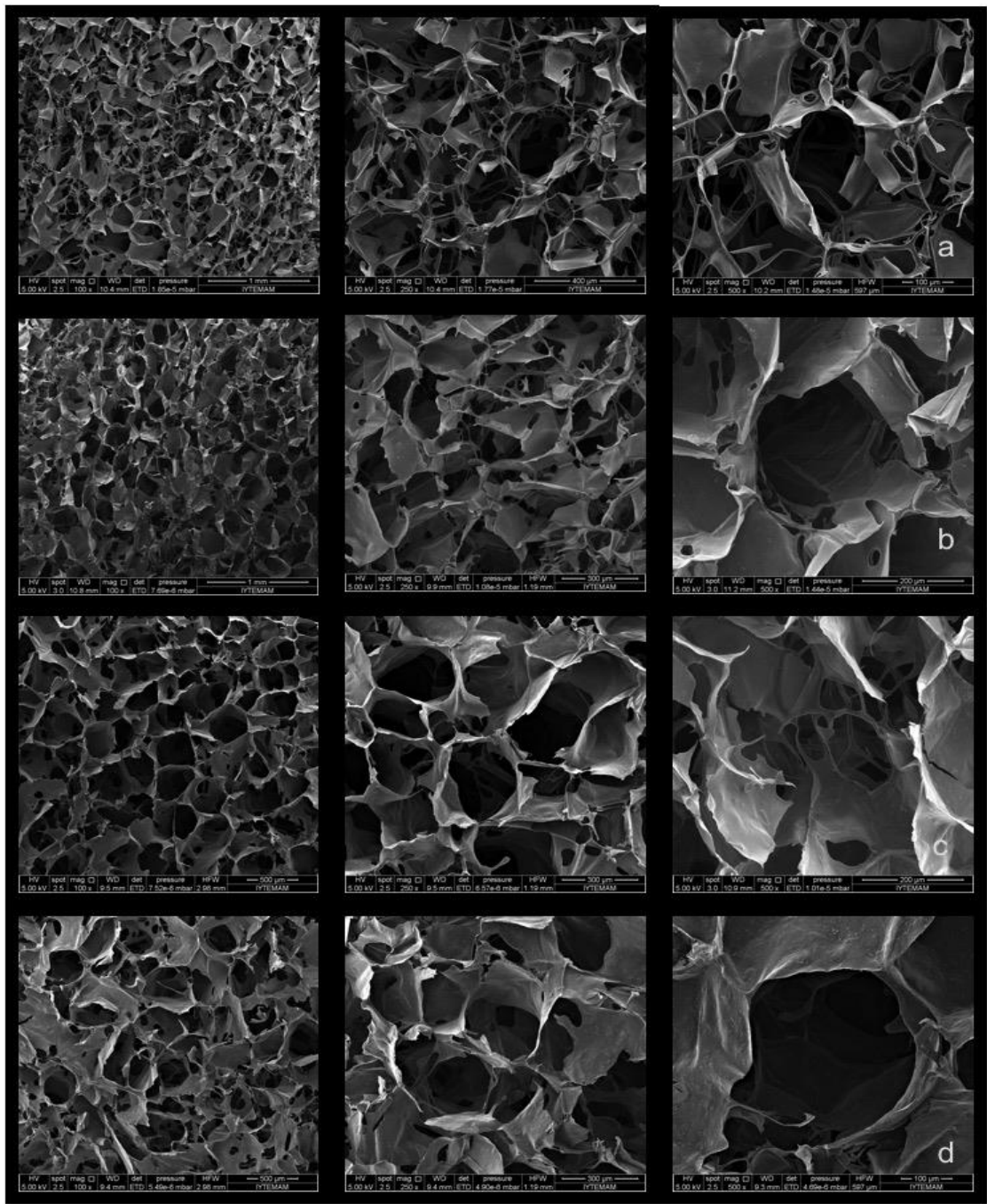
Figure 4.15. Scanning electron micrographs of chitosan/diatomite scaffolds with 100x 250x and 500x magnifications: 1%diatomite (a); 3% diatomite (b); 5% diatomite (c); 10% diatomite (d)
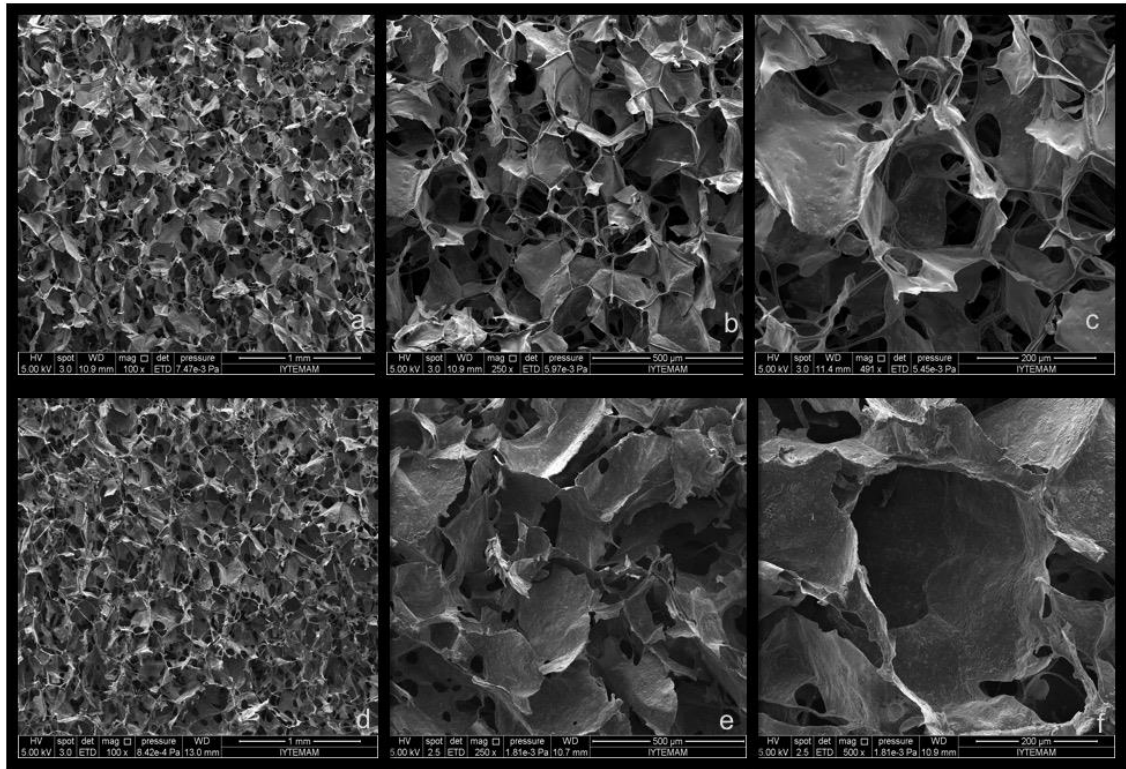
Figure 4.16. Scanning electron micrographs of chitosan/diatomite scaffolds with 100x, 250x and 500x magnifications: 20% Diatomite (a); 40% Diatomite (b)

Table 4.8. Lateral pore size distribution of chitosan and chitosan/Diatomite composite scaffolds.

Scaffold Groups	Average Pore Size (µm)
Chitosan	213 ± 44
Chitosan- 1 % Diatomite	297 ± 102.4
Chitosan- 3 % Diatomite	218 ± 44.8
Chitosan- 5 % Diatomite	260 ± 65
Chitosan- 10 % Diatomite	319 ± 76
Chitosan- 20 % Diatomite	287 ± 49.4
Chitosan- 40 % Diatomite	219 ± 56.3
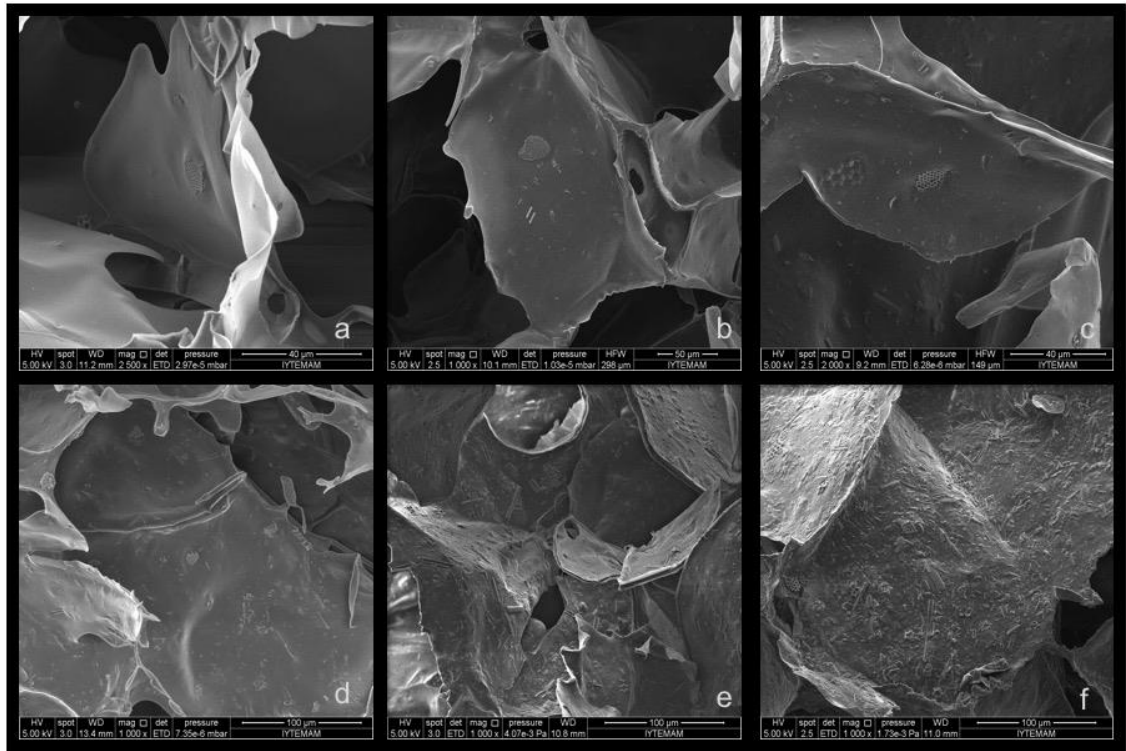
Figure 4.17. Distribution of diatom frustules on scaffold surface: 1%diatomite
(a); 3% diatomite (b); 5% diatomite (c); 10% diatomite (d); 20%
diatomite (e);40% diatomite(f) with 1000x and 2500x magnifications.
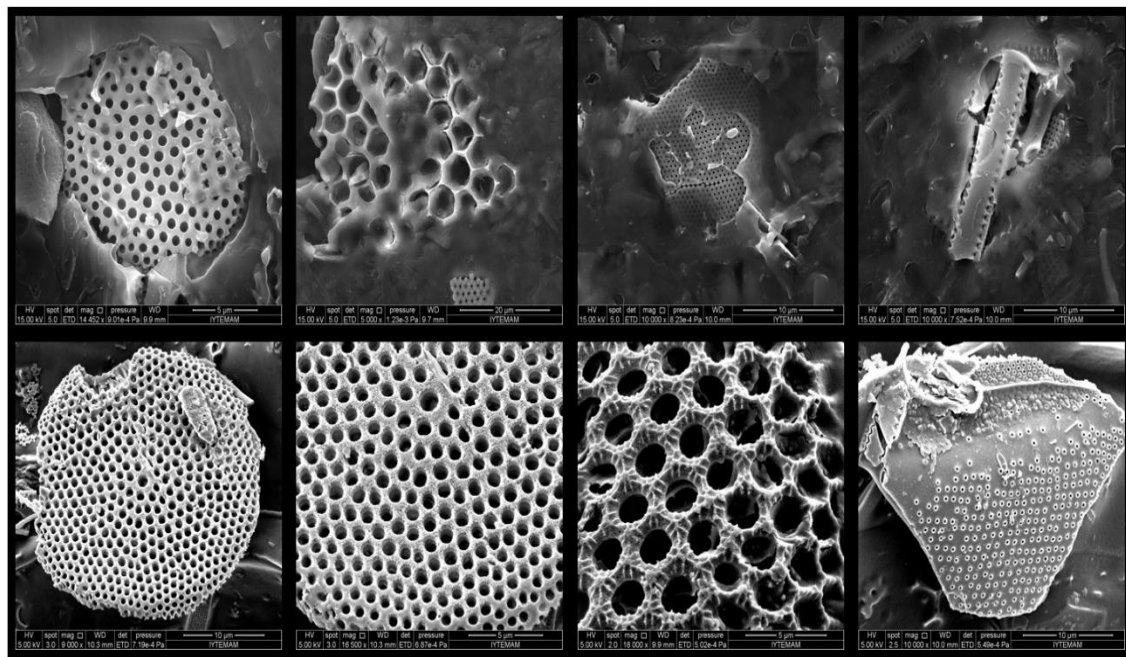
Figure 4.18. Diatom frustules on scaffold surface (5000x,10000x,15000x)

4.1.5. Porosity Determination

In this study scaffold porosity was determined by using two different methods; mercury porosimeter and micro CT analysis.

4.1.5.1. Mercury Porosimeter

Mercury porosimetry is a characterization technique investigating only open pores between 500 μm and 3.5 nm in a size range (Giesche, 2006). In this technique porosimeter applies pressure on material in order to provide penetration of mercury inside the material. Therefore, sample may collapse and compressed during the analysis. This causes error in measurements. For this reason, mercury porosimetry technique may not be not suitable for flexible scaffolds with porosity higher than 90%. Mercury porosimetry has a limitation of measuring the largest entrance towards a pore. Therefore, this measurement does not represent the actual inner size of pore which may be larger than the entrance diameter (Ho and Hutmacher, 2006).

Adjusting the pore size is a crucial factor in scaffold design. Larger pores may be able to enhance the mass transport and neo-vascularization within the implants, whereas smaller pores are preferred to provide larger surface per volume ratio. Furthermore, pore shape is also a key factor to affect the tissue regeneration efficiency.

Cooney et al. demonstrated that in an aqueous chitosan system the formation of oval pores is more likely to occur at the higher temperature (0 to -50°C) and if the temperature gradient is high, the oval ice crystals can evolve into lamellar structures (Cooney et al., 2008). In this study, chitosan-silica composite scaffolds were prefreezed at -20 ℃ and freze dried at -45℃. Therefore, oval pore structures were obtained.

Some specific pore sizes can enhances the cellular activity, but optimal size and geometry are highly dependent on specific cell types grown on injured sites. For bone in-growth, the optimal pore size is in the range of 75–250 μm (Cheung et al., 2007).

In this study, open pore size range and porosity were determined by mercury porosimeter. Scaffolds were analysed under low pressure in order to prevent compression and possible disruption. Micro/macro pore sizes and porosity % of scaffolds were depicted in Table 4.9. Both chitosan-POSS and chitosan-diatomite

composite scaffolds showed a morphology including micropores and macropores. All composite scaffold groups showed high porosity % in a range of 83-91%. As seen in Table 4.9, micropores size ranges were found to be similar between groups obtained in the range of 10 to 97 μm. However, macropores size ranges differed within groups. Increasing both diatomite and POSS concentrations decreased the size of macropores in the structure.

Table 4.9. Pore size range and porosity % of composite scaffolds determined by mercury porosimete

Groups	Micro-Pore Range (μm)	Macro-Pore Range (μm)	Porosity (%)
Chitosan	10-70	110-390	89.25
Chitosan-5% Diatomite	13-71	105-267	86.70
Chitosan-20% Diatomite	10-98	124-278	90.80
Chitosan-40% Diatomite	10-85	108-225	86.81
Chitosan-5% POSS	10-93	129-346	87.95
Chitosan-20% POSS	10-86	118-321	88.82
Chitosan-40% POSS	10-97	100-106	82.58

4.1.5.2. Micro CT Analysis

Recently several studies used Micro CT analysis to determine the porosity and three dimensional structure of scaffolds (Peyrin, 2011). Scaffolds with intricate interior structures can be analyzed using micro CT. Different spatial locations of the scaffold architecture exhibiting different geometric layouts can be digitally isolated out (Ho and Hutmacher, 2006).

In this study, micro CT analysis was also perfomed to determine the 3D morphology and porosity % of composite scaffolds. Porosity data of composite scaffolds is tabulated in Table 4.10. Chitosan-POSS scaffolds showed similar porosity in a range of 82.6-86.8 % compared to pure chitosan scaffold with 87.5% porosity. Scaffolds with high POSS concentration (20wt %) had lower porosity of 82.6%. On the

other hand, for diatomite containing scaffolds, an increase in diatomite concentration increased the porosity of scaffold from 86.7 to 90.7%. Results indicate that all chitosan-POSS and chitosan-diatomite scaffolds can mimic the structure of cancellous bone and provide required porosity % for bone cell growth.

Table 4.10. Porosity% of composite scaffolds determined by micro-CT analysis

Groups	Porosity (%)
Chitosan	87.50
Chitosan-5%Diatomite	86.71
Chitosan-20% Diatomite	90.76
Chitosan-5% POSS	86.78
Chitosan-20% POSS	82.62

Figure 4.19. presents the three dimensional images of pure chitosan scaffolds. Highly interconnected porous structure was observed in which small micropores are located at the center of scaffold whereas larger macropores are located at the peripheral sites of the scaffold.
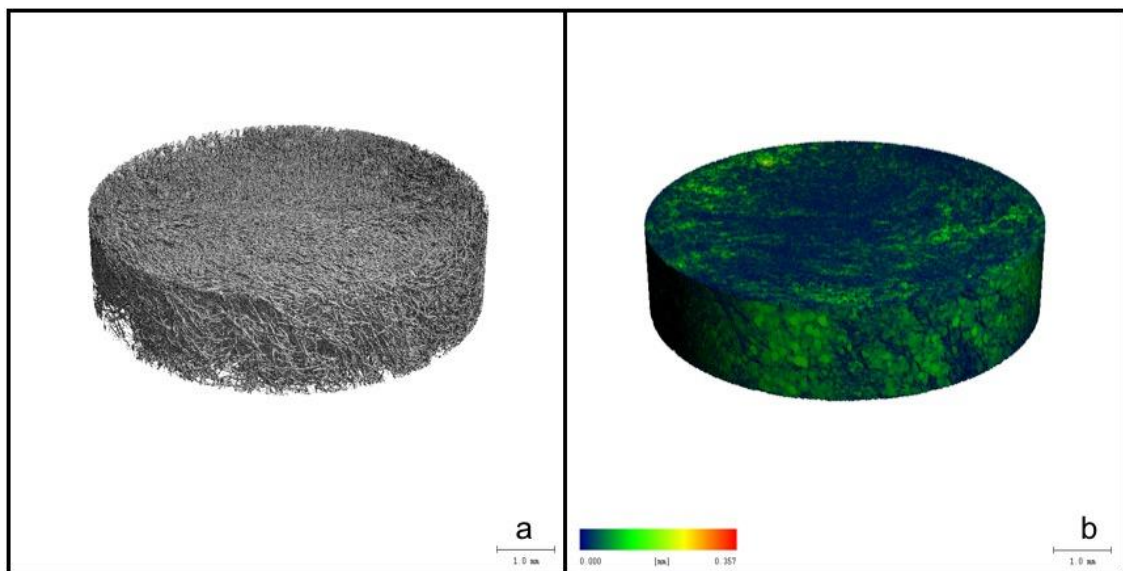
Figure 4.19. Micro CT images of chitosan scaffold showing morphology and 3D colored pore distribution respectively.

Figure 4.20. shows the micro CT images of 5 and 20 wt % POSS loaded chitosan composite scaffolds. 3D images of the chitosan-POSS scaffolds showed morphology with high porosity with interconnected pores whereas, increasing POSS content from 5 to 20wt% changed the 3D structure of chitosan-POSS scaffold. 20 wt % POSS containing chitosan composite scaffold exhibited a different three dimensional structure as also observed in SEM images (Figure 4.14). Pore wall surfaces increased and interconnections between pores decreased with increasing POSS content (Figure 4.20.) This change in pore surface may arise from possible agglomerations of POSS nanoparticles on scaffold surface. However, homogenous pore size distribution was observed in chitosan-20%POSS scaffolds.

Figure 4.20. Micro CT images of chitosan/diatomite scaffolds showing morphology and 3D colored pore distribution respectively. Chitosan-5%POSS (a,b); chitosan- 20%POSS (c,d).

Figure 4.21. depicted the three dimensional structure and morphology of 5 and 20 wt % diatomite incorporated chitosan composite scaffolds. Micro CT images showed that both chitosan-diatomite composites exhibited highly porous structure. Chitosan-diatomite 5% composite showed a homogeneous distribution of larger pores. However, increasing diatomite concentration altered the pore size distribution. Chitosan-20% diatomite composite scaffold exhibited smaller pores at the center whereas, larger pores at the peripheral region.
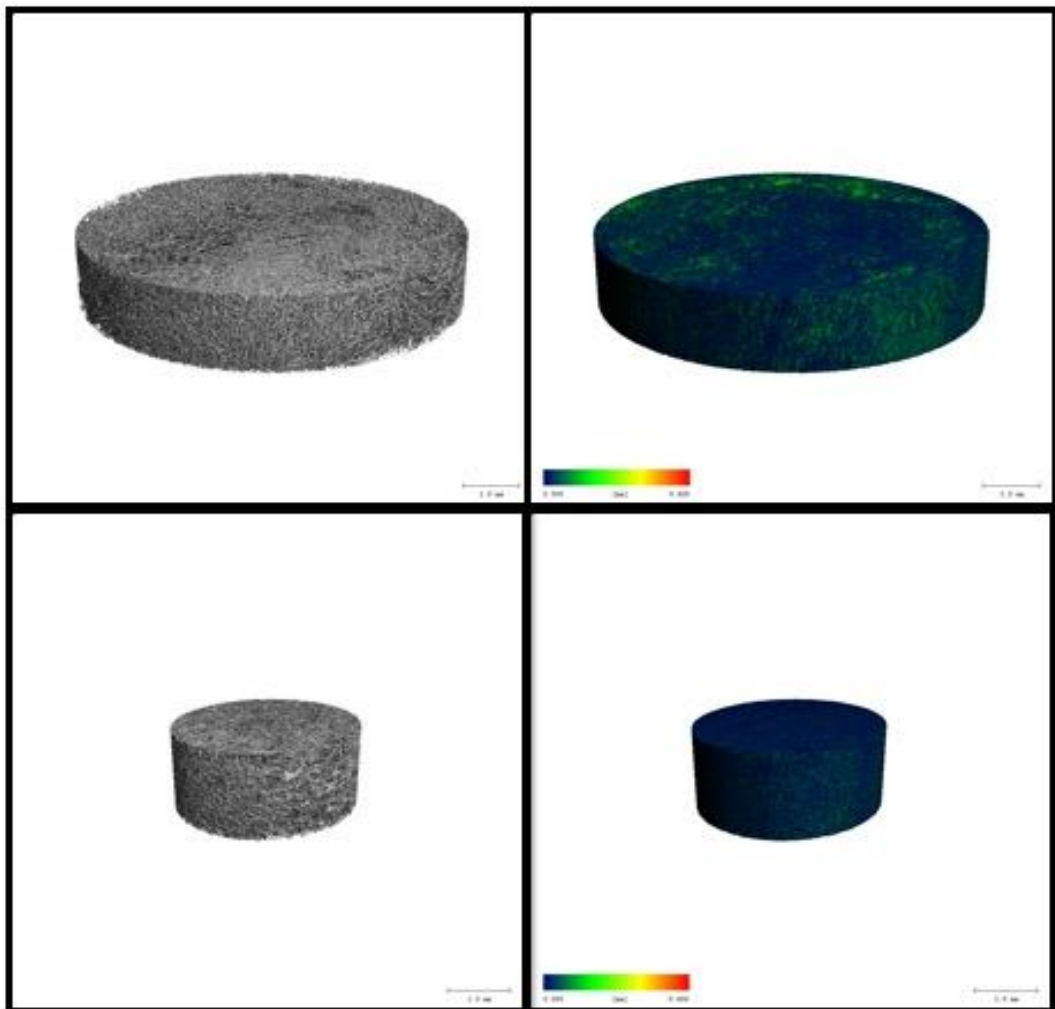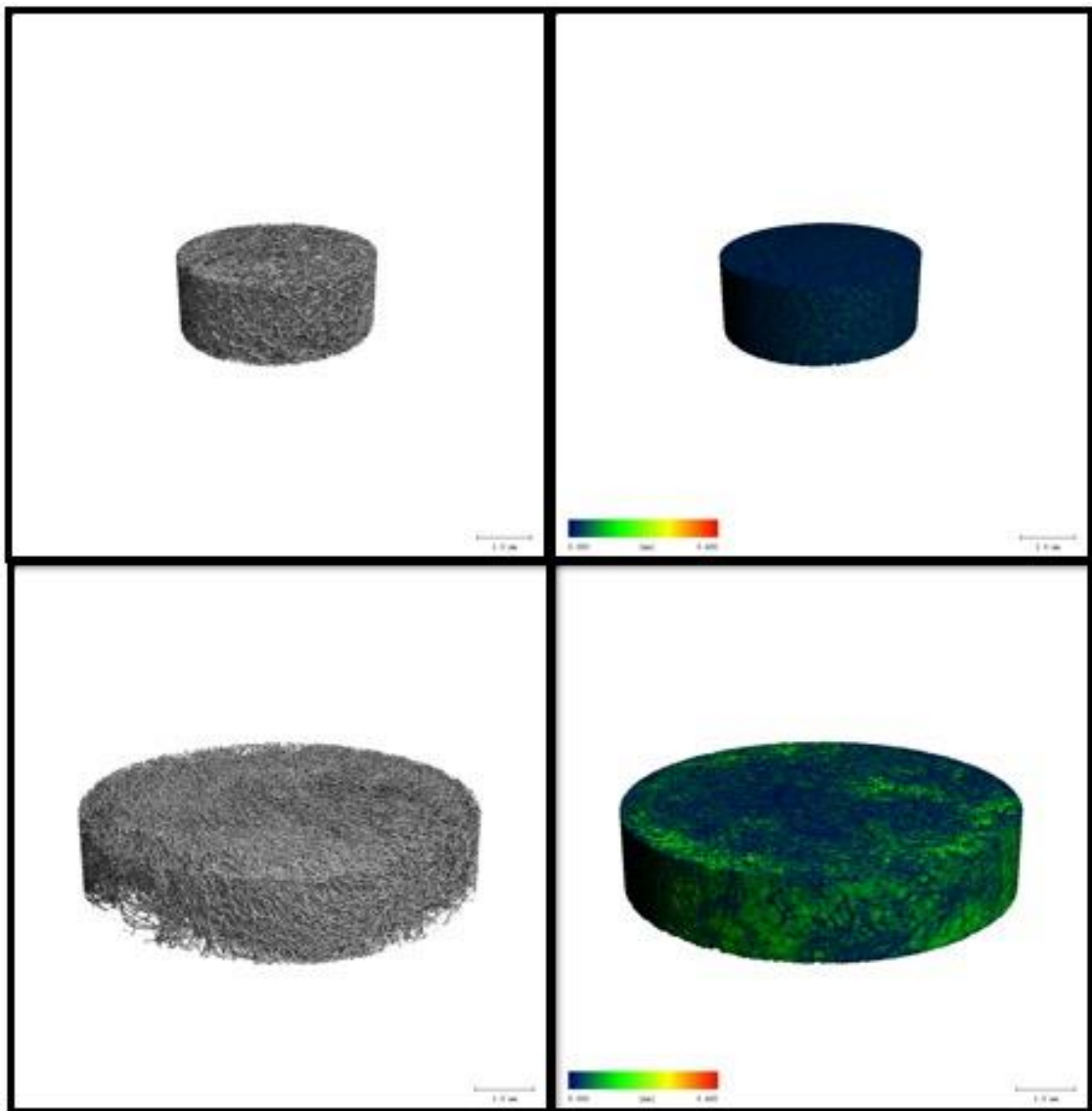

Figure 4.21. Micro CT images of chitosan/diatomite scaffolds showing morphology and 3D colored pore distribution respectively. Chitosan-5%diatomite (a,b); chitosan-20% diatomite (c,d).

The porosity of the scaffold prepared in this study showed higher porosity as compared to the porosity results of Oliveria and coworkers (Oliveira et al., 2006). They prepared bilayered chitosan-hap composite and micro ct images showed that chitosan part of the bilayered chitosan-hap composite scaffold had a porosity of 74%. In addition, Wang and co workers fabricated silica-chitosan hybrid scaffolds and investigated the three dimensional structure and pore morphology of scaffolds by micro ct analysis. They indicated that, high amount of silica and GPTMS resulting formation of a condensed silica network, disrupted the ice crystallization and reduced the length of the growing ice crystals. In addition, the pore morphology changed from more lamellar for chitosan to more tube-like as the content of silica and GPTMS increased. Scaffolds were obtained with a mean porosity of 97% due to the low chitosan concentration (Wang et al.,2015).

4.1.6. Protein Adsorption

The understanding of protein-material interaction in biomaterial design provides a correlation between biomaterial and in vivo tissue responses at the defect site (Servoli et al., 2009). Cell adhesion, proliferation and migration are significant parameters for tissue engineering. The cell-substrate interaction the major factor during cell adhesion. Fibronectin, fibrinogen, and vitronectin are the serum proteins that play role in cell adhesion. After cell adhesion, cell monolayer is formed and cell-cell interactions come into prominence for cell migration and proliferation in tissue formation (Menzies and Jones, 2010). When biomaterial contacts with a fluid containing soluble proteins (blood, body fluid or cell culture media), protein adsorption on material surface takes place. Thus, cell do not contact the molecular structure of biomaterial when seeded. They contact and interact with the adsorbed protein layer. Cell receptor-protein binding process plays an important role in the interaction of cells with adsorbed protein layer. This binding process determines the cell response on biomaterial surface (Latour, 2005). Therefore, protein adsorption is an important factor for biocompatibility of biomaterials.

In this study, protein adsorption on both types of chitosan scaffolds was determined by using BCA colorimetric protein assay kit for 24 hr. Protein adsoprtion on neat chitosan scaffolds was obtained as 108μg/ml. For chitosan-diatomite composite scaffolds, protein adsorption increased up to 10% diatomite content when compared to

pure chitosan scaffolds (Figure 4.22). Maximum adsorbed protein amount was determined on chitosan-10% diatomite composite scaffolds as 264 μg/ml. Above this concentration, the protein adsorption decreased. This decrease may result from microstructure and pore surface alterations with increasing diatomite concentration. Figure 4.23 represents the amount of protein adsorbed on chitosan-POSS composite scaffold for 24h incubation. Highest protein adsorption was determined in chitosan-5 wt % POSS scaffolds with 223μg/ml. It can be said that POSS nanoparticle incorporation did not effect protein adsorption significantly except 5% POSS content.

In literature, Sowjanya and co workers fabricated chitosan/alginate/nano-silica biocomposite scaffolds and examined the effect of nano-silica particles on protein adsorption of scaffolds. Chitosan/alginate/nano-silica scaffolds showed a marked increase in the proteins adsorption at the initial period of 1h incubation compared to chitosan/alginate scaffolds (Sowjanya et al., 2013). Similar increase in protein adsorption was obtained for all chitosan-diatomite composite. However, for chitosan – POSS composite, a marked increase in protein adsorption was only obtained only for 5 wt% POSS loaded composites.

Kavya and co workers fabricated chitosan/chondrotin sulfate-nano SiO_2 indicated composite scaffolds for bone tissue engineering application and reported that nano-SiO_2 incorporation slightly increased serum protein adsorption on chitosan/chondrotin sulfate scaffolds (Kavya et al., 2012). Sowjanya and co workers investigated the effect of nano silica particles on chitosan/alginate scaffolds. Similar trend of increased protein adsorption was found on CS/Alg/nSiO2 scaffolds with the incubation period of 4 h and 8 h. They reported that the significant increase in the proteins adsorbed was due to the increased surface area achieved by the presence of nano silica particles (Sowjanya et al., 2013).
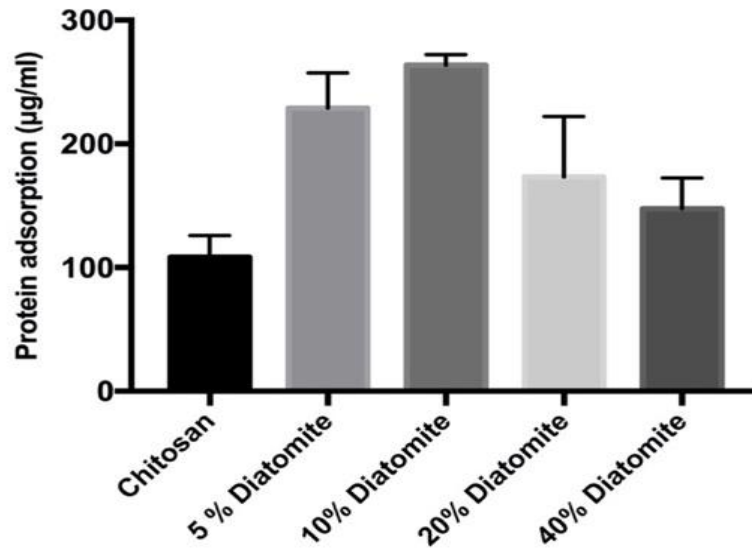
Figure 4.22. Protein adsorption on chitosan/diatomite scaffolds for 24h
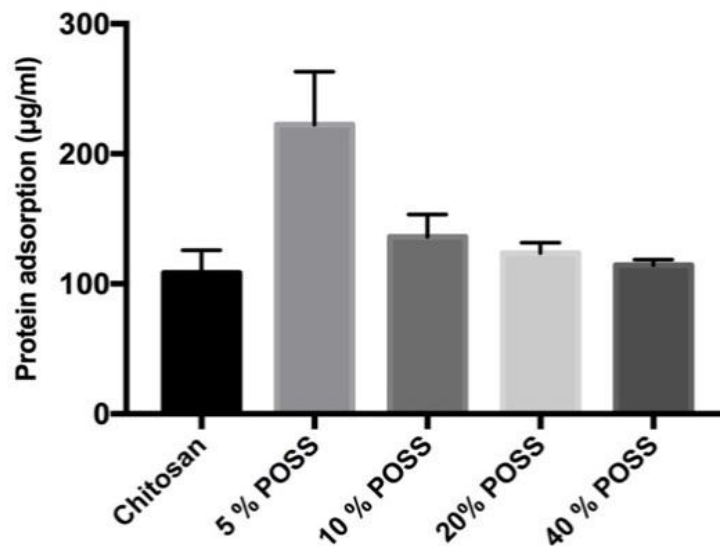
Figure 4.23. Protein adsorption on chitosan/POSS scaffolds for 24h

4.1.7. Water Uptake Capacity Determination

Water uptake capacity of a biomaterial plays an important role when interacting with body fluids. Biomaterial must have hydrophilic character in order to provide a chemical interaction with the body fluids contents (i.e. proteins). Besides, blood or body fluid must be absorbed efficiently by the graft at the defect site. In this study, water uptake capacity of scaffolds was determined by calculating swelling ratio (SR) with

weight uptake determination. In order to simulate body fluid conditions, scaffolds were incubated in PBS solution at 37 ^{o}C for 24hour. Swelling ratio of chitosan composite composite scaffolds were calculated using Eq 3.1 and depicted in Tables 4.11 & 4.12. For chitosan-diatomite scaffolds, water uptake capacity of scaffolds increased with increasing diatomite concentration due to the hydrophilic character of diatomite frustules. The water uptake values were found be in the range of 25.3-44.2. Similarly, as seen in Table 4.12., the swelling ratio of chitosan/POSS composite scaffolds increased with POSS incorporation. Increasing POSS concentration enhanced the swelling ratio of scaffolds in the range of 29.1-32. It was found that diatomite incorporated composites had higher water uptake values compared to chitosan/POSS composites due to the microparticle nature of diatomite frustules. Diatomite and POSS are both composed of silica particles and incorporation of silica in chitosan leads to enhancement in the water uptake capacity of chitosan scaffold. The pore size and pore surface area differences obtained with increasing silica content effected water uptake capacity of scaffolds positively. Composites with higher silica content showed higher pore sizes and pore surface areas. This gave rise to an increase in water uptake capacity.

Table 4.11. Swelling ratio of chitosan/diatomite composite scaffolds. The data is presented as the mean ±SE for three measurements.

Groups	Swelling Ratio (24h)
Chitosan	26.8 ± 0.34
Chitosan-1% Diatomite	25.3 ± 0.66
Chitosan-3% Diatomite	27.5 ± 0.24
Chitosan-5% Diatomite	29.7 ± 0.44
Chitosan-10% Diatomite	37.1 ± 0.41
Chitosan-20% Diatomite	41.3 ± 1.84
Chitosan-40% Diatomite	44.22 ± 2.62

Table 4.12. Swelling ratio of chitosan/POSS composite scaffolds. The data is presented as the mean ±SE for three measurements.

Groups	Swelling Ratio (24h)
Chitosan	26.8 ± 1.02
Chitosan-1% POSS	29.1 ± 0.08
Chitosan-3% POSS	27.8 ± 0.7
Chitosan-5% POSS	27.5 ± 0.64
Chitosan-10% POSS	34.8 ± 3.2
Chitosan-20% POSS	35.2 ± 0.22
Chitosan-40% POSS	32 ± 0.1

Similar findings were observed in the literature, silica loading in polymer matrix increased the swelling properties positively. Enhanced water uptake capacity was obtained for chitin-nanosilica composites. Silica incorporation increased the swelling ratio (R) of chitin based scaffolds from 5 to 15 (Madhumati et al., 2009). Similarly, higher water retention capacity was obtained for mesoporous silica nanoparticle loaded chitosan nanofibers (Li et al., 2015).

4.1.8. Enzymatic Degradation

In vitro degradation of biomaterials is generally tested by incubating samples in enzymatic solutions which are available in human body at the same concentrations. Biomaterial is degraded by an enzyme physically and this causes a weight loss in the structure. Composite scaffolds were incubated in phosphate-buffered solution (PBS, pH 7.4) including 1.5 µg/ml lysozyme at 37°C. 0,01% sodium azide was used in solution to prevent bacterial contamination in medium.

Ideally, the degradation rate of the scaffold should be matched with neo-tissue formation rate in order to procure a smooth transition of the load transfer from the scaffold to the newly formed tissue. However, studies showed that the degradation rate differs with the type and composition of the polymer, conditions of loading and ambient environment. The enzymatic degradation rate proceeds from the surface of the polymer. Therefore, surface area and porosity of the scaffold are major factors to control the

degradation rate (Cheung et al.,2007). In literature, lysozyme enzyme has been used for degradation studies of chitosan. The degradation process is generally dependent on the degree of acetylation of chitosan. Highly acetylated chitosan showes faster degradation rate (Kean and Thanou, 2010). It is well known that, in human serum, N-acetylated chitosan is mainly depolymerized enzymatically by lysozyme which biodegrades the polysaccharide by hydrolyzing the glycosidic bonds present in the chemical structure. Lysozyme contains a hexameric binding site, and hexasaccharide sequences containing 3–4 or more acetylated units contribute mainly to the initial degradation rate of N-acetylated chitosan. (Freier et al., 2005).

In this work, higher weight loss% were obtained for chitosan/diatomite and chitosan/POSS composites in the first 3 weeks due to the high degree of acetylation of chitosan (75-85%). Freier and co workers studied the effect of degree of acetylation on biodegradation of chitosan films.Chitosan films with 79.5% degree of acetylation degraded in a range of 10-40 % weight loss for 28day incubation period. They found that the degradation rate of the samples generally appeared to slow down after a high initial mass loss which is a result of the loss of appropriate hexasaccharide sequences with progressing degradation. Degradation results indicated that the lack of consecutive N-acetylglucosamine residues was found to be also responsible for the slow degradation of samples with very low degree of acetylation (DA). However, samples having a high DA showed a decreasing degradation rate with increasing DA (Freier et al., 2005). Similarly, degradation rate of chitosan control groups with (75-85%) DA increased with time. However, lower weight loss% in the range 5-23.5% was obtained for chitosan scaffolds compared to the results of Freier and co workers.

Biodegradation results of chitosan-POSS composite showed that weight loss% of samples increased with POSS incorporation during incubation time. Weight loss% of POSS groups changed in a range of 9.3-32.7 and 22.5-32.8 for 7 day and 21 day incubation periods respectively. Results indicated that increase in POSS content increased the degradation rate of chitosan scaffolds for 7 and 21th day incubation period. However, 20% and 40%POSS loaded groups showed lower weight loss% as compared to 21 day incubation.

Weight loss% decreased from 40.5 to 24.3 for 20%POSS and 33 to 28 for 40%POSS group. This weight loss% decrease may proceed with due to possible ionic accumulation on scaffolds during degradation process. In addition, three dimensional structure and high porosity of composite scaffolds had a promoting effect on

degradation rate. Chitosan-POSS composites with high content (20-40%) showed a decrease in weight loss% for 28day incubation.
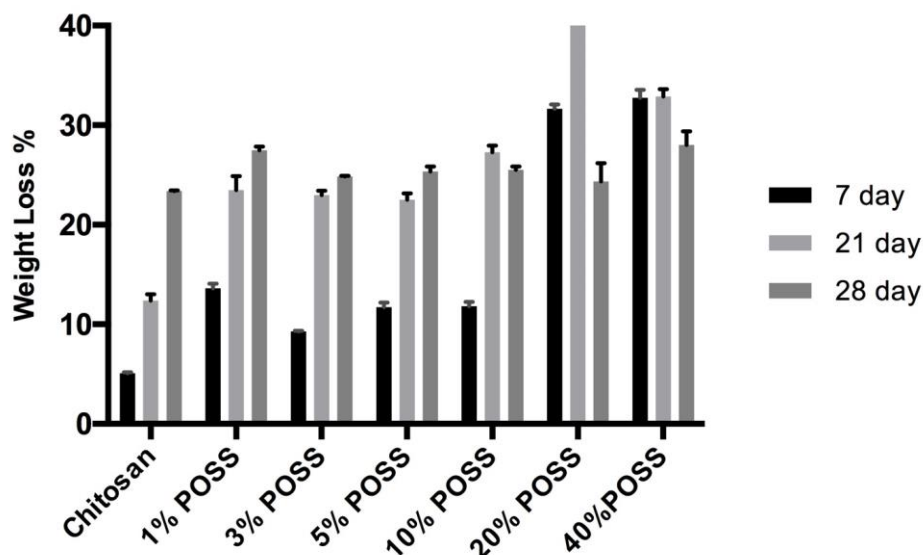
Figure 4.24. Weight loss% of chitosan and chitosan-POSS composite scaffolds for 7,21and 28 day respectively.

Chitosan-diatomite (1-10wt%) composite.scaffolds degraded in a range of 12% to 30% weight loss with 7-28 day of incubation. It was seen that degradation rate of chitosan-POSS composites was higher compared to chitosan-diatomite composites due to having organic degradable R groups and cause the break down of the structural integrity. In addition, all diatomite groups showed similar degradation behavior between 7-28 day and increasing diatomite concentration increased the degradation rate. However, above 10% diatomite loading, a decrease on degradation rate was observed from 21 to 28 day of incubation as observed in chitosan-POSS composite groups. This may stem from possible mineralization on composite surface with high diatomite concentration. Chitosan-20% diatomite and chitosan-40%diatomite showed a decrease in weight loss% from 40 to 24.3 and 32.7 to 28% , respectively between 21-28 day.

Sowjanya and co workers studied the effect of nano-silica particles on chitosan/alginate scaffolds. They found that silica incorporation increased degradation rate% of chitosan/alginate scaffolds for all incubation periods (Sowjanya et al., 2013). In addition, Pourhaghgouy et al studied the physicochemical properties of chitosan/bioactive glass nanoparticle (BGNP) nanocomposites. Biodegradation study

results showed that increase in BGNP content led to increase in weight loss amount. Degradation of Chi-BGNPs nanocomposites was found to be the result of three mechanisms; first, degradation of the chitosan; second, degradation of the BGNPs and third; separation of BGNPs from chitosan surfaces due to degradation of interfacial areas (Pourhaghgouy et al., 2015). In a similar way, diatomite and POSS as silica particles become part of this degradation steps.

Since chitosan is hydrophilic polymer, its degradation is due to bulk erosion. Diffusion of water into chitosan matrices is faster than degradation, the chitosan matrices first begin to swell prior to degradation due to its hyrophilic nature. This was also reported by Gopherich. Ren and co-workers reported that chitosan has two main degradation stages. In first stage chitosan interacts with water in the lysozyme solution, swells and this hydration process initiates the bond cleavage causing degradation. Degradation and weight loss is observed in second stage (Ren et al., 2 005). Similarly, composite groups first began to absorb enzymatic solution and swell at the first stage of degradation (1-7 days) as Ren et al reported for chitosan matrices. Then chitosan-silica groups showed a similar increase in weight loss % trend compared to results of Ren and co workers for 7-28day of incubation.
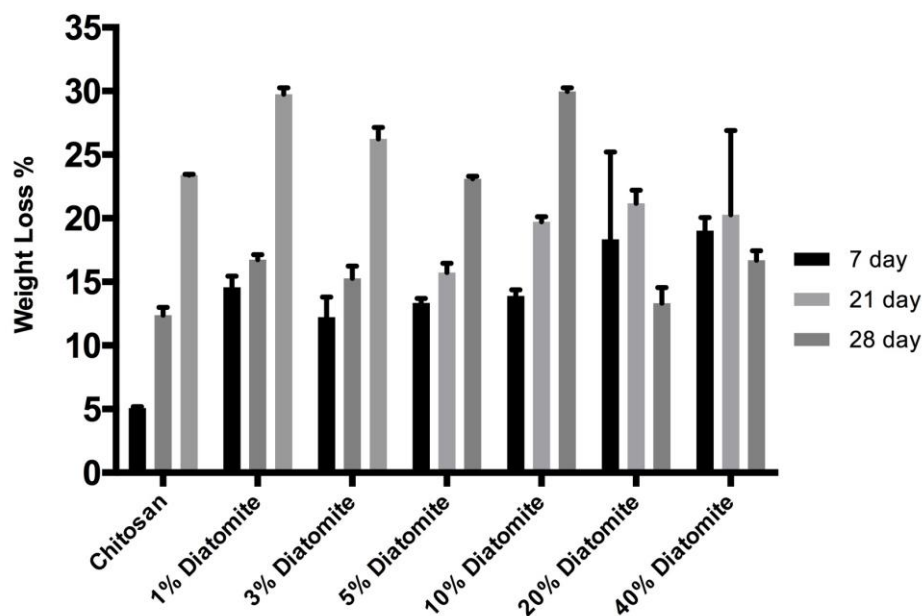

Figure 4.25. Weight loss% of chitosan and chitosan-diatomite composite scaffolds for 7,21 and 28day respectively.

Wan et al. indicated that the scaffold weight loss% changes with pore size and porosity that large pores and high porosity leads to higher weight loss%. Besides the weight loss% does not change linearly with the degradation time. Thus, scaffolds tend to degrade relatively fast in the first weeks. During this period, lysozyme can cleave chitosan molecules on the surface layer of scaffolds (Wan et al., 2005). Similarly, in this work, higher weight loss% was obtained for chitosan/diatomite and chitosan/POSS composites in the first 3 weeks.

4.1.9. Mineralization on Scaffold Surface

Generally, mineralization on scaffold is tested by immersing into simulated body fluid (SBF) in weeks and analyzing deposited minerals by EDX periodically. Ca and P deposition on scaffold surface lead to growth and formation of apatite crystals which is an important phenomenon for bone tissue formation. Bio-mineralization is a process in which release of biomolecules control the nucleation and growth of minerals such as carbonates, phosphates, silica and iron oxide (Ruiz-Hitzky et al., 2008). SBF was first produced and used by Kokubo et al. in 1990. Simulated body fluid (SBF) is a solution having ion concentrations similar to that of human blood plasma. SBF is used as a biomimetic surface modification technique to form apatite layer on biomaterial surface.

There are many different types of SBF, which are all different modifications of the Kokubo's first SBF recipe (Katsanevakis et al 2010).

In this study, exogenous biomineralization was determined by immersing scaffolds in m-SBF solution at 37 ^{o}C for 21 days. SEM analysis was performed with backscatter mode to investigate mineralisation on scaffold surface. Figures 4.25- 4.29 illustrate SEM images of neat chitosan and chitosan composites scaffolds incubated in SBF solution for 7 and 21days. SEM images indicated that, mineralization was observed on chitosan-diatomite and chitosan-POSS composite scaffolds. Apatite deposition which is the initiator of mineralization process was prominently determined on surfaces. Table 4.13. shows the Ca/P ratio of chitosan/silica composite scaffolds for 7 and 21 day incubations.

EDX spectral analysis of the precipitates of composite scaffolds showed a Ca/P ratio similar to stochiometric Ca/P (1.67) ratio of bone mineral. Composite surfaces showed showed a better mineral coating compared to neat chitosan. Increasing

diatomite and POSS concentrations and soaking time increased mineral formation on scaffold surface. Ca ion accumulation was found to be significantly higher than phosphate ion accumulation on composite surfaces which have higher silica content. This fact may arise from calcium silicate formation on surface instead of calcium phosphate formation.

It was concluded that silica particles initiated this mineral formation. The Si–OH groups are involved in the apatite deposition through the hydration and dissolution of the silica network itself. The degradation of the silica network leads to the formation of Si–OH groups at the bioactive composite–solution interface. In literature it is indicated that silanol (Si–OH) groups, have favourable sites for the calcium phosphate nucleation. Moreover, in SBF solution the water molecules react with the Si–O–Si bond to form additional Si–OH groups. The silanol groups first chelate the calcium ions (Ca^{2+}). Then clusters of critical size are formed by adsorbing phosphates. These functional groups induce apatite nucleation, and the released Ca^{2+} and Na^+ ions accelerate apatite nucleation by inducing the ionic activity product (IAP) of apatite in the fluid. It has been suggested the calcium silicate continuously gains more positive charges until it begins to interact with the negatively charged phosphate ions in the SBF fluid to form amorphous calcium phosphate. This amorphous material would then be transformed into the crystalline apatite. Tanahashi et al. showed that Si–OH groups were effective in apatite nucleation. Therefore, the mineralization process is induced by Si–OH groups which are specific surface functional groups and serve as effective sites for heterogeneous nucleation of Ca–P (Alves et al., 2010; Jongwattanapisan et al., 2011). Similarly in a study, $nSiO_2$ addition to chitin showed enhanced biomineralization when immersed in SBF for 7 and 14 days (Kavya et al., 2013). Sowjanya et al. reported that nano-silica particles in $CS/Alg/nSiO_2$ scaffolds may initiate formation of a calcium phosphate layer due to electrostatic interactions of negatively charged Si-O units which are formed by Si-OH dissociation, with the positively charged calcium ions in the SBF solution. As a result, calcium silicate layer was formed and exhibited a positive charge interacting with the negatively charged phosphate ions. By this way, amorphous calcium phosphate formation was observed (Sowjanya et al., 2013). Pourhaghgouy and co workers examined *in vitro* biomineralization of chitosan/bioactive glass nanoparticle nanocomposites and revealed that over soaking time, the intensity of the P–O bonds developed toward the Si–O–Si bond (Pourhaghgouy et al., 2015).

Table 4.13. Ca/P ratio of Chitosan/silica composite scaffolds for 7 and 21 day incubations

Groups	Ca/P ratio (7 days)	Ca/P ratio (21 days)
Chitosan	1.73	2.3
Chitosan-5% POSS	1.55	2
Chitosan-10% POSS	1.58	1.66
Chitosan-20% POSS	3.1	1.5
Chitosan-40% POSS	3.4	1
Chitosan-5% Diatomite	1.4	2
Chitosan-10% Diatomite	3.7	2
Chitosan-20% Diatomite	1.89	3
Chitosan-40% Diatomite	3.6	5
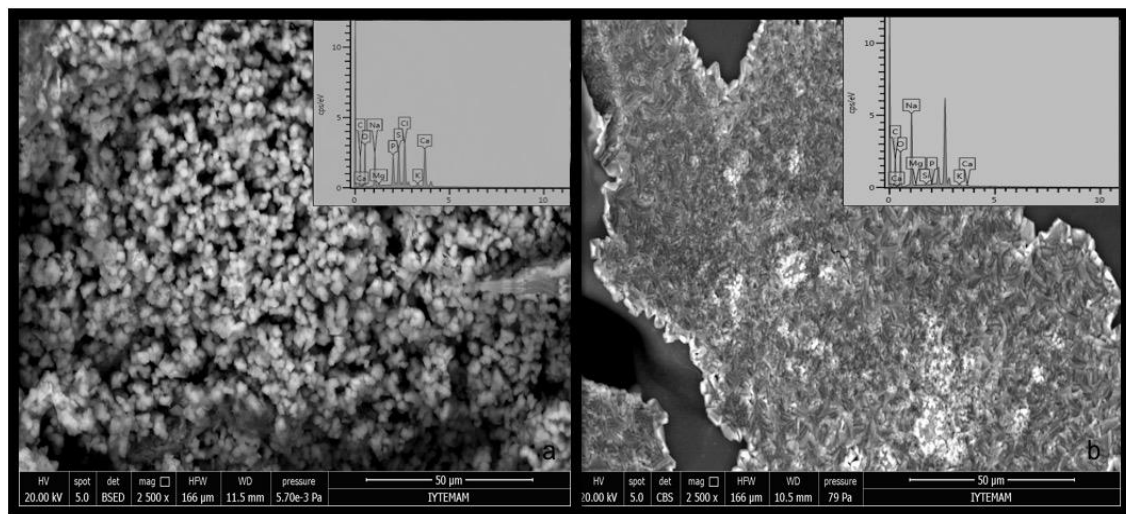
Figure 4.26. Scanning electron micrographs of chitosan scaffolds incubated in SBF solution for 7 and 21day respectively
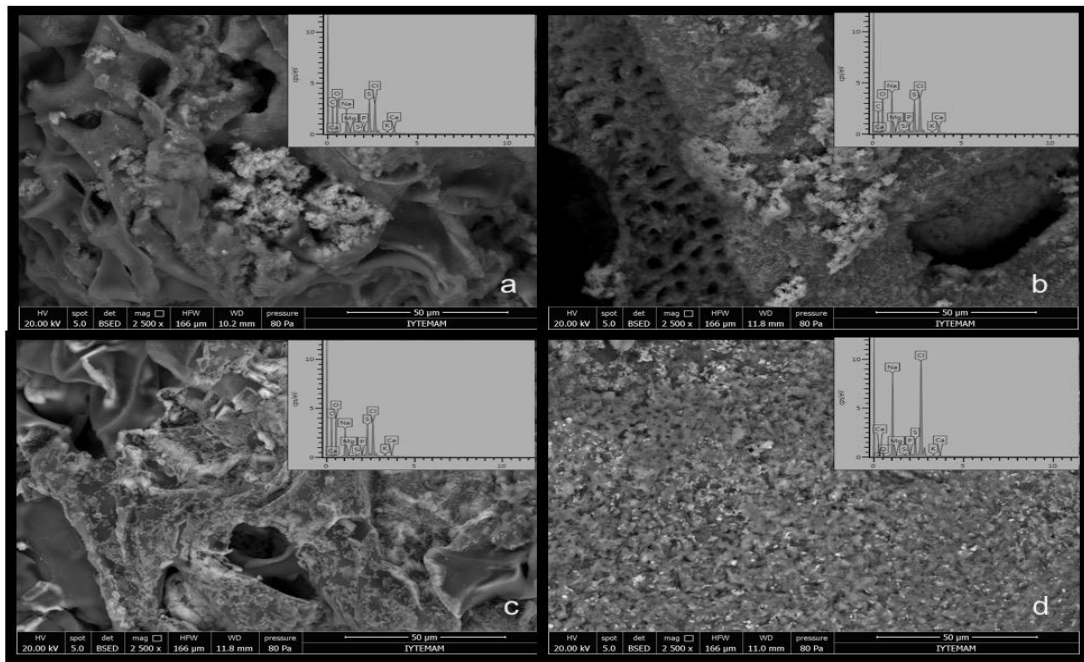
Figure 4.27. Scanning electron micrographs of chitosan-POSS composite scaffolds incubated in SBF solution for 7day 5% POSS (a); 10% POSS (b); 20% POSS (c); 40% POSS (d).

Figure 4.28. Scanning electron micrographs of chitosan-POSS composite scaffolds incubated in SBF solution for 21day 5% POSS (a); 10% POSS (b); 20% POSS (c); 40% POSS (d).

Figure 4.29. Scanning electron micrographs of chitosan-diatomite composite scaffolds incubated in SBF solution for 7day 5% Diatomite (a); 10% Diatomite (b); 20% Diatomite (c); 40% Diatomite (d).
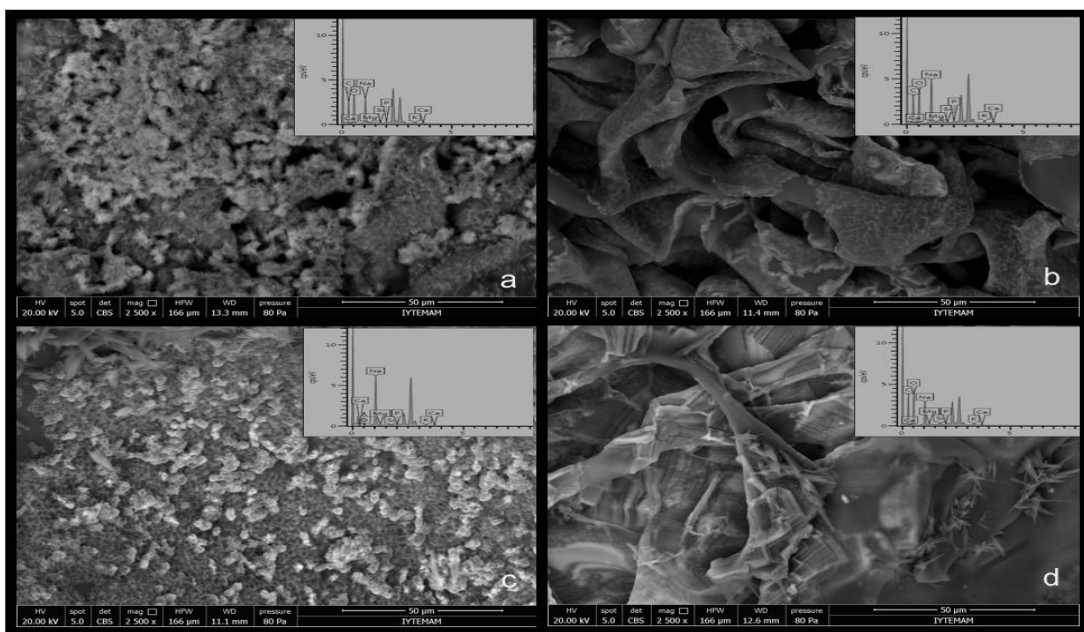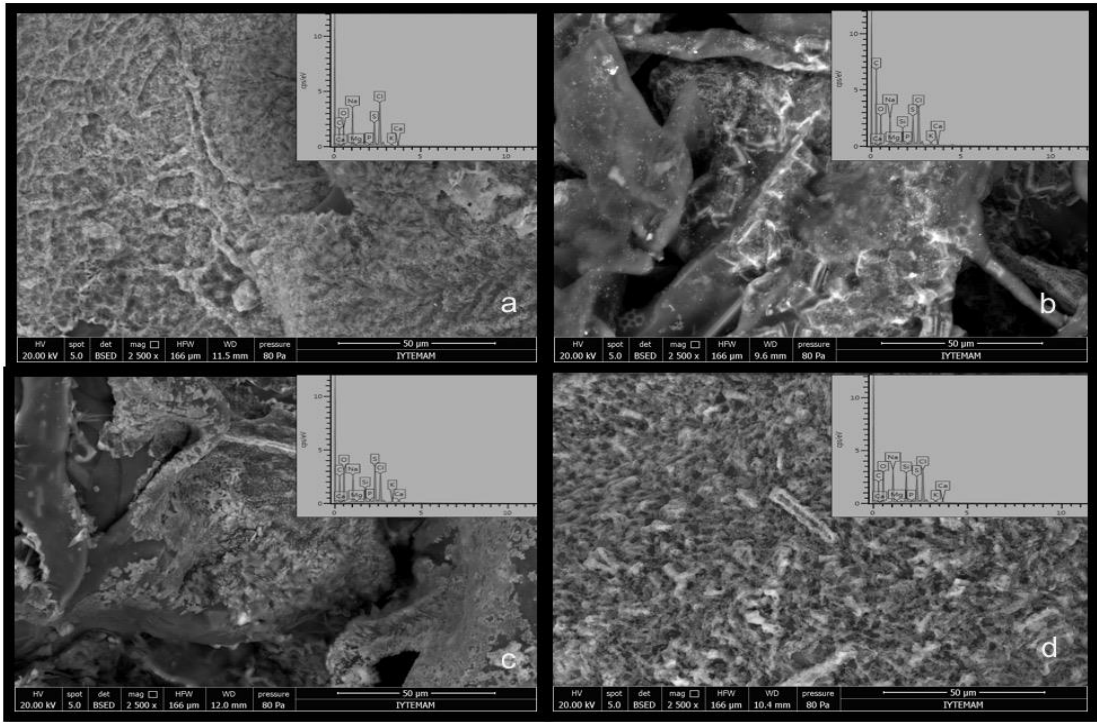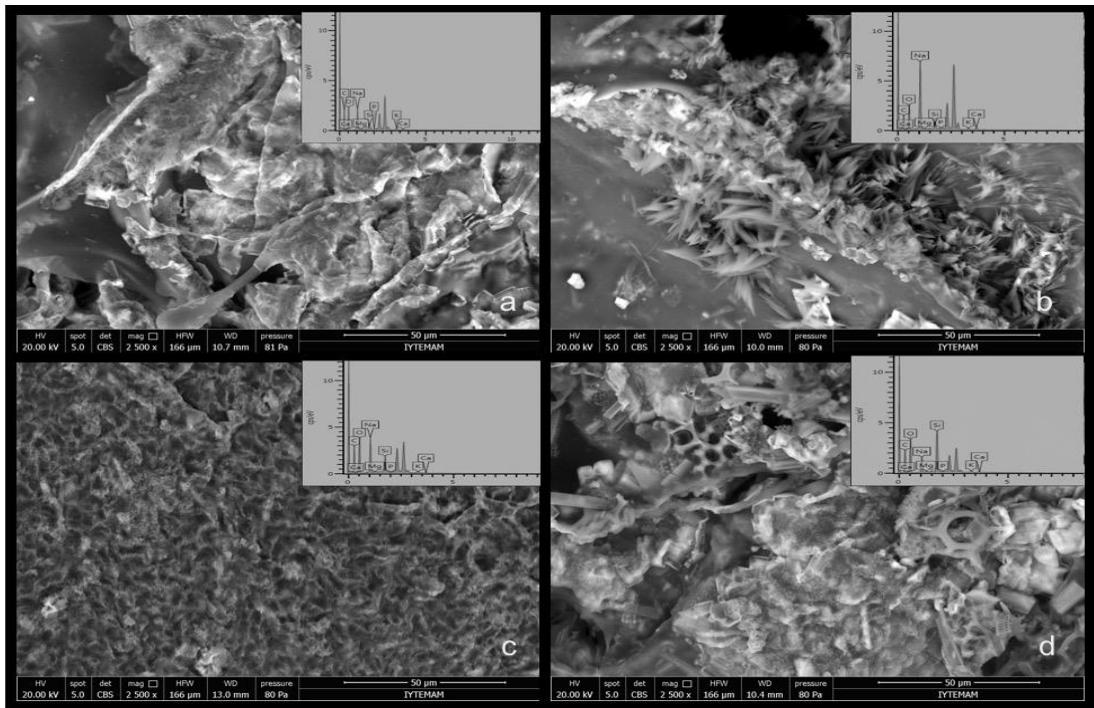

Figure 4.30. Scanning electron micrographs of chitosan-diatomite composite scaffolds incubated in SBF solution for 21day 5% Diatomite (a); 10% Diatomite (b); 20% Diatomite (c); 40% Diatomite (d).

4.2. *In vitro* Studies

4.2.1. *In vitro* Cytotoxicity Determination

Sterilised composite scaffolds were extracted for 24h in cell culture medium at 37°C according to ISO 10993 standards. WST 1 assay was performed on 3T3 cell line as specified in ISO standards for biocompatibility of materials. In addition, cytotoxicity determination was performed on MG-63 and Saos-2 cell lines which were used as bone cell models for *in vitro* cell culture studies. Cytotoxicity assay was not performed on Hfob cell line due to its lower proliferation rate and different incubation conditions (33°C) compared to MG-63 and Saos-2 osteosarcoma cell lines. Cells seeded on 96-well plates were observed with microscope during incubation periods.

Cytotoxicity on 3T3 cells was not observed with both chitosan/diatomite and chitosan/POSS scaffolds during 24h, 48h and 72h (Figures 4.31-4.32). 3T3 cell viability results indicated that both chitosan/diatomite and chitosan/POSS scaffolds didn't show any cytotoxic effect on 3T3 cell line. In addition to this, chitosan-diatomite composite scaffolds showed proliferative effect on 3T3 cell line with high diatomite concentrations (5-40%) (Figure 4.31). Similarly, 5-40% POSS incorporated composite scaffolds showed a significant proliferative effect on cells in 24h incubation period. This proliferation in 24 h led to slight viability decrease further, caused by the contact inhibition for 48h and 72h periods. Cell viability results obtained for 48h incubation were found to be statistically significant between chitosan and 3% diatomite, 1% and 20% diatomite, 3% and 5% diatomite concentrations (Figure 4.31). POSS groups showed statistically significant differences between 3% , 10% and 20% POSS in 48h incubation (Figure 4.32.).

Figure 4.31. 3T3 cell viability results of chitosan-diatomite composite scaffolds for 24,48 and 72h incubation periods (* represents significant differences).

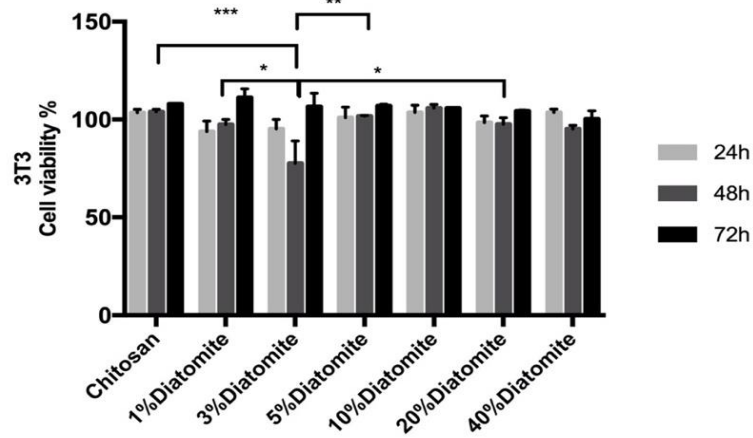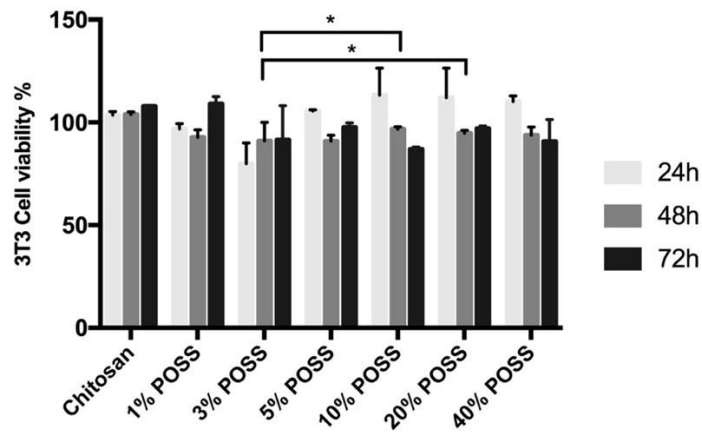Figure 4.32. 3T3 cell viability results of chitosan-POSS composite scaffolds for 24,48 and 72h incubation periods (*represents significant differences).

Figure 4.33. MG-63 cell viability results of chitosan-diatomite composite scaffolds for 24, 48 and 72h incubation periods.

Similarly, chitosan-diatomite and chitosan-POSS extracts did not show any cytotoxic effect on MG-63 cell line during 24h, 48h and 72h incubation time periods. (Figures 4.33-4.34). As seen in Figures 4.33., MG-63 cell viability results of chitosan-diatomite showed that the differences for 24h incubation were found to be statistically significant between 1% diatomite and 20% diatomite, 3% and 20% diatomite, 5% and 20% diatomite concentrations. In addition, the differences between 1% and 10%, 1% and 40%, 3% and 40%diatomite concentrations were found to be statistically significant for 48h incubation. 1% and 3% diatomite concentrations caused a rapid increase on cells in 48h. Similar proliferative effect on cells was observed for POSS incorporation with 1-10 wt% concentration range. The differences between 1% and 40%, 3% and 40%, 5% and 40%, 10% and 40% POSS concentrations were found statistically significant for 48h incubation (Figure 4.36).

Figure 4.34. MG-63 cell viability results of chitosan-POSS composite scaffolds for 24,48 and 72h incubation periods.

In literature, *in vitro* cytocompatibility studies reported for various polymer-nSiO$_2$ nanocomposites showed nontoxic behavior. Results indicated that the toxicity of nSiO$_2$ could be highly reduced by blending it into composites and nanocomposite scaffolds were found to be biocompatible with MG63, hMSCs, bMSCs cell lines (Deepthi et al., 2016).

As shown in Figures 4.35-4.36, Saos-2 cell viability results indicated that both chitosan-diatomite and chitosan-POSS composites showed no toxic effect on Saos-2 cells incubated for 72h. Increasing diatomite loading in 20-40% range decreased cell viability for 24h incubation. However, increasing diatomite loading between 1-10 wt%, increased the cell viability for 24h incubation. Statistical analysis indicated that interactions between groups with changing incubation time were found to be significantly different. In addition, 1%, 3%, 5%, and 10% diatomite loaded groups were found to be statistically different from 40% diatomite loaded group (Figure 4.35).
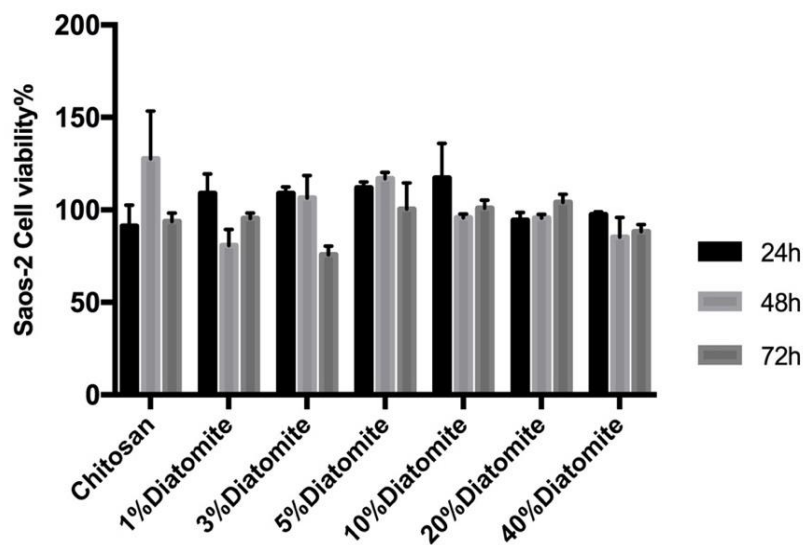
Figure 4.35. Saos-2 cell viability results of chitosan-diatomite composite scaffolds for 24,48 and 72h incubation periods.
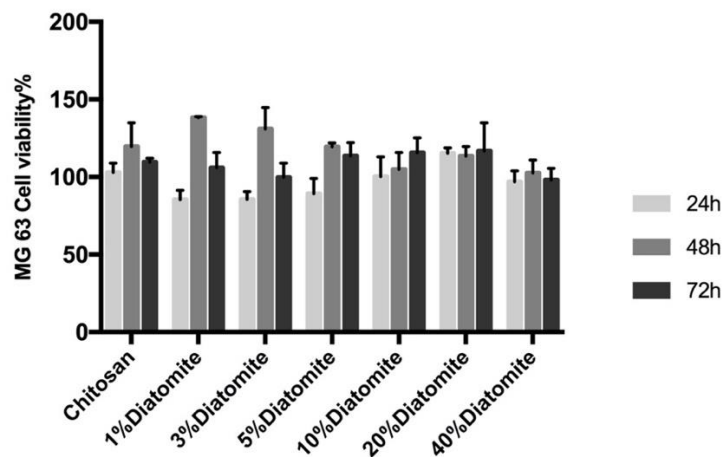
Similarly, chitosan-POSS composite scaffolds showed no toxic effect on Saos-2 cells. Composite scaffolds with 5-40% POSS loading showed an increase in cell viability for 24h compared to neat chitosan group. The decrease of cell viability for 48-72h period stem from cell population increase at 24h period and contact inhibition of cells due to lack of monolayer surface for attachment and proliferation. Interaction between composite groups was found to be statistically different. Anova results indicated that 1%, 10%, 20% and 40% diatomite loading were found to be statistically different from neat chitosan group for 48h (Figure 4.36).
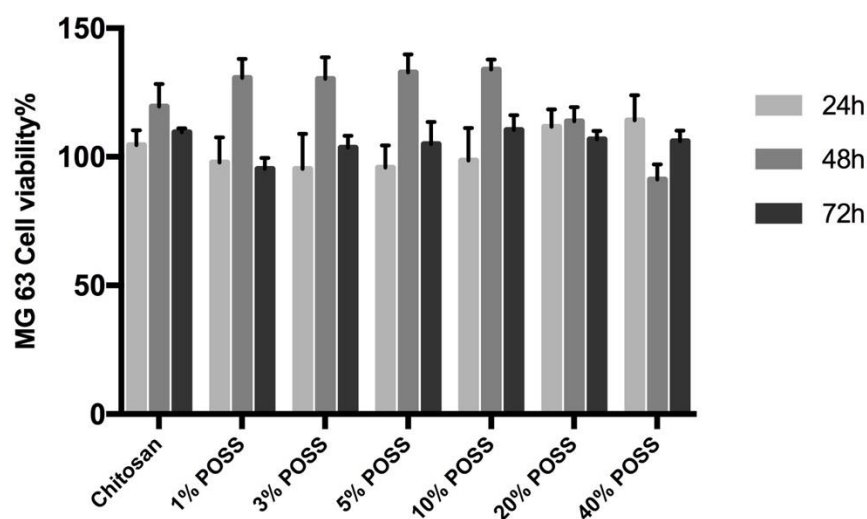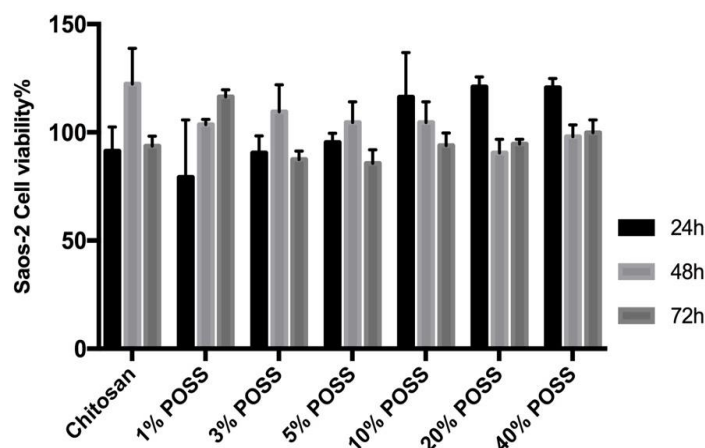
Figure 4.36. Saos-2 cell viability results of chitosan-POSS composite scaffolds for 24,48 and 72h incubation periods.

4.2.2. *In vitro* Cell Proliferation on Composite Scaffolds

In vitro cell proliferation studies were performed 7, 14, 21 and 28day incubation periods with hFob, MG 63 and Saos-2 cell lines which are generally used as *in vitro* models for bone regeneration studies. Highly sensitive fluorometric rezasurin assay was used to determine cellular metabolic activity on scaffolds. Although osteosarcoma cells show osteoblastic properties, they differ in various terms, concerning proliferation kinetics and the osteoid production (Pautke et al., 2004). hFob cell line mimics healthy human osteoblast cells with its morphology and osteogenic properties by comparison with osteosarcoma cell lines. Therefore, in this study, the effect of diatomite frustules and POSS nanoparticles in the prepared composite scaffolds was investigated on hFob proliferation. Pautke and co-workers reported that osteosarcoma cell lines lack physiological features such as contact inhibition. Therefore, cell growth in culture is not restricted to monolayers. They have a typical characteristic of the malignant nature altering cellular functions like cell-to-cell communication (Pautke et al., 2004). In this study, as seen in Figures 4.37-4.38, hFob cells proliferated on composite scaffolds during 28day incubation. Increasing diatomite concentrations showed a positive effect on hFob proliferation. The differences between groups (chitosan-20%diatomite, 5%-10% diatomite, 10%- 20% diatomite) were found statistically significant for 7day incubation. In addition, chitosan-40% diatomite composite scaffolds showed significant difference compared to chitosan control group for 21day. On the other hand, POSS

nanoparticles did not show a significant effect on hFob proliferation when compared to pure chitosan scaffold (Figure 4.37-4.38).

Figure 4.37. hFob cell proliferation on chitosan-diatomite composite scaffolds for 7,14, 21, 28day incubation period.
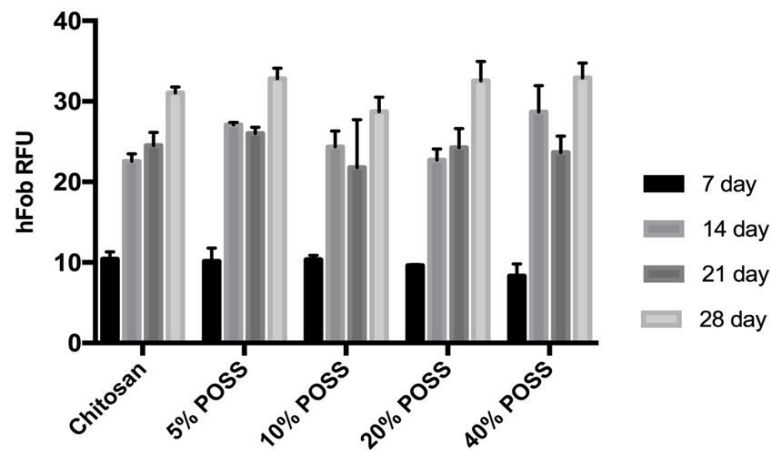
Figure 4.38. hFob cell proliferation on chitosan-POSS composite scaffolds for 7,14, 21, 28day incubation period.

Studies indicated that MG-63 cell line may provide a good alternative for initial attachment to various materials. MG-63 cells were also found to be appropriate for studying the regulation and production of osteocalcin. Contrary to this, MG-63 cells were not very representative regarding proliferation and alkaline phosphatase activities (Clover and Owen, 1994). Different from literature, MG-63 cell culture results showed a good proliferation trend on composite scaffolds. MG-63 cell proliferation results of chitosan-diatomite composites indicated that cells on the composite showed an increasing trend with incubation time (Figure 4.39). 14day proliferation results showed that MG-63 cells proliferated rapidly on composite scaffolds compared to chitosan

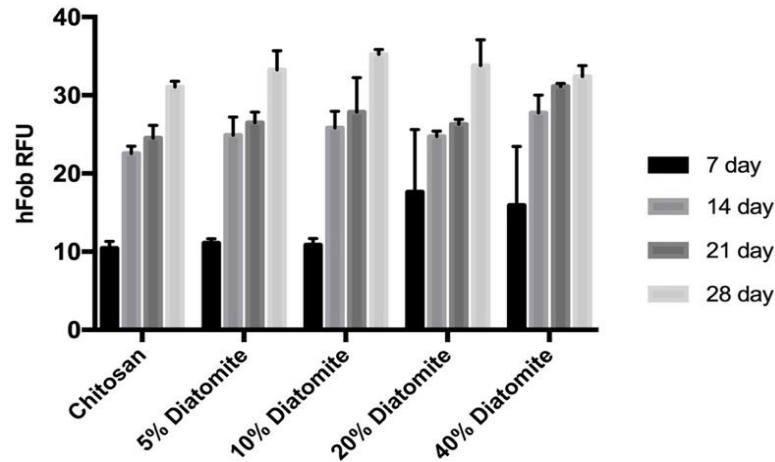control group. No statistical difference was found between groups and incubation periods.

Figure 4.39. MG-63 cell proliferation on chitosan-diatomite composite scaffolds for 7, 14, 21, 28day incubation period.

Proliferation of MG-63 cells on chitosan-POSS composites was shown in Figure 4.40. MG-63 proliferation on chitosan-POSS (5%-10%) scaffolds showed an upward trend compared with chitosan control group. However, proliferation reduced for 20 and 40 wt% incorporated composite scaffolds. POSS agglomerations inducing heterogenity on scaffold structure and increasing organic R groups (metyl ammonium) of POSS agglomerations may lead to low cell proliferation on scaffolds. Highest proliferation results with MG 63 cell line was obtained on 5% POSS scaffold among chitosan/POSS groups. Statistical differences were found between groups for 7, 21 and 28day incubation periods. At 7th day, 20% POSS group was found statistically different compared to control group. At 21th day, significant differences were obtained for 10% and 20% POSS groups compared to control group.
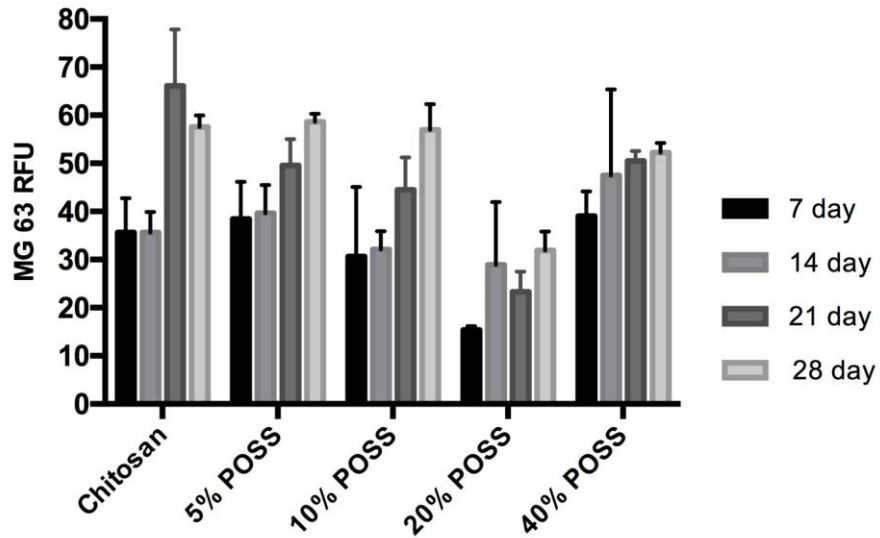
Figure 4.40. MG-63 cell proliferation on chitosan-POSS composite scaffolds for 7, 14, 21, 28 day incubation period.

Saos-2 cell proliferation showed an upward trend with increasing diatomite and POSS concentrations (Figure 4.41, Figure 4.42). Cells were highly proliferated on scaffolds at the end of 21day. Chitosan-POSS and chitosan-diatomite scaffolds supplied suitable environment for Saos-2 cells.
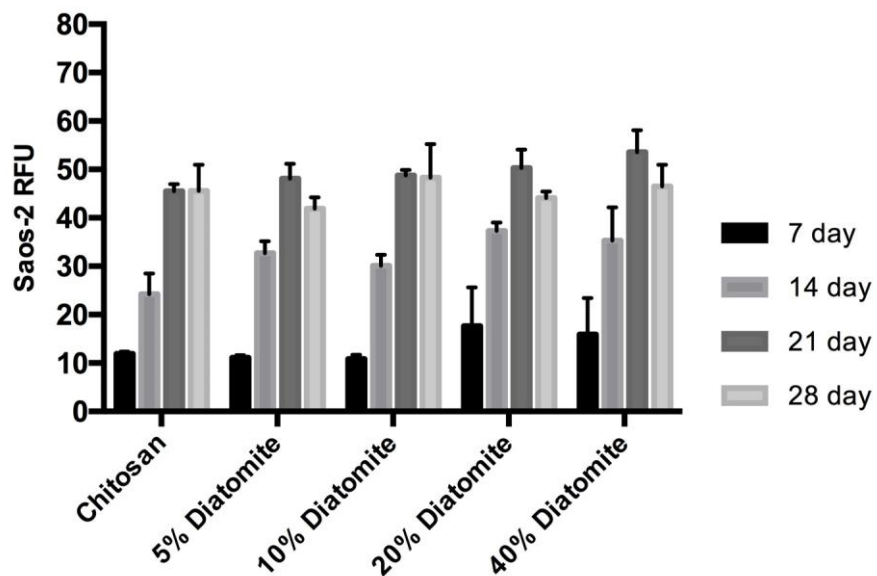
Figure 4.41. Saos-2 cell proliferation on chitosan-diatomite composite scaffolds for 7, 14, 21, 28day incubation period.
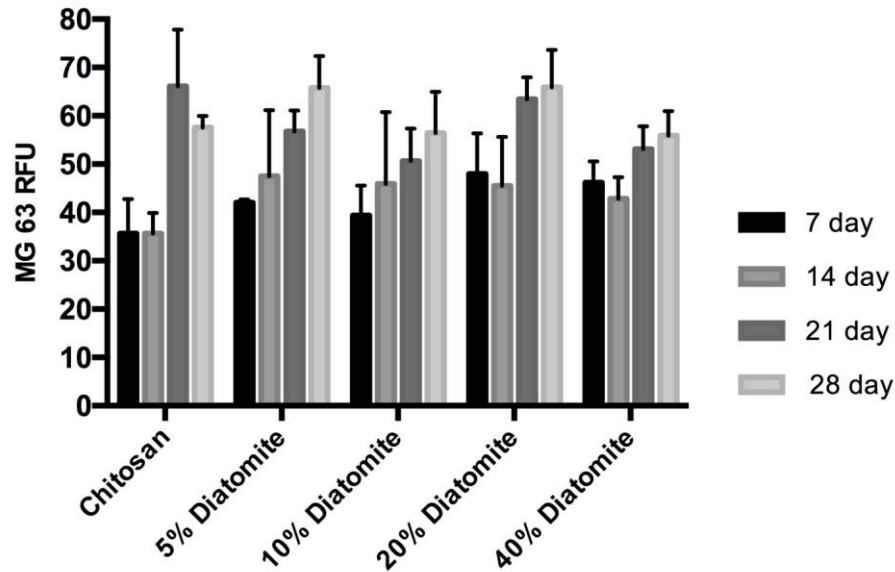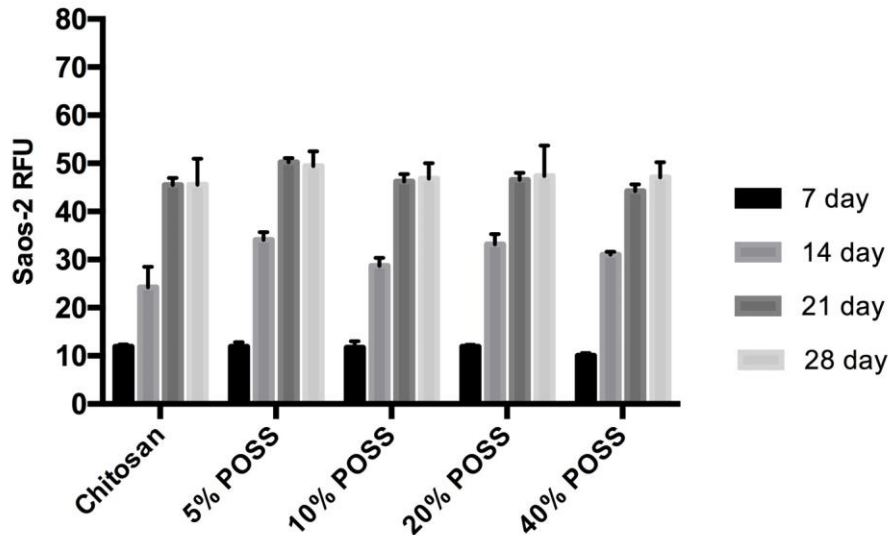
Figure 4.42. Saos-2 cell proliferation on chitosan-POSS composite scaffolds for 7, 14, 21, 28 day incubation period.

4.2.3. Cell Attachment and Spreading on Scaffold

In this study, MG-63 cells were incubated on scaffolds for 3 and 7 days. Proliferated cells were stained with Alexa fluor 488 phalloidin and DAPI to investigate cell attachment and spreading on scaffold surface. MG-63 cells were observed using florescence microscopy under 10x, 20x and 40x magnifications.

Osteoblast/material interaction depends on the surface aspects of materials which can be defined regarding their topography, chemistry or surface energy. These surface characteristics determine the adsorption of biological molecules to the material surface and the orientation of adsorbed molecules (Anselme, 2000). Surface topography has been shown to affect cell/biomaterial interaction. Studies reported that enhanced cell attachment was obtained on textured polymer substrates. Cells preferentially adhere to the edges of pores (10μm in diameter) and pillars (50 μm in depth) and also stretch between closely positioned features. Defining the topographic parameters has an influence on cell–biomaterial adhesion, by improving cell attachment and spreading (Rizzi et al., 2000).

In this study, cell attachment and spreading study results showed that both diatomite and POSS particles had a positive effect on cell attachment on scaffold surface by altering surface topography and increasing surface roughness. SEM images showed that chitosan-silica composite scaffolds was found to be favorable for cell attachment and spreading. Figure 4.43 shows the SEM image of MG-63 cells on chitosan scaffold surface. Cells attached on chitosan-diatomite and chitosan-POSS scaffolds were shown in Figure 4.44 and Figure 4.45 respectively.
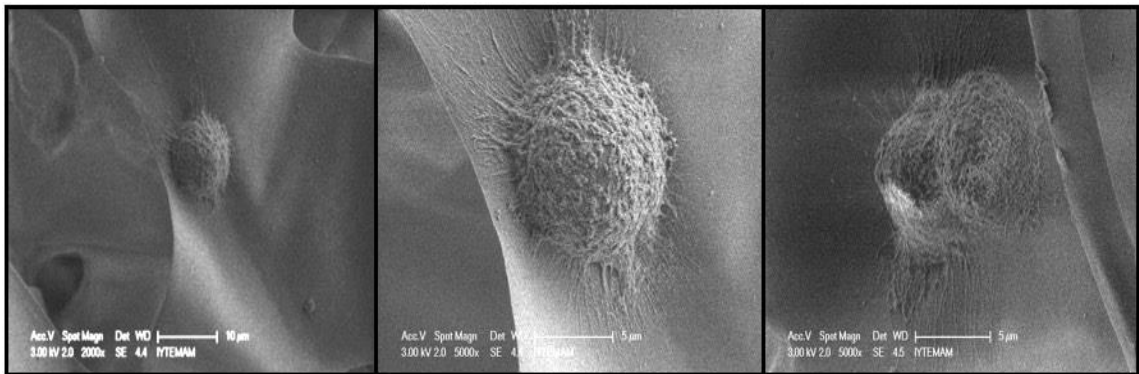
Figure 4.43. SEM image of MG-63 cells incubated for 3 days on chitosan scaffold
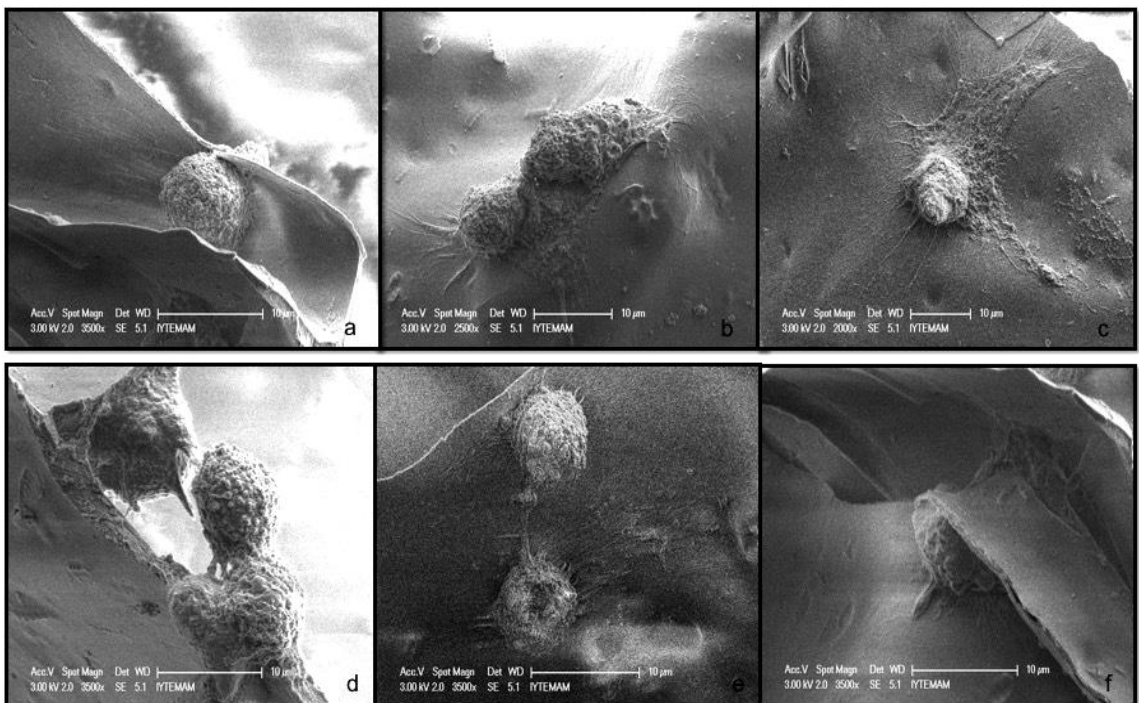
Figure 4.44. SEM images of MG-63 cells incubated for 3 days on chitosan-diatomite composite scaffolds: 5% diatomite (a,b,c); 20% diatomite (d,e,f).
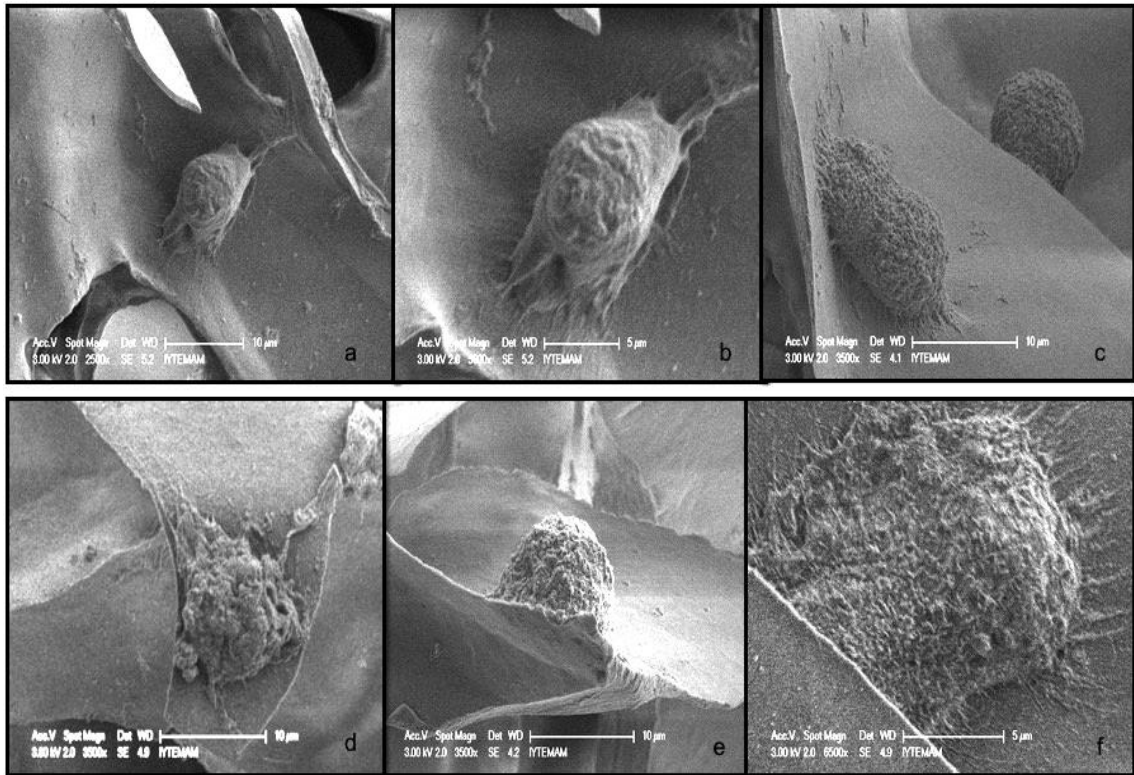
Figure 4.45. SEM images of MG-63 cells incubated for 3 days on chitosan-POSS composite scaffolds: 5% POSS (a,b,c); 20% POSS (d,e,f).

Figure 4.46. shows the fluorescence image of MG-63 cells on chitosan scaffold. Cells were observed under brightfield and fluorescence modes. It was seen that cells were attached and spread on chitosan scaffold surface at the end of 7day incubation. Nuclei of MG-63 cells were stained with DAPI. As a result of DAPI staining, the nuclei of MG-63 cells were observed as blue. High magnification fluorescence image of chitosan showed that MG-63 osteoblast-like cells on surface were in close contact with each other and colonized on the chitosan scaffold and strongly adhered to the surface of scaffold.
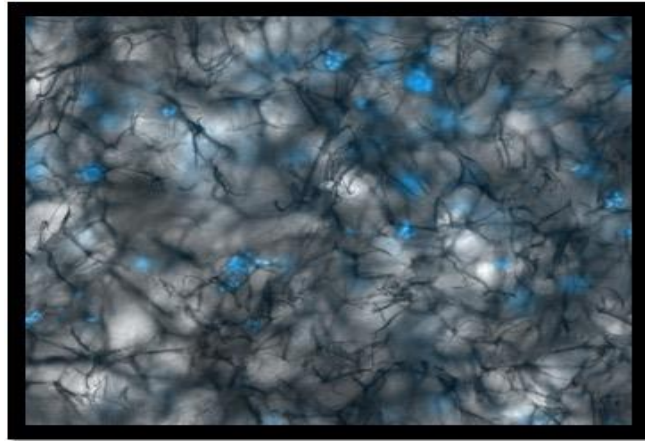
Figure 4.46. MG-63 cells proliferated on chitosan scaffolds

MG-63 cell attachment and spreading on chitosan-diatomite and chitosan-POSS composite scaffolds were depicted in Figure 4.47. Addition of silica enhanced MG-63 cell attachment and uniform cell spreading for both type of chitosan-silica composites compared to those on chitosan scaffold.
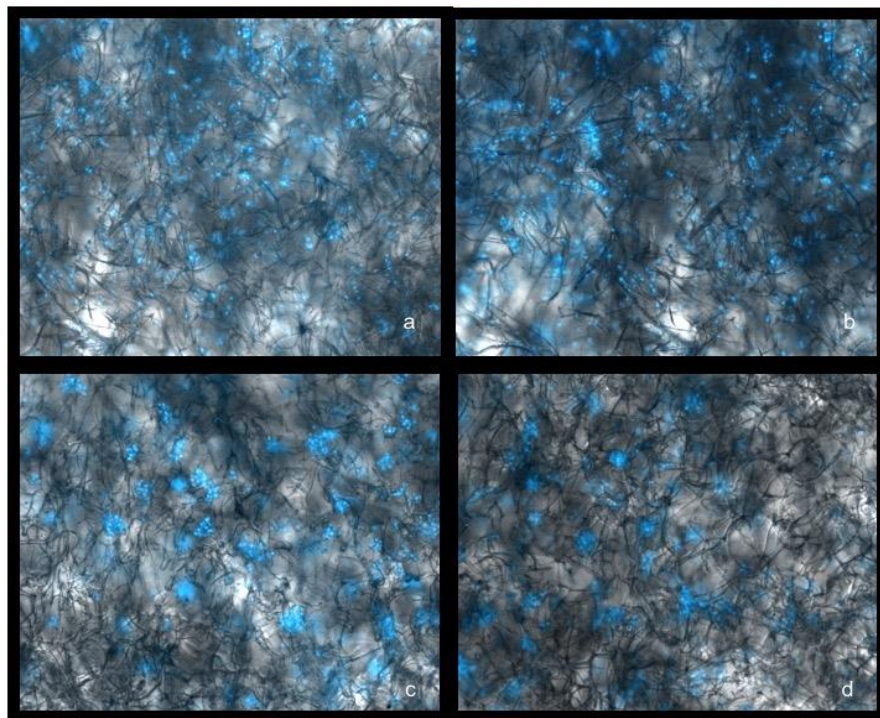
Figure 4.47. Fluorescence images of MG-63 cells proliferated on chitosan-diatomite and chitosan-POSS scaffolds under brightfield with 10x magnification. Chitosan-5% diatomite (a); chitosan-20% diatomite(b); chitosan-5% POSS (c);chitosan-20% POSS (d) respectively.

Cell spreading on chitosan scaffolds for 7 days is shown in Figure 4.48. According to fluorescence images, limited number of MG-63 cells was observed on chitosan scaffolds compared to chitosan-silica composite scaffolds.
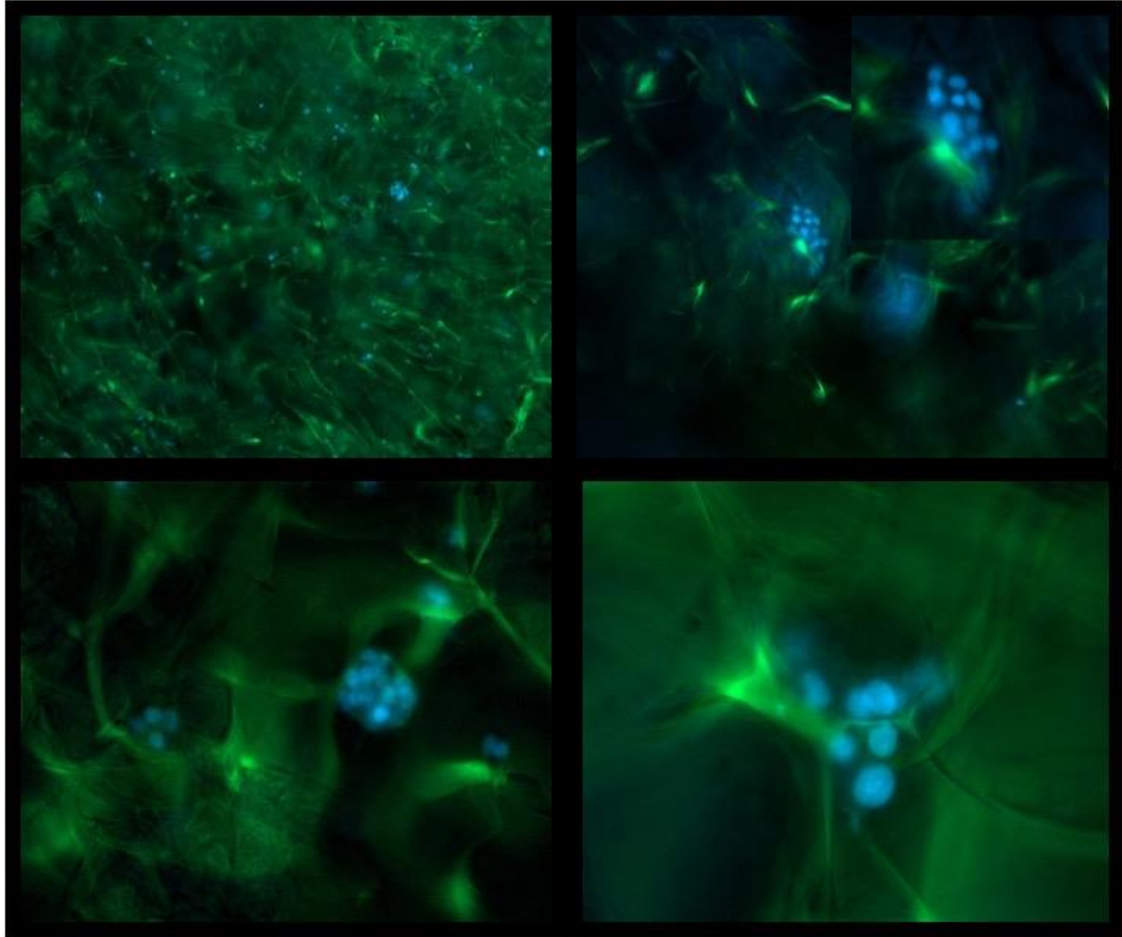
Figure 4.48. Fluoresence images of MG-63 cells on chitosan scaffolds under 10x, 20x and 40x magnifications for 7 day.

Fluorescence images of MG-63 cells on chitosan-diatomite scaffolds were depicted in Figures 4.49. and 4.50. for 7 th days. Images showed that MG-63 cells spread on composite scaffolds uniformly and attached on pore walls successfully. Diatomite incorporation supported cell adhesion, enhanced cell spreading and proliferation on scaffolds. Increasing diatomite loading enhanced cell attachment and spreading.
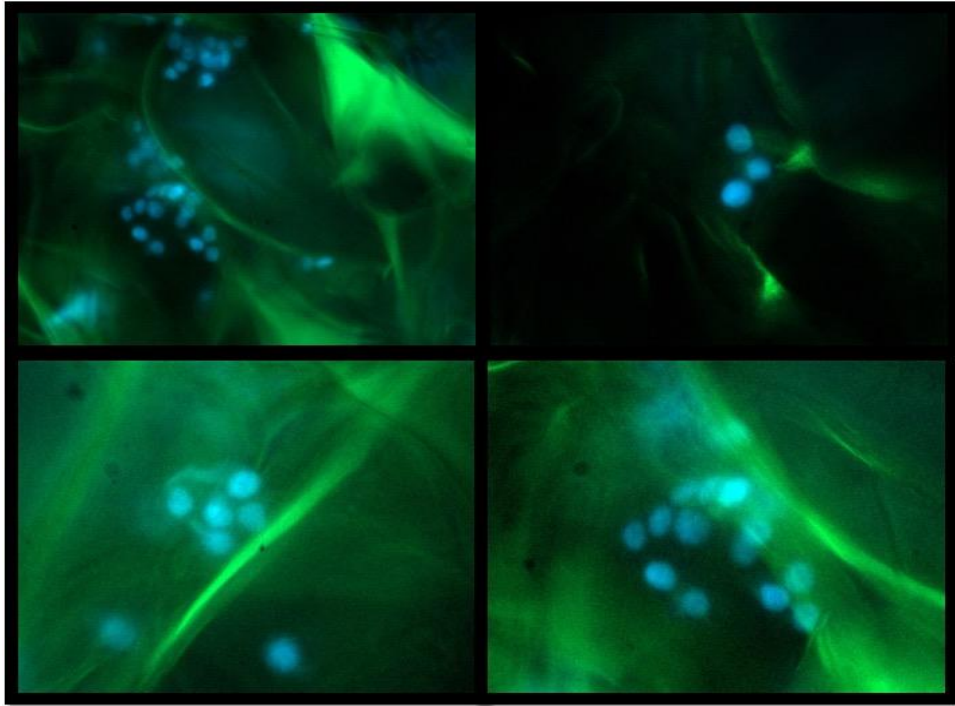
Figure 4.49. Fluoresence images of MG-63 cells on chitosan-5%diatomite scaffolds under 20x and 40x magnifications for 7 day.
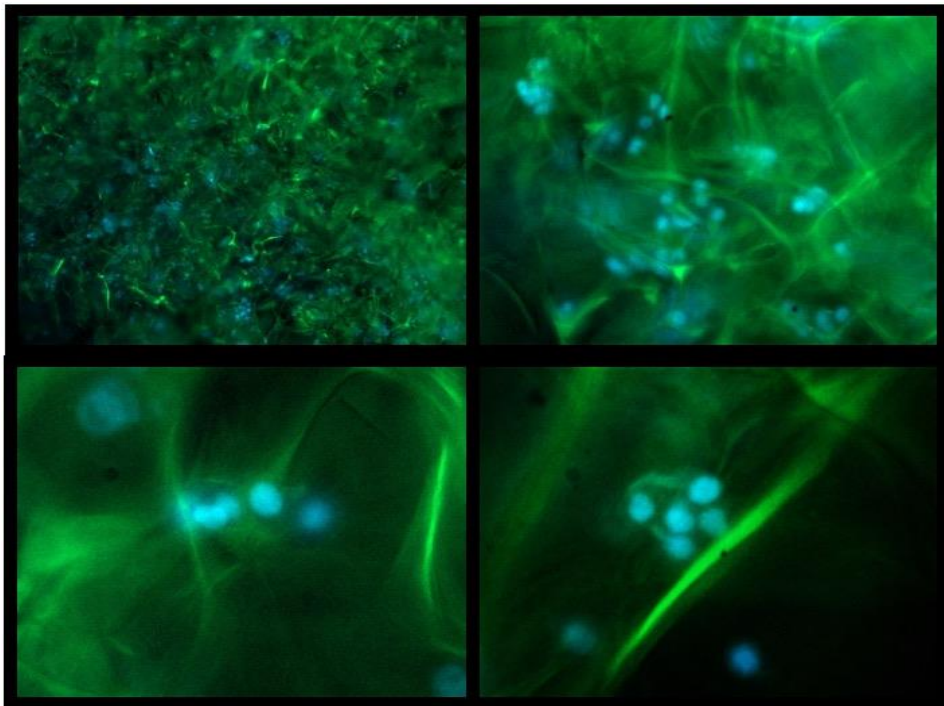
Figure 4.50. Fluoresence images of MG-63 cells on chitosan-20%diatomite scaffolds under 10x, 20x and 40x magnifications for 7 day.

Fluorescence images of MG-63 cells on chitosan-POSS scaffolds were shown in Figure 4.51. and Figure 4.52. Images showed that MG-63 cells spread on composite scaffolds uniformly and attached on pore walls successfully. POSS addition to chitosan matrix enhanced cell adhesion and cell spreading on scaffolds.
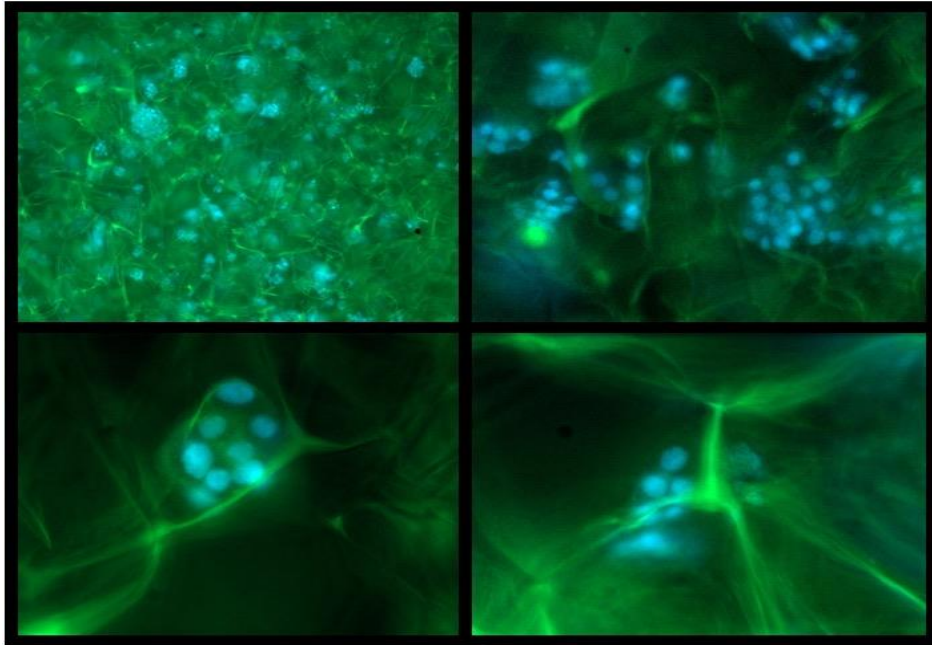
Figure 4.51. Fluoresence images of MG-63 cells on chitosan-5%POSS scaffolds under 10x, 20x and 40x magnifications for 7 day.
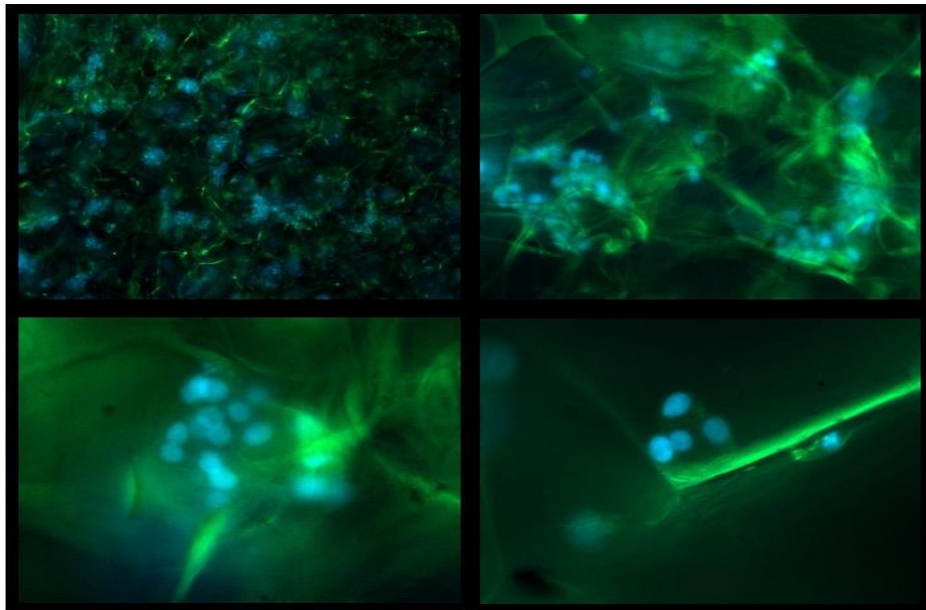
Figure 4.52. Fluoresence images of MG-63 cells on chitosan-20%POSS scaffolds under 10x, 20x and 40x magnifications for 7 day.

4.2.4. Alkaline Phosphatase (ALP) Activity Determination

In this study, ALP activity was determined by fluorometric quantification. Then fluorometric unit was converted to ALP concentration using standard curve and normalized with total protein concentration (μg/mL) during incubation periods. ALP studies were performed with MG-63, Saos-2 and hFob cell lines in osteogenic medium to determine the different osteogenic responses of these cell lines on composite scaffolds.

Literature studies reported that, although MG-63 cells were identified as expressing a similar integrin subunit profile to HOb cells, they had low ALP enzyme activity and did not mineralise (Pierschbacher et al., 1988; Saldana et al., 2011). Saos-2 cells with a mature osteoblast phenotype, possessed a high matrix mineralisation capacity and showed higher ALP activity than other osteosarcoma cell lines, such as MG-63 (Murray et al., 1987). Saldana and co-workers indicated that Saos-2 showed similar ALP activity compared to human primary osteoblast cells at the early time points, but 120-fold higher ALP activity was observed after 14day incubation (Saldana et al., 2011). Cytokine and growth factor expression of SaOs-2 cells have been shown to be similar to primary normal human osteoblast cells (Bilbe *et al.*, 1996). SaOs-2 cells have been shown to express receptors specifically for parathyroid hormone (PTH) and calcitrol ($1,25(OH)_2D_3$) similar when compared to osteoblasts *in vitro* and *in vivo* (Rao *et al.*, 1996). As a consequence, SaOs-2 cells show responses resembling HOb cells more closely, regarding the expression of osteoblastic factors (Czekanska et al., 2012).

ALP activity is an early osteogenic differentiation marker for bone tissue regeneration. So high ALP activity results were expected for 7 and 14 day incubations. As expected, Saos-2 cells seeded on chitosan-POSS composite scaffolds showed high ALP activity at 7th and 14th day (Figure 4.53.). POSS incorporation increased the ALP activity of Saos-2 cells for 14 day incubation. ALP activity of Saos-2 cells decreased after 14 day of incubation as expected. Cell showed similar ALP activity on chitosan-POSS composites compared to chitosan control group. Chitosan-20% POSS composite found to be significantly different compared to chitosan control group for 7 day incubation. 5% and 10% POSS groups were significantly differed from control chitosan group for 14 day. Only 40% POSS composite scaffolds showed significant difference for 21 and 28 day incubation.
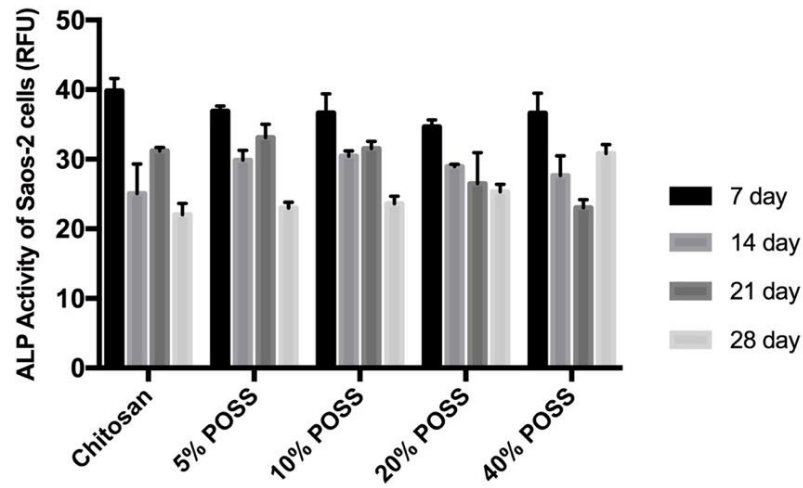
Figure 4.53. Alkaline Phosphatase Activity of Saos-2 cells on chitosan/POSS composite scaffolds.

ALP activity of Saos-2 cells on chitosan-diatomite scaffolds were shown in Figure 4.54. Similarly, higher ALP activity of Saos-2 cells on chitosan-diatomite composites were obtained for 7 and 14 days. Increasing diatomite concentrations showed a positive effect on Saos-2 cell at 14th day and increased the ALP activity. Table 4.14. shows the ALP concentrations of Saos-2 cells on composite scaffolds.
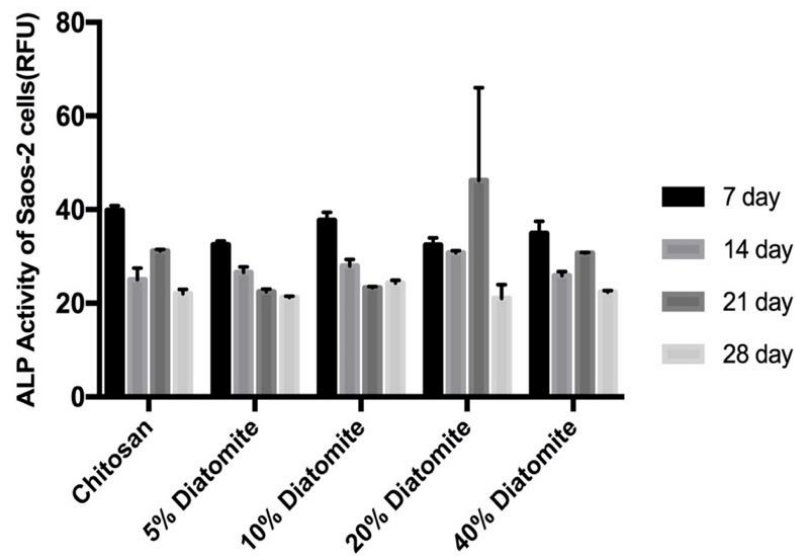
Figure 4.54. Alkaline Phosphatase Activity of Saos-2 cells on chitosan/diatomite composite scaffolds.

Table 4.13. ALP concentrations of Saos-2 cells on composite scaffolds. The data was presented as the mean ±SE for three measurements.

Saos-2	ALP concentration (nM)			
Group	7 day	14 day	21 day	28 day
Chitosan	113.7±12.1	69.5±5.2	88±4.3	60.5±3.7
5% POSS	103.4±7.1	84±5.6	93.6±5.1	63.4±3.4
10% POSS	104.2±8.3	85.6±4.5	89±2.6	65.2±6.3
20% POSS	98.3±3.5	81.1±4.2	73.8±3.7	70.3±5.3
40% POSS	104±13.1	77.3±9.5	63.5±4.6	86.7±5.1
5% Diatomite	92±17	74.1±9.2	61.7±7.8	58±4.1
10% Diatomite	104±12.4	78.3±9.4	64.3±5.4	67.3±5.7
20% Diatomite	93±0.14	88±10.1	132.8±55.2	57.4±4.8
40% Diatomite	99±0.14	72.3±3.6	86.4±5.6	61.5±

ALP activity of MG-63 cells on chitosan-diatomite scaffolds were shown in Figure 4.55. In contradiction to Saos-2 cell line, an increase in ALP activity was observed at the late stages of incubation. At higher diatomite concentrations (20% and 40%) ALP activity of MG-63 cell decreased. ALP activity of cell increased with incubation time for all chitosan-diatomite composite groups. There was no significant difference between groups for 7 and 14day incubation periods. 10% and 40% diatomite groups were found to be significantly different for 21day incubation. Also 40% diatomite group showed a significant difference at 28th day. High ALP activity results were obtained on chitosan-diatomite scaffolds for 7 and 14day incubation periods. As

expected ALP acitivity decreased with incubation time. 5% and 10% diatomite groups exhibited high ALP activity compared to control chitosan group. Above 10% diatomite addition led to decrease in ALP activity (Figure 4.55). Statistically no significant difference was found between groups. Similarly, higher ALP activity results were obtained on chitosan-POSS composite scaffolds at the end of incubation period (Figure 4.56.). POSS incorporation increased the ALP activity on 28th day of incubation contrary to diatomite incorporation. The ALP concentrations of MG-63 cells on composite scaffolds were depicted in Table 4.15. At 14th day, all POSS groups showed statistically significant differences compared to chitosan control group.
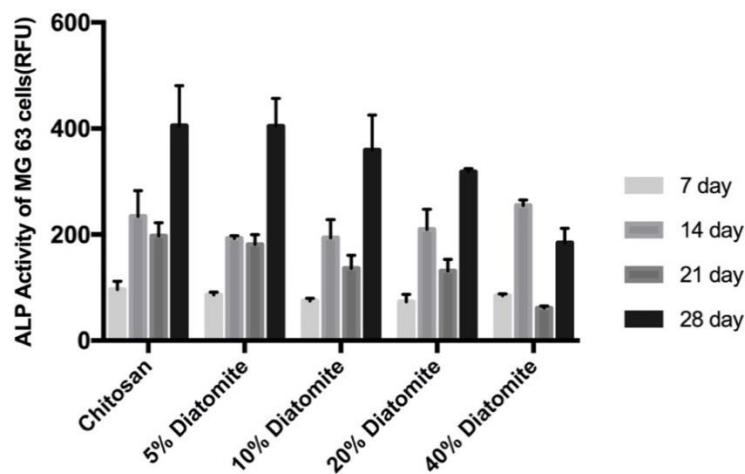
Figure 4.55. Alkaline Phosphatase Activity of MG-63 cells on chitosan/diatomite composite scaffolds
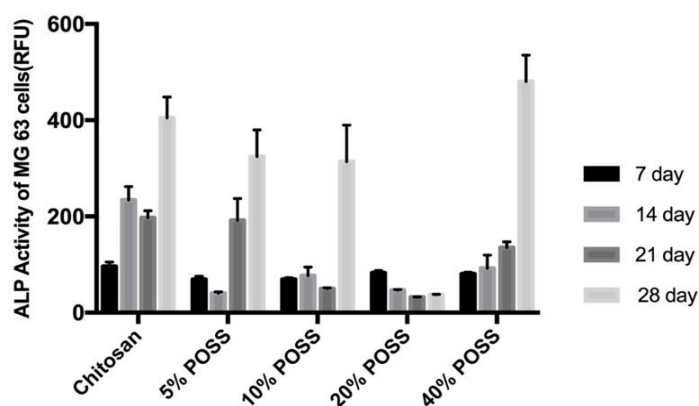
Figure 4.56. Alkaline Phosphatase Activity of MG-63 cells on chitosan/POSS composite scaffolds.

Kavya and co-workers reported that the incorporation of $nSiO_2$ particles into chitin/chitosan matrix enhanced the osteogenic activity of the composite (Kavya et al.,2009). Similarly, in this study, incorporation of Diatomite and POSS particless showed a positive effect on ALP activity of Hfob, Saos-2 and MG-63 cell lines.

Table 4.14. ALP concentrations of MG-63 cells on composite scaffolds. The data was presented as the mean ±SE for three measurements.

MG-63	ALP concentration (nM)			
Group	7 day	14 day	21 day	28 day
Chitosan	282±37.7	694.5±119	548±62.02	1200.8±185.3
5% POSS	181.2± 26.4	114.6±12.6	414.8±85.7	879.7±125.2
10% POSS	217.8±13.8	224.2±75.4	124.3±22.6	818.4±170.6
20% POSS	270.9±20.7	104.3±11.8	91±2.3	71.26±4.2
40% POSS	229.8±13.7	270±116	286±49.6	1175,4±306.3
5% Diatomite	240±12	571.3±11.6	364.2±71.6	1086.7±149.4
10% Diatomite	220±12.4	574.5±83.8	313.2±44	1123±169
20% Diatomite	261.6±34.7	622.2±92.2	340.5±41.2	870±99.5
40% Diatomite	236.8±8.7	763.6±28	163±6.8	488.8±75.1
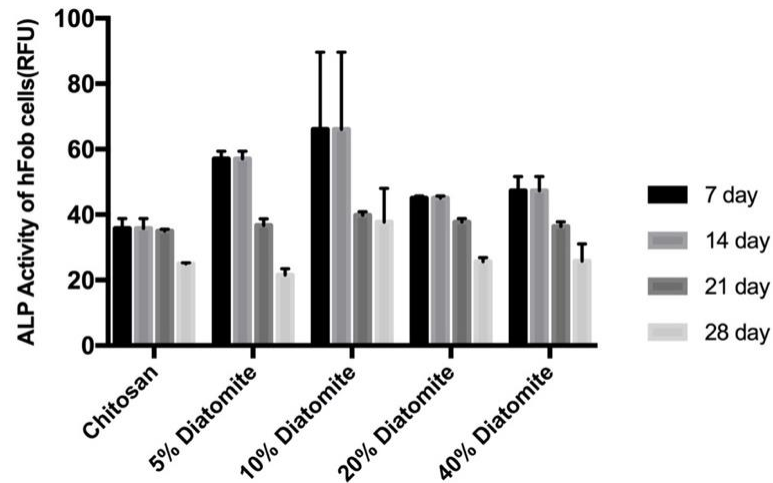
Figure 4.57. Alkaline Phosphatase Activity of hFob cells on chitosan/diatomite composite scaffolds.

On the other hand, Alkaline Phosphatase Activity of hFob cells on chitosan/diatomite and chitosan/POSS composite scaffolds was also studied and illustrated in Figures 4.57. and 4.58. Results indicated that addition of 5-10% diatomite increased the ALP activity of hFob cells. Above 10% diatomite ALP acitivity of hFob decreased. Results of chitosan/POSS composites indicated that 5% POSS sharply increased the ALP activity of hFob cells. Above this concentration, ALP activity decreased. However, all POSS groups showed higher ALP activity compared to chitosan control group for 7 and 14 day incubation periods. At 7th day, 5%POSS group was found to be statistically different compared to control. 40% POSS group showed significant difference with control group for 14 day of incubation. ALP concentrations of hFob cells on composite scaffolds were depicted in Table 4.16.

Consequently, Saos-2 and hFob cell lines showed similar responses in terms of ALP activity as indicated in literature studies. MG-63 cells exhibited ALP activity at the late term of incubation. However, much higher ALP concentrations were obtained with MG-63 cell line contrary to literature. Saos-2 and hFob cell lines showed lower ALP concentrations compared to MG63 cell line
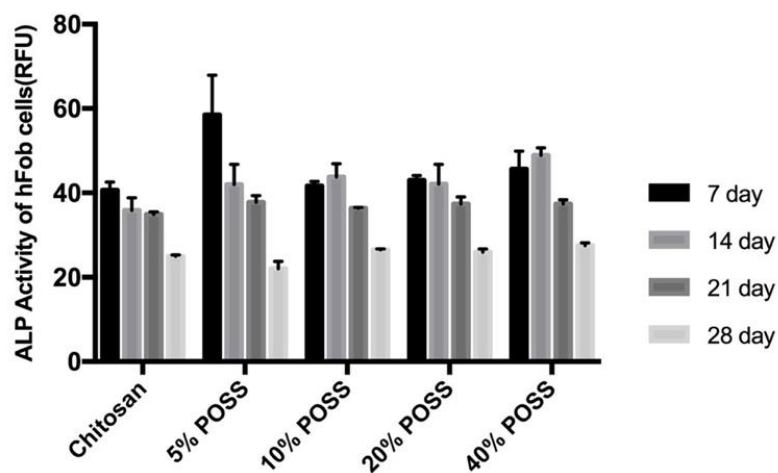
Figure 4.58. Alkaline Phosphatase Activity of hFob cells on chitosan/POSS composite scaffolds.

Table 4.15. ALP concentrations of hFob cells on composite scaffolds. The data was presented as the mean ±SE for three measurements.

hFob	ALP concentration (nM)			
Group	**7 day**	**14 day**	**21 day**	**28 day**
Chitosan	116.1±8.1	101.7±12.5	99±2.5	69.2±4.7
5% POSS	199.5±6.4	165±10.1	107.51±6.7	60.4±5.2
10% POSS	119±4.5	192±9.9	103.3±1.1	73.8±3.7
20% POSS	123±4.8	129.2±2.9	106.4±6.9	72.2±8.6
40% POSS	131±18.3	136.1±18.4	106.3±4.3	76.8±6.4

(Cont. on next page)

Table 4.15. cont.

5% Diatomite	165±10.1	165±10.1	104.5±8.1	57.4±5.2
10% Diatomite	201.2±94	192±100	113.7±4.3	107.4±5.1
20% Diatomite	140.8±18.3	131.3±18.4	107.3±4.7	71.2±3.2
40% Diatomite	136.1±18.4	130.5±13.5	103.3±6	71.8±2.5

4.2.5. In vitro Biomineralization on Composite Scaffolds

4.2.5.1. Von Kossa Staining

Von kossa staining protocol which detected phosphate ions bounding calcium deposits, was used to observe mineral formation of MG-63 and Saos-2 cells incubated on composite scaffolds. Von kossa stained scaffolds were observed under stereomicroscopy. In addition, cross section of scaffold is observed and mineral formation was detected at the inner parts of all scaffolds.

Figure 4.59 shows mineral formation on chitosan scaffolds for 21 and 28th day incubations. Slight amount of mineral formation was observed on MG-63 seeded chitosan scaffolds. But mineral formation was homogeneous on scaffold surface and increased with incubation time (Figure 4.59. a,b).
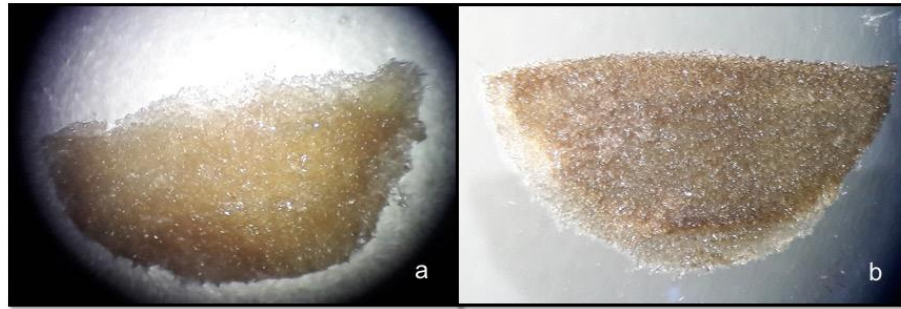
Figure 4.59. Von Kossa staining of MG-63 cells on chitosan scaffolds for 21day and 28day incubation respectively.

Figures 4.60 and 4.61 present the mineral formation of MG-63 cells on chitosan-diatomite & chitosan -POSS composites, respectively for 21 and 28day incubations. As seen in the figures, von kossa stained composite scaffolds showed that MG-63 cells induced mineral formation on both chitosan-diatomite and chitosan-POSS composite scaffolds. However, mineral formation was heterogenous changing concentrations at the center and peripheral regions due to the distribution of cells. This may stem from the morphology differences (porosity and pore size distribution) of composite scaffolds.

Figure 4.60. Von Kossa staining of MG-63 cells on chitosan-diatomite composites for 21 and 28day incubation respectively. Chitosan-5% diatomite scaffold (a,b); chitosan-20% diatomite scaffold (c,d).

Figure 4.61. Von Kossa staining of MG-63 cells on chitosan-POSS composites for 21 and 28day incubation respectively. Chitosan-5% POSS scaffold (a,b); chitosan-20% POSS scaffold (c,d).

On the other hand, Saos-2 cells prominently induced mineral formation on chitosan scaffolds. Mineral formation observed on scaffolds increased with incubation period. Figure 4.62 shows that Saos-2 cells prominently induced mineral formation on chitosan scaffolds. Mineral formation observed on scaffolds increased with incubation period.
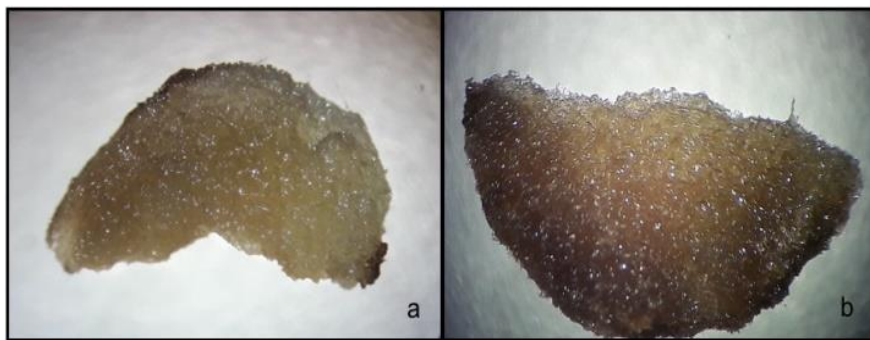
Figure 4.62. Von Kossa staining of Saos-2 cells on chitosan scaffolds for 21day and 28day incubation respectively.

Von kossa stained composite scaffolds showed that Saos-2 cells were distributed homogenously and induced mineral formation on both chitosan-diatomite and chitosan-POSS composite scaffolds (Figure 4.63, Figure 4.64).

Figure 4.63. Von Kossa staining of Saos-2 cells on chitosan-diatomite composites for 21 and 28day incubation respectively. Chitosan-5% diatomite scaffold (a,b); chitosan-20% diatomite scaffold (c,d).

Figure 4.64. Von Kossa staining of Saos-2 cells on chitosan-POSS composites for 21 and 28day incubation respectively. Chitosan-5% POSS scaffold (a,b); chitosan-20% POSS scaffold (c,d).

4.2.5.2. Alizarin Red Staining

Alizarin red staining is commonly used to detect and quantify calcium, while von Kossa staining is used to visualize phosphate, within the deposited mineral (Hoemann et al., 2009). Calcium ions precipitate with alizarin, calcium deposits turn into red immediately when immersed in alizarin stain (Puchtler et al., 1969).

Mineral formation of MG-63 and Saos-2 cells on chitosan and chitosan composite scaffolds were determined by alizarin red staining. Stereomicroscopy images depicted in Figures 4.65.-4.70. showed that MG-63 and Saos-2 cells induced mineralization on chitosan, chitosan-diatomite and chitosan-POSS composite scaffolds for 21 and 28 day incubation periods. Scaffolds were cut into slices by surgical blade to observe the colour change. However a distinctive difference of colour change couldn't be observed between groups and incubation times as observed in von kossa staining. Consequently, mineral formation was detected on all composite groups.
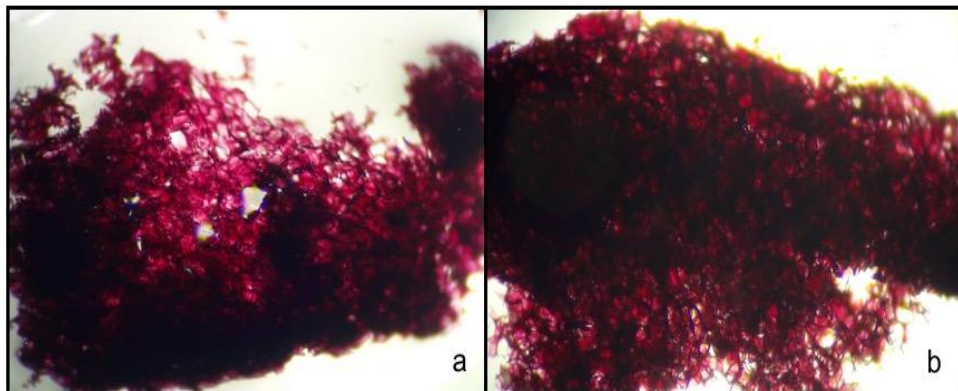
Figure 4.65. Alizarin red staining of MG-63 cells on chitosan scaffolds for 21day and 28day incubation respectively.
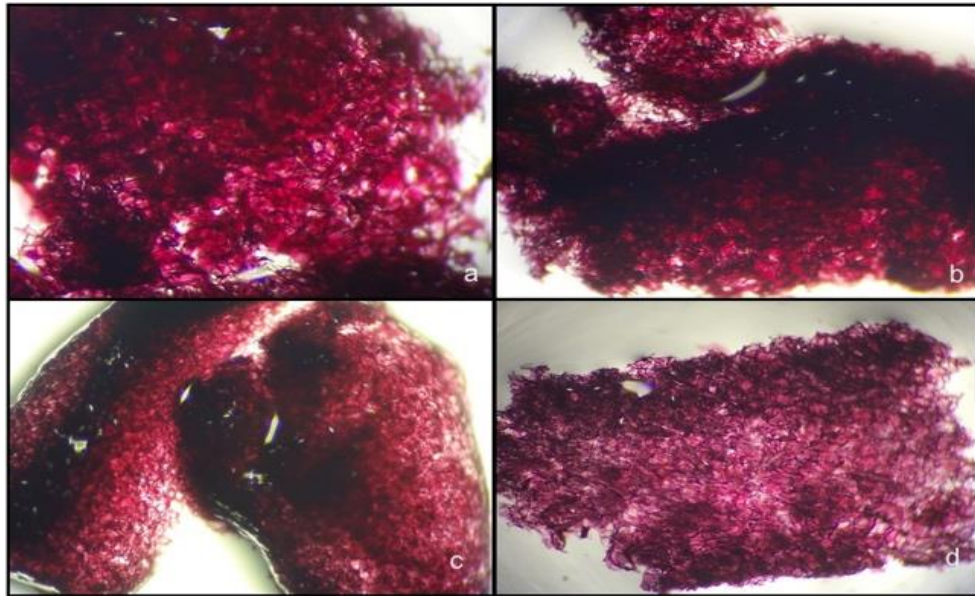
Figure 4.66. Alizarin red staining of MG-63 cells on chitosan-diatomite composites for 21 and 28day incubation respectively. Chitosan-5% diatomite scaffold (a,b); chitosan-20% diatomite scaffold (c,d).
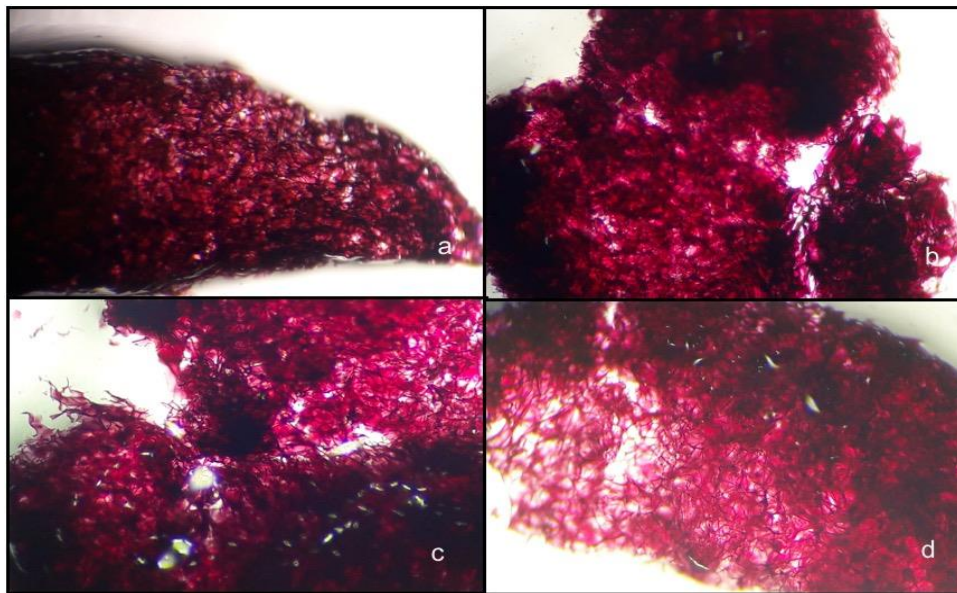
Figure 4.67. Alizarin red staining of MG-63 cells on chitosan-POSS composites for 21 and 28day incubation respectively. Chitosan-5% POSS scaffold (a,b); chitosan-20% POSS scaffold (c,d).
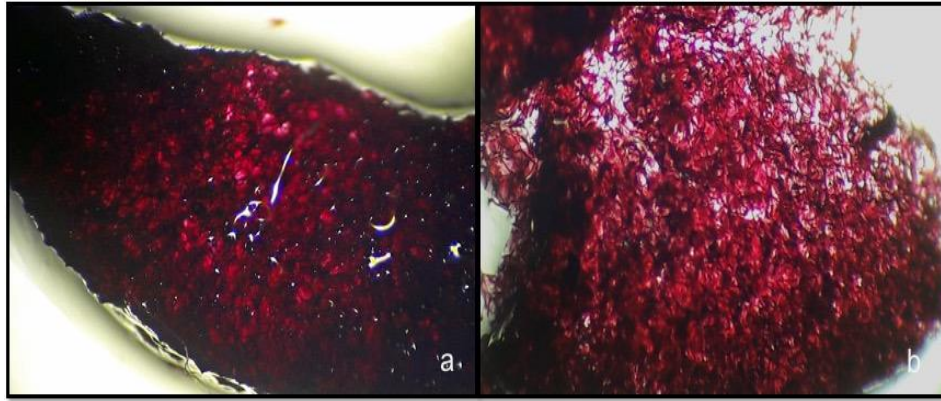
Figure 4.68. Alizarin red staining of Saos-2 cells on chitosan scaffolds for 21day and 28day incubation respectively.
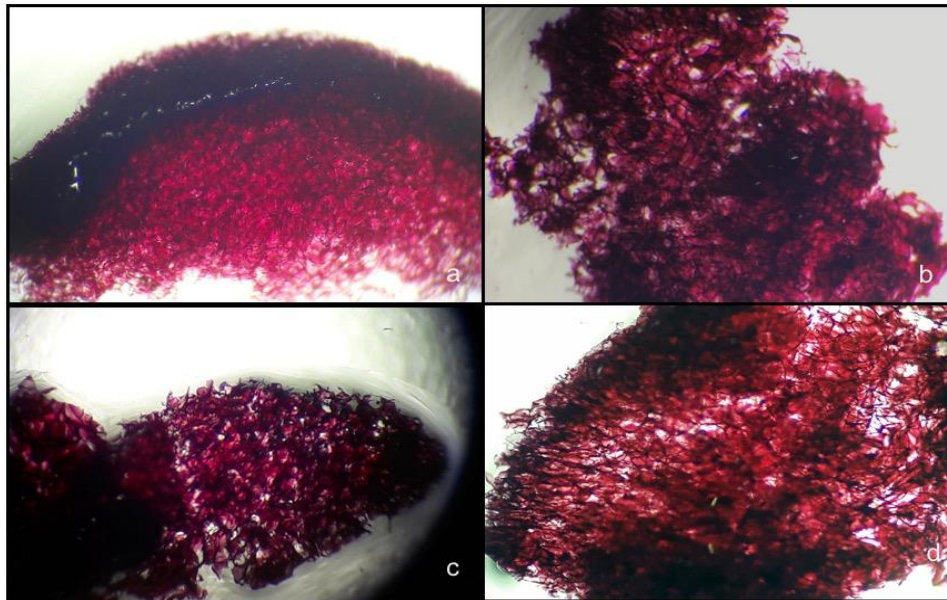
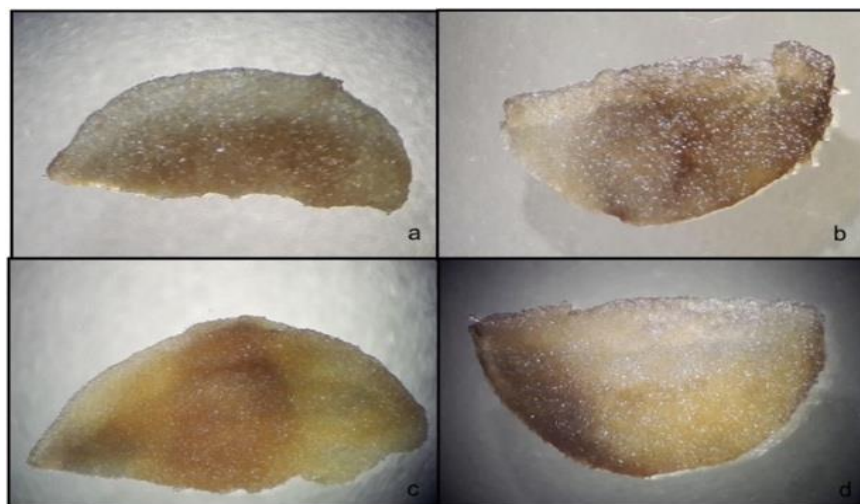Figure 4.69. Alizarin red staining of Saos-2 cells on chitosan-diatomite composites for 21d and 28day incubation respectively. Chitosan-5% diatomite scaffold (a,b); chitosan-20% diatomite scaffold (c,d).
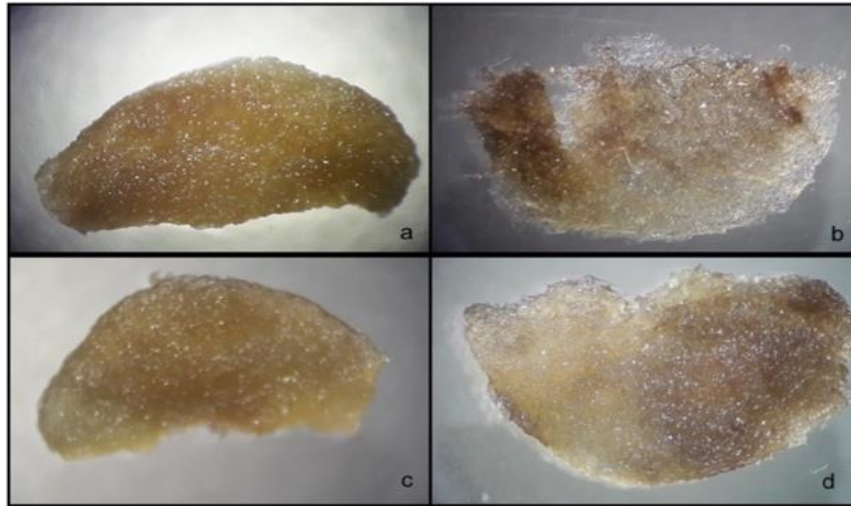
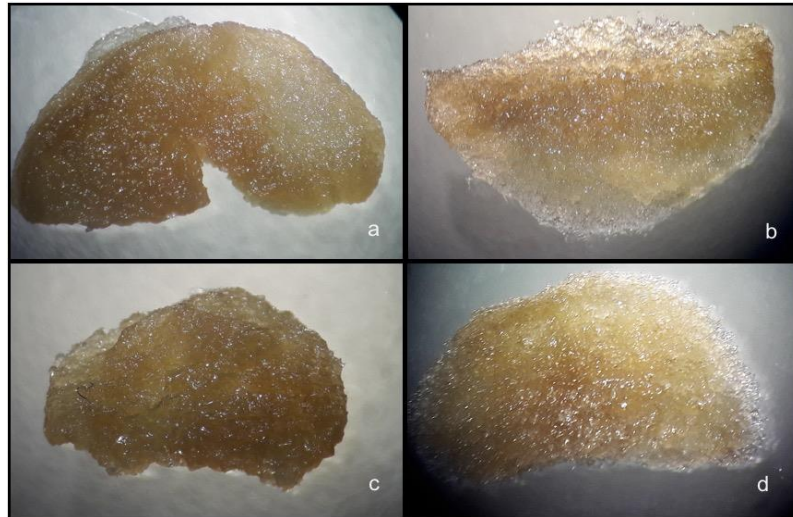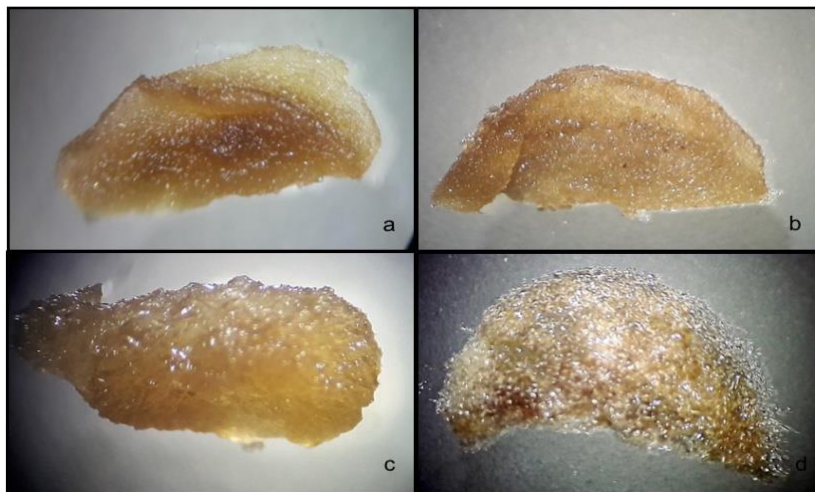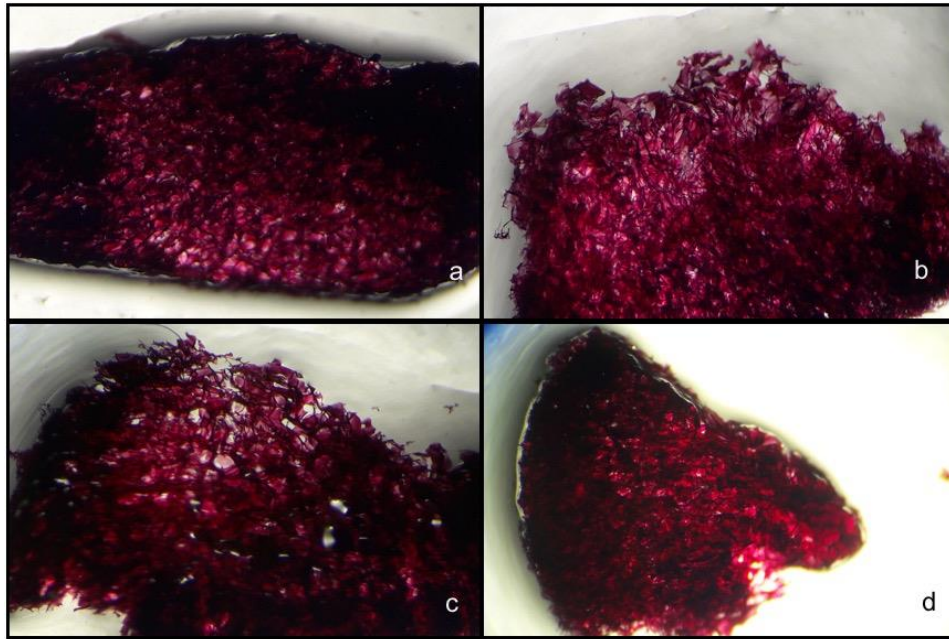Figure 4.70. Alizarin red staining of Saos-2 cells on chitosan-POSS composites for 21 and 28day incubation respectively. Chitosan-5% POSS scaffold (a,b); chitosan-20% POSS scaffold (c,d).

CHAPTER 5

CONCLUSIONS

The main objective of this dissertation was to develop a novel composite biomaterial for bone tissue engineering applications by silica incorporation in order to enhance mechanical properties and bioactivity. Therefore, this dissertation comprises the optimization of silica concentration in polymer matrix to determine desired mechanical, surface characteristics and bioactivity. In this study, chitosan-silica composite scaffolds were fabricated by freeze drying method by using two different silica sources; natural silica; *Diatomite* and *synthetic silica*, octa (tetramethylammonium) polyhedral oligomeric silsesquioxanes (OctaTMA-POSS). Diatomaceous earth (SiO_2-nH_2O) as a natural occurring mineral compound from microscopic skeletal remains of unicellular algae-like plants called diatoms has a mineralised exoskeleton termed as "frustule". In respect to the biogenic sources, the diatomaceous earth (diatomite) constitutes biogenic amorphous silica source and the most abundant form of silica on earth. POSS, regarded as the smallest possible particles of silica which has a hybrid chemical composition intermediate ($RSiO_{1.5}$) between that of silica (SiO_2) and silicone (R_2SiO). The effects of silica type and loading on the mechanical, morphological, chemical, and surface properties, wettability and biocompatibility of composite membranes were investigated and characterized by using SEM, AFM, contact angle analysis, swelling study, protein adsorption assay, biodegradation and biomineralization tests. *In vitro* cytotoxicity of chitosan-silica composites were determined by WST-1 cytotoxicity assay. *In vitro* cell culture studies were performed with three different osteoblast cell line, MG-63, Saos-2 and hFob due to the different characteristics and bone forming capacity. Cell proliferation on composite scaffolds was determined by using highly sensitive fluorometric rezasurin assay. Alkaline phosphatase activity which is an early indicator of bone tissue formation assay was performed by fluorometric ALP assay. *In vitro* biomineralization of osteoblast cells on composite scaffolds was determined by Von Kossa and Alizarin red staining.

SEM images of chitosan-silica composite scaffolds showed uniform highly porous structures. Chitosan-silica composites exhibited 82-90% porosity. Average pore size range of chitosan-diatomite and chitosan-POSS composite scaffolds was obtained

in the range of 15-180μm and 220-300μm, respectively. Composites with higher silica content showed higher pore sizes and pore surface areas.Wet chitosan-silica composite scaffolds exhibited higher compression moduli when compared to pure chitosan scaffold in the range of 67.3-81.4 kPa for chitosan -diatomite and 78.1 to 107.6 kPa for chitosan-POSS composites, respectively. Results clearly showed that the scaffold porosity and mechanical properties were strongly related. Despite being an important factor for bone ingrowth, higher pore size and porosity conduced decrease in compressive strength of composite scaffolds in dry condition. The decrease in the pore wall thickness lead to larger and more interconnected pores with a higher void volume. This caused lower mechanical strength in all scaffold groups. Silica nanoparticle incorporation represented promising osteomimetic architecture with inherent properties such as increased wettability, roughness, and surface area. Comparison of two different composite systems, AFM images presented different surface topographies for chitosan-diatomite and chitosan-POSS composites. AFM results indicated that POSS and diatomite incorporation in chitosan scaffolds increased the surface roughness in the desired level for cell attachment. Static air-water contact angle analysis showed that diatomite and POSS particles did not conduce a significant change on the surface hydrophilicity of membranes. However, measured contact angles showed that composites had hydrophilic character in a range of 73.7-80.2 °. The pore size and pore surface area differences obtained with increasing silica content effected water uptake capacity of scaffolds positively. Besides, Diatomite and POSS silica particles lead to enhancement in the water uptake capacity of chitosan scaffold. Diatomite incorporated composites had higher water uptake values compared to chitosan/POSS composites due to the microparticle nature of diatomite frustules. Enzymatic degradation results indicated that chitosan-POSS composites showed higher weight loss% when compared with chitosan-diatomite composites. Both diatomite and POSS composites with high content (20-40%) showed a decrease in weight loss% for 28day incubation due to possible dissolution of silica particles simultaneously with degradation process. This fact may cause the break down of the structural integrity of scaffolds. In addition, three dimensional structure and high porosity of composite scaffolds had a promoting effect on degradation rate. Mineralization studies indicated that silica particles initiated the mineral formation on scaffold surface. As reported in literature, the Si–OH groups had a role in initiation of the apatite formation through the hydration and dissolution of the silica network.

In vitro cytotoxicity results indicated that chitosan-silica composites did not show any cytotoxic effect on 3T3 fibroblast, MG-63 and Saos-2 osteoblast like cell lines. Cell attachment and spreading study results showed that diatomite and POSS particles had a positive effect on cell attachment on scaffold surface by altering surface topography and increasing surface roughness. Chitosan-silica composites were found to be favorable for osteoblast proliferation. Diatomite and POSS incorporated chitosan scaffolds showed high ALP activity which is an early osteogenic differentiation marker for bone tissue regeneration. Mineral formation of cells incubated on composite scaffold was detected by Von kossa and Alizarin Red staining. Stereomicroscopy images showed that MG-63 and Saos-2 cells induced mineralization on chitosan-diatomite and chitosan-POSS composite scaffolds for 21 and 28day incubation periods. However, a distinctive difference of colour change couldn't be observed between groups and incubation times. As a result, novel chitosan-diatomite and chitosan-POSS composite scaffolds prepared in this study could be used as promising biomaterials for bone tissue engineering applications.

In future studies, calcinated diatomite particles and different POSS structures could be used as reinforcements and the effect of this structural differences can be examined to design new composites. In addition to the performed *in vitro* studies, collagen formation, which is an important factor for bone regeneration, could be observed by immuno histochemical staining. Besides silica incorporation, scaffold microarchitecture can be designed as a multilayer structure comprising different morphological characteristics in order to provide favourable biomaterial for soft to hard tissue interfaces such as bone-ligament, bone-cartilage and bone-tendon which are critical for joint motion and stabilization. The complex interface between damaged soft and hard tissues can be damaged during reconstructive surgery using fixation grafts, which fail to integrate into the host tissues. Therefore, it is critical to develop gradient organization and regeneration. These interfaces can be designed and characterized by gradient biomaterials with anisotropical properties, such as composition, structure, mechanics and biomolecular properties.

REFERENCES

Arca, H. Ç., & Şenel, S. (2008). Chitosan based systems for tissue engineering part 1: hard tissues. *FABAD J. Pharm. Sci*, *33*, 35-49.

Alves, N. M., Leonor, I. B., Azevedo, H. S., Reis, R. L., & Mano, J. F. (2010). Designing biomaterials based on biomineralization of bone. *Journal of Materials Chemistry*, *20*(15), 2911-2921.

Amini, A. R., Laurencin, C. T., & Nukavarapu, S. P. (2012). Bone tissue engineering: recent advances and challenges. *Critical Reviews™ in Biomedical Engineering*, *40*(5).

Anselme, K. (2000). Osteoblast adhesion on biomaterials. *Biomaterials*, *21*(7), 667-681.

Arboleya, L., & Castaneda, S. (2013). Osteoimmunology: the study of the relationship between the immune system and bone tissue. *Reumatología Clínica (English Edition)*, *9*(5), 303-315.

Bakr, H. E. G. M. M. (2010). Diatomite: its characterization, modifications and applications. *Asian journal of materials science*, *2*(3), 121-136.

Balas, F., Pérez-Pariente, J., & Vallet-Regí, M. (2003). In vitro bioactivity of silicon-substituted hydroxyapatites. *Journal of Biomedical Materials Research Part A*, *66*(2), 364-375.

Bainor, A., Chang, L., McQuade, T. J., Webb, B., & Gestwicki, J. E. (2011). Bicinchoninic acid (BCA) assay in low volume. *Analytical biochemistry*, *410*(2), 310-312.

Beniash, E. (2011). Biominerals-hierarchical nanocomposites: the example of bone. *Wiley Interdisciplinary Reviews: Nanomedicine and Nanobiotechnology*, *3*(1), 47-69.

Berridge, M. V., Tan, A. S., McCoy, K. D., & Wang, R. (1996). The biochemical and cellular basis of cell proliferation assays that use tetrazolium salts. *Biochemica*, *4*(1), 14-19.

Bellucci, D., Sola, A., & Cannillo, V. (2015). Hydroxyapatite and tricalcium phosphate composites with bioactive glass as second phase: State of the art and current applications. *Journal of Biomedical Materials Research Part A*.

Bhatia, S. K. (2010). Tissue engineering for clinical applications. *Biotechnology journal*, *5*(12), 1309-1323.

Billiau, A., Edy, V. G., Heremans, H., Van Damme, J., Desmyter, J., Georgiades, J. A., & De Somer, P. (1977). Human interferon: mass production in a newly established cell line, MG-63. *Antimicrobial agents and chemotherapy*, *12*(1), 11-15.

Boccaccini, A. R., Keim, S., Ma, R., Li, Y., & Zhitomirsky, I. (2010). Electrophoretic deposition of biomaterials. *Journal of The Royal Society Interface*, *7*(Suppl 5), S581-S613.

Bonfield, W. (2006). Designing porous scaffolds for tissue engineering. *Philosophical Trnsactions of the Royal Society of London A: Mathematical, Physical and Engineering Sciences*, *364*(1838), 227-232.

Bose, S., Roy, M., & Bandyopadhyay, A. (2012). Recent advances in bone tissue engineering scaffolds. *Trends in biotechnology*, *30*(10), 546-554.

Bueno, E. M., & Glowacki, J. (2009). Cell-free and cell-based approaches for bone regeneration. *Nature Reviews Rheumatology*, *5*(12), 685-697.

Burg, K. J., Porter, S., & Kellam, J. F. (2000). Biomaterial developments for bone tissue engineering. *Biomaterials*, *21*(23), 2347-2359.

Cai, L., Chen, J., Rondinone, A. J., & Wang, S. (2012). Injectable and biodegradable nanohybrid polymers with simultaneously enhanced stiffness and toughness for bone repair. *Advanced Functional Materials*, *22*(15), 3181-3190.

Chen, G., Ushida, T., & Tateishi, T. (2002). Scaffold design for tissue engineering. *Macromolecular Bioscience*, *2*(2), 67-77.

Chen, Q., Roether, J. A., & Boccaccini, A. R. (2008). Tissue engineering scaffolds from bioactive glass and composite materials. *Topics in tissue engineering*, *4*, 1-27.

Cheung, H. Y., Lau, K. T., Lu, T. P., & Hui, D. (2007). A critical review on polymer-based bio-engineered materials for scaffold development. *Composites Part B: Engineering*, *38*(3), 291-300.

Chew, S. L., Wang, K., Chai, S. P., & Goh, K. L. (2011). Elasticity, thermal stability and bioactivity of polyhedral oligomeric silsesquioxanes reinforced chitosan-based microfibres. *Journal of Materials Science: Materials in Medicine*, *22*(6), 1365-1374.

Cooney, M. J., Lau, C., Windmeisser, M., Liaw, B. Y., Klotzbach, T., & Minteer, S. D. (2008). Design of chitosan gel pore structure: towards enzyme catalyzed flow-through electrodes. *Journal of Materials Chemistry*, *18*(6), 667-674.

Costa-Pinto, A. R., Reis, R. L., & Neves, N. M. (2011). Scaffolds based bone tissue engineering: the role of chitosan. *Tissue Engineering Part B: Reviews*, *17*(5), 331-347. Croisier, F., & Jérôme, C. (2013). Chitosan-based biomaterials for tissue engineering. *European Polymer Journal*, *49*(4), 780-792.

Czekanska, E. M., Stoddart, M. J., Richards, R. G., & Hayes, J. S. (2012). In search of an osteoblast cell model for in vitro research. *Eur Cell Mater*, *24*(4), 1-17.

Dash, M., Chiellini, F., Ottenbrite, R. M., & Chiellini, E. (2011). Chitosan-A versatile semi-synthetic polymer in biomedical applications. *Progress in polymer science*, *36*(8), 981-1014.

DeArmitt, C. (2010). Polyherdral Oligomeric Silesquioxane Handbook. *Phanom Plastics*.

Deepthi, S., Venkatesan, J., Kim, S. K., Bumgardner, J. D., & Jayakumar, R. (2016). An overview of chitin or chitosan/nano ceramic composite scaffolds for bone tissue engineering. *International journal of biological macromolecules*.

Di Martino, A., Sittinger, M., & Risbud, M. V. (2005). Chitosan: a versatile biopolymer for orthopaedic tissue-engineering. *Biomaterials, 26*(30), 5983-5990.

Du, Y., Yu, M., Chen, X., Ma, P. X., & Lei, B. (2016). Development of Biodegradable Poly (citrate)-Polyhedral Oligomeric Silsesquioxanes Hybrid Elastomers with High Mechanical Properties and Osteogenic Differentiation Activity. *ACS applied materials & interfaces*, 8(5), 3079-3091.

El Yacoubi, A., Massit, A., Fathi, M., El Idrissi, B. C., & Yamni, K. (2014). Characterization of silicon-substituted hydroxyapatite powders synthesized by a wet precipitation method. *IOSR J. Appl. Chem.*, 7(11), 24-29.

Faucheux, N., Schweiss, R., Lützow, K., Werner, C., & Groth, T. (2004). Self-assembled monolayers with different terminating groups as model substrates for cell adhesion studies. *Biomaterials*, 25(14), 2721-2730.

Feng, X. (2009). Chemical and biochemical basis of cell-bone matrix interaction in health and disease. *Current chemical biology*, 3(2), 189-196.

Fernandez-Yague M.A., Abbah S.A., McNamara L., Zeugolis D.I., Pandit A., Biggs M.J. (2015.) Biomimetic approaches in bone tissue engineering: Integrating biological and physicomechanical strategies. *Advanced Drug Delivery Reviews*, 84, 1-29.

Fernández, M. D., Fernández, M. J., & Cobos, M. (2016). Effect of polyhedral oligomeric silsesquioxane (POSS) derivative on the morphology, thermal, mechanical and surface properties of poly (lactic acid)-based nanocomposites. *Journal of Materials Science*, 51(7), 3628-3642.

Freemont, A. J. (1993). Basic bone cell biology. *International journal of experimental pathology*, 74(4), 411.

Freier, T., Koh, H. S., Kazazian, K., & Shoichet, M. S. (2005). Controlling cell adhesion and degradation of chitosan films by N-acetylation. *Biomaterials*, 26(29), 5872-5878.

Frohlich, M., Grayson, W. L., Wan, L. Q., Marolt, D., Drobnic, M., & Vunjak-Novakovic, G. (2008). Tissue engineered bone grafts: biological requirements, tissue culture and clinical relevance. *Current stem cell research & therapy*, 3(4), 254-264.

Fuhrmann, T., Landwehr, S., El Rharbi-Kucki, M., & Sumper, M. (2004). Diatoms as living photonic crystals.*Applied Physics B*, 78(3-4), 257-260.

Gaddis, C. S., & Sandhage, K. H. (2004). Freestanding microscale 3D polymeric structures with biologically-derived shapes and nanoscale features. *Journal of materials research*, *19*(09), 2541-2545.

Ghanbari, H., Cousins, B. G., & Seifalian, A. M. (2011). A nanocage for nanomedicine: polyhedral oligomeric silsesquioxane (POSS). *Macromolecular rapid communications*, *32*(14), 1032-1046.

Gibson, I. R., Best, S. M., & Bonfield, W. (1999). Chemical characterization of silicon-substituted hydroxyapatite. *Journal of biomedical materials research*, *44*(4), 422-428.

Giesche, H. (2006). Mercury porosimetry: a general (practical) overview. *Particle & particle systems characterization*, *23*(1), 9-19.

Golub, E. E., & Boesze-Battaglia, K. (2007). The role of alkaline phosphatase in mineralization. *Current Opinion in Orthopaedics*, *18*(5), 444-448.

Gong, T., Xie, J., Liao, J., Zhang, T., Lin, S., & Lin, Y. (2015). Nanomaterials and bone regeneration. *Bone research*, *3*, 15029.

Gordon, R., & Parkinson, J. (2005). Potential roles for diatomists in nanotechnology. *Journal of Nanoscience and Nanotechnology*, *5*(1), 35-40.

Gültürk, E., & Güden, M. (2011). Thermal and acid treatment of diatom frustules.

Ha, Y. M., Amna, T., Kim, M. H., Kim, H. C., Hassan, M. S., & Khil, M. S. (2013). Novel silicificated PVAc/POSS composite nanofibrous mat via facile electrospinning technique: potential scaffold for hard tissue engineering. *Colloids and Surfaces B: Biointerfaces*, *102*, 795-802.

Hadjar, H., Hamdi, B., Jaber, M., Brendlé, J., Kessaissia, Z., Balard, H., & Donnet, J. B. (2008). Elaboration and characterisation of new mesoporous materials from diatomite and charcoal. *Microporous and Mesoporous Materials*, *107*(3), 219-226.

Hamilton, V., Yuan, Y., Rigney, D. A., Puckett, A. D., Ong, J. L., Yang, Y.,& Bumgardner, J. D. (2006). Characterization of chitosan films and effects on fibroblast cell attachment and proliferation. *Journal of Materials Science: Materials in Medicine*, *17*(12), 1373-1381.

Hamm, C. E., Merkel, R., Springer, O., Jurkojc, P., Maier, C., Prechtel, K., & Smetacek, V. (2003). Architecture and material properties of diatom shells provide effective mechanical protection. *Nature*, *421*(6925), 841-843.

Han, T., Nwe, N., Furuike, T., Tokura, S., & Tamura, H. (2012). Methods of N-acetylated chitosan scaffolds and its in-vitro biodegradation by lysozyme.

Harris, S. A., Enger, R. J., Riggs, L. B., & Spelsberg, T. C. (1995). Development and characterization of a conditionally immortalized human fetal osteoblastic cell line. *Journal of Bone and Mineral Research*, *10*(2), 178-186.

Hench, L. L., & Wilson, J. (Eds.). (1993). *An introduction to bioceramics* (Vol. 1). World Scientific.

Hench, L. L., & Polak, J. M. (2002). Third-generation biomedical materials. *Science*, *295*(5557), 1014-1017.

Henkel, J., Woodruff, M. A., Epari, D. R., Steck, R., Glatt, V., Dickinson, I. C.&Hutmacher, D. W. (2013). Bone regeneration based on tissue engineering conceptions—a 21st century perspective. *Bone research*, *1*(3), 216.

Hoppe, A., Güldal, N. S., & Boccaccini, A. R. (2011). A review of the biological response to ionic dissolution products from bioactive glasses and glass-ceramics. *Biomaterials*, *32*(11), 2757-2774.

Heremans, H., Billiau, A., Cassiman, J. J., Mulier, J. C., & De Somer, P. (1978). In vitro cultivation of human tumor tissues II. Morphological and virological characterization of three cell lines. *Oncology*, *35*(6), 246-252.

Hoemann, C. D., El-Gabalawy, H., & McKee, M. D. (2009). In vitro osteogenesis assays: influence of the primary cell source on alkaline phosphatase activity and mineralization. Pathologie Biologie, 57(4), 318-323.

Holzwarth, J. M., & Ma, P. X. (2011). Biomimetic nanofibrous scaffolds for bone tissue engineering. *Biomaterials*, *32*(36), 9622-9629.

Hu, Q., Li, B., Wang, M., & Shen, J. (2004). Preparation and characterization of biodegradable chitosan/hydroxyapatite nanocomposite rods via in situ hybridization: a potential material as internal fixation of bone fracture. *Biomaterials*, *25*(5), 779-785.

Ho, S. T., & Hutmacher, D. W. (2006). A comparison of micro CT with other techniques used in the characterization of scaffolds. *Biomaterials*, *27*(8), 1362-1376.

Hutmacher, D. W., Schantz, J. T., Lam, C. X. F., Tan, K. C., & Lim, T. C. (2007). State of the art and future directions of scaffold-based bone engineering from a biomaterials perspective. *Journal of tissue engineering and regenerative medicine*, *1*(4), 245-260.

Jayakumar, R., Menon, D., Manzoor, K., Nair, S. V., & Tamura, H. (2010). Biomedical applications of chitin and chitosan based nanomaterials—A short review. *Carbohydrate Polymers*, *82*(2), 227-232.

Jayakumar, P., & Di Silvio, L. (2010). Osteoblasts in bone tissue engineering. *Proceedings of the Institution of Mechanical Engineers, Part H: Journal of Engineering in Medicine*, *224*(12), 1415-1440.

Johnson, D. J., Miles, N. J., & Hilal, N. (2006). Quantification of particle–bubble interactions using atomic force microscopy: A review. *Advances in colloid and interface science*, *127*(2), 67-81.

Jones, J. R. (2009). New trends in bioactive scaffolds: the importance of nanostructure. *Journal of the European Ceramic Society*, *29*(7), 1275-1281.

Jones, J. R. (2013). Review of bioactive glass: from Hench to hybrids. *Acta biomaterialia*, *9*(1), 4457-4486.

Jongwattanapisan, P., Charoenphandhu, N., Krishnamra, N., Thongbunchoo, J., Tang, I. M., Hoonsawat, R., & Pon-On, W. (2011). In vitro study of the SBF and osteoblast-like cells on hydroxyapatite/chitosan–silica nanocomposite. *Materials Science and Engineering: C*, *31*(2), 290-299.

Kavya, K. C., Dixit, R., Jayakumar, R., Nair, S. V., & Chennazhi, K. P. (2012). Synthesis and characterization of chitosan/chondroitin sulfate/nano-SiO2 composite scaffold for bone tissue engineering. *Journal of biomedical nanotechnology*, *8*(1), 149-160.

Kanezashi, M., Shioda, T., Gunji, T., & Tsuru, T. (2012). Gas permeation properties of silica membranes with uniform pore sizes derived from polyhedral oligomeric silsesquioxane. *AIChE Journal*, *58*(6), 1733-1743.

Kannan, R. Y., Salacinski, H. J., Butler, P. E., & Seifalian, A. M. (2005). Polyhedral oligomeric silsesquioxane nanocomposites: the next generation material for biomedical applications. *Accounts of chemical research*, *38*(11), 879-884.

Kastis, D., Kakali, G., Tsivilis, S., & Stamatakis, M. G. (2006). Properties and hydration of blended cements with calcareous diatomite. *Cement and concrete research*, *36*(10), 1821-1826.

Katti, K. S., Katti, D. R., & Dash, R. (2008). Synthesis and characterization of a novel chitosan/montmorillonite/hydroxyapatite nanocomposite for bone tissue engineering. *Biomedical Materials*, *3*(3), 034122.

Katsanevakis, E., Wen, X. J., Shi, D. L., & Zhang, N. (2010). Biomineralization of polymer scaffolds. In *Key Engineering Materials* (Vol. 441, pp. 269-295). Trans Tech Publications.

Karageorgiou, V., & Kaplan, D. (2005). Porosity of 3D biomaterial scaffolds and osteogenesis. *Biomaterials*, *26*(27), 5474-5491.

Karande, T. S., Ong, J. L., & Agrawal, C. M. (2004). Diffusion in musculoskeletal tissue engineering scaffolds: design issues related to porosity, permeability, architecture, and nutrient mixing. *Annals of biomedical engineering*, *32*(12), 1728-1743.

Kartsogiannis, V., & Ng, K. W. (2004). Cell lines and primary cell cultures in the study of bone cell biology. *Molecular and cellular endocrinology*, *228*(1), 79-102.

Kaur, G., Pandey, O. P., Singh, K., Homa, D., Scott, B., & Pickrell, G. (2014). A review of bioactive glasses: their structure, properties, fabrication and apatite formation. *Journal of Biomedical Materials Research Part A*, *102*(1), 254-274.

Kavya, K. C., Jayakumar, R., Nair, S., & Chennazhi, K. P. (2013). Fabrication and characterization of chitosan/gelatin/nSiO 2 composite scaffold for bone tissue engineering. *International journal of biological macromolecules*, *59*, 255-263.

Ke, Y. C., & Stroeve, P. (2005). *Polymer-layered silicate and silica nanocomposites*. Elsevier.

Kepa, K., Coleman, R., & Grøndahl, L. (2015). In vitro mineralization of functional polymers. *Biosurface and Biotribology*, *1*(3), 214-227.

Kean, T., & Thanou, M. (2010). Biodegradation, biodistribution and toxicity of chitosan. *Advanced drug delivery reviews*, *62*(1), 3-11.

Kim, I. Y., Seo, S. J., Moon, H. S., Yoo, M. K., Park, I. Y., Kim, B. C., & Cho, C. S. (2008). Chitosan and its derivatives for tissue engineering applications. *Biotechnology advances*, *26*(1), 1-21.

Latour, R. A. (2005). Biomaterials: protein-surface interactions. *Encyclopedia of biomaterials and biomedical engineering*, *1*, 270-278.

Le, T. D. H., Bonani, W., Speranza, G., Sglavo, V., Ceccato, R., Maniglio, D., & Migliaresi, C. (2016). Processing and characterization of diatom nanoparticles and microparticles as potential source of silicon for bone tissue engineering. *Materials Science and Engineering: C*, *59*, 471-479.

Lee, K. T., Liu, D. M., Liang, Y. Y., Matsushita, N., Ikomac, T., & Lu, S. Y. (2014). Materials Chemistry B.

Lehmann, G., Cacciotti, I., Palmero, P., Montanaro, L., Bianco, A., Campagnolo, L., & Camaioni, A. (2012). Differentiation of osteoblast and osteoclast precursors on pure and silicon-substituted synthesized hydroxyapatites. *Biomedical Materials*, *7*(5), 055001.

Levengood, S. K. L., & Zhang, M. (2014). Chitosan-based scaffolds for bone tissue engineering. *Journal of Materials Chemistry B*, *2*(21), 3161-3184.

Li, L. H., Zhao, M. Y., Ding, S., & Zhou, C. R. (2011). Rapid biomimetic mineralization of chitosan scaffolds with a precursor sacrificed method in ethanol/water mixed solution. *Express Polym. Lett*, *5*(6), 545-554.

Li, K., Sun, H., Sui, H., Zhang, Y., Liang, H., Wu, X., & Zhao, Q. (2015). Composite mesoporous silica nanoparticle/chitosan nanofibers for bone tissue engineering. *RSC Advances*, *5*(23), 17541-17549.

Liao, F., Chen, Y., Li, Z., Wang, Y., Shi, B., Gong, Z., & Cheng, X. (2010). A novel bioactive three-dimensional β-tricalcium phosphate/chitosan scaffold for periodontal tissue engineering. *Journal of Materials Science: Materials in Medicine*, *21*(2), 489-496.

Liu, X., Lim, J. Y., Donahue, H. J., Dhurjati, R., Mastro, A. M., & Vogler, E. A. (2007). Influence of substratum surface chemistry/energy and topography on the human fetal

osteoblastic cell line hFOB 1.19: phenotypic and genotypic responses observed in vitro. *Biomaterials*, *28*(31), 4535-4550.

Lopez-Alvarez, M., Solla, E. L., González, P., Serra, J., Leon, B., Marques, A. P., & Reis, R. L. (2009). Silicon–hydroxyapatite bioactive coatings (Si–HA) from diatomaceous earth and silica. Study of adhesion and proliferation of osteoblast-like cells. *Journal of Materials Science: Materials in Medicine*, *20*(5), 1131-1136.

Lyons, F., Partap, S., & O'Brien, F. J. (2008). Part 1: scaffolds and surfaces. *Technology and Health Care*, *16*(4), 305-317.

Madhumathi, K., Kumar, P. S., Kavya, K. C., Furuike, T., Tamura, H., Nair, S. V., & Jayakumar, R. (2009). Novel chitin/nanosilica composite scaffolds for bone tissue engineering applications. *International journal of biological macromolecules*, *45*(3), 289-292.

Mekayarajjananonth, T., & Winkler, S. (1999). Contact angle measurement on dental implant biomaterials. *Journal of Oral Implantology*, *25*(4), 230-236.

Meloan, S. N., & Puchtler, H. (1985). Chemical mechanisms of staining methods: von Kossa's technique: what von Kossa really wrote and a modified reaction for selective demonstration of inorganic phosphates. *Journal of Histotechnology*, *8*(1), 11-13.

Menzies, K. L., & Jones, L. (2010). The impact of contact angle on the biocompatibility of biomaterials. *Optometry & Vision Science*, *87*(6), 387-399.

Mieszawska, A. J., Fourligas, N., Georgakoudi, I., Ouhib, N. M., Belton, D. J., Perry, C. C., & Kaplan, D. L. (2010). Osteoinductive silk–silica composite biomaterials for bone regeneration. *Biomaterials*, *31*(34), 8902-8910.

Moura, J., Teixeira, L. N., Ravagnani, C., Peitl, O., Zanotto, E. D., Beloti, M. M., ... & de Oliveira, P. T. (2007). In vitro osteogenesis on a highly bioactive glass-ceramic (Biosilicate®). *Journal of Biomedical Materials Research Part A*, *82*(3), 545-557.

Murray, E., Provvedini, D., Curran, D., Catherwood, B., Sussman, H., & Manolagas, S. (1987). Characterization of a human osteoblastic osteosarcoma cell line (SAOS-2) with high bone alkaline phosphatase activity. *Journal of Bone and Mineral Research*, *2*(3), 231-238.

Muzzarelli, R. A. (2011). Chitosan composites with inorganics, morphogenetic proteins and stem cells, for bone regeneration. *Carbohydrate Polymers*, *83*(4), 1433-1445.

Nair, B. P., Gangadharan, D., Mohan, N., Sumathi, B., & Nair, P. D. (2015). Hybrid scaffold bearing polymer-siloxane Schiff base linkage for bone tissue engineering. *Materials Science and Engineering: C*, *52*, 333-342.

Navarro, M., Michiardi, A., Castano, O., & Planell, J. A. (2008). Biomaterials in orthopaedics. *Journal of the Royal Society Interface*, *5*(27), 1137-1158.

Noll, F., Sumper, M., & Hampp, N. (2002). Nanostructure of diatom silica surfaces and of biomimetic analogues. Nano Letters, 2(2), 91-95.

Oliveira, J. M., Rodrigues, M. T., Silva, S. S., Malafaya, P. B., Gomes, M. E., Viegas, C. A., & Reis, R. L. (2006). Novel hydroxyapatite/chitosan bilayered scaffold for osteochondral tissue-engineering applications: Scaffold design and its performance when seeded with goat bone marrow stromal cells. *Biomaterials*, *27*(36), 6123-6137.

Oliveira, Joaquim M., et al. "Novel hydroxyapatite/carboxymethylchitosan composite scaffolds prepared through an innovative "autocatalytic" electroless coprecipitation route." *Journal of Biomedical Materials Research Part A* 88.2 (2009): 470-480.

Oyane, A., Kim, H. M., Furuya, T., Kokubo, T., Miyazaki, T., & Nakamura, T. (2003). Preparation and assessment of revised simulated body fluids. *Journal of Biomedical Materials Research Part A*, *65*(2), 188-195.

Palmer, L. C., Newcomb, C. J., Kaltz, S. R., Spoerke, E. D., & Stupp, S. I. (2008). Biomimetic systems for hydroxyapatite mineralization inspired by bone and enamel. *Chemical reviews*, *108*(11), 4754-4783.

Pandis, C., Madeira, S., Matos, J., Kyritsis, A., Mano, J. F., & Ribelles, J. L. G. (2014). Chitosan–silica hybrid porous membranes. *Materials Science and Engineering: C*, *42*, 553-561.

Parkinson, J., & Gordon, R. (1999). Beyond micromachining: the potential of diatoms.*Trends in biotechnology*,*17*(5), 190-196.

Pautke, C., Schieker, M., Tischer, T., Kolk, A., Neth, P., Mutschler, W., & Mılz, S. (2004). Characterization of osteosarcoma cell lines MG-63, Saos-2 and U-2 OS in comparison to human osteoblasts. *Anticancer research*, *24*(6), 3743-3748.

Peter, M., Ganesh, N., Selvamurugan, N., Nair, S. V., Furuike, T., Tamura, H., & Jayakumar, R. (2010). Preparation and characterization of chitosan–gelatin/nanohydroxyapatite composite scaffolds for tissue engineering applications. *Carbohydrate Polymers*, *80*(3), 687-694.

Peyrin, F. (2011). Evaluation of bone scaffolds by micro-CT. *Osteoporosis International*, *22*(6), 2043-2048.

Pietak, A. M., Reid, J. W., Stott, M. J., & Sayer, M. (2007). Silicon substitution in the calcium phosphate bioceramics. *Biomaterials*, *28*(28), 4023-4032.
Prashanth, K. H., & Tharanathan, R. N. (2007). Chitin/chitosan: modifications and their unlimited application potential—an overview. *Trends in food science & technology*, *18*(3), 117-131.

Pielichowska, K., & Blazewicz, S. (2010). Bioactive polymer/hydroxyapatite (nano) composites for bone tissue regeneration. In *Biopolymers* (pp. 97-207). Springer Berlin Heidelberg.

Ponten, J., & Saksela, E. (1967). Two established in vitro cell lines from human mesenchymal tumours. *International journal of cancer*, *2*(5), 434-447.

Puchtler, H., Meloan, S. N., & Terry, M. S. (1969). On the history and mechanism of alizarin and alizarin red S stains for calcium. *Journal of Histochemistry & Cytochemistry*, *17*(2), 110-124.

Puppi, D., Chiellini, F., Piras, A. M., & Chiellini, E. (2010). Polymeric materials for bone and cartilage repair. *Progress in Polymer Science*, *35*(4), 403-440.

Quarles, L. D., Yohay, D. A., Lever, L. W., Caton, R., & Wenstrup, R. J. (1992). Distinct proliferative and differentiated stages of murine MC3T3-E1 cells in culture: An in vitro model of osteoblast development. *Journal of Bone and Mineral Research*, *7*(6), 683-692.

Ramay, H. R., & Zhang, M. (2003). Preparation of porous hydroxyapatite scaffolds by combination of the gel-casting and polymer sponge methods. *Biomaterials*, *24*(19), 3293-3302.

Rahaman, M. N., Day, D. E., Bal, B. S., Fu, Q., Jung, S. B., Bonewald, L. F., & Tomsia, A. P. (2011). Bioactive glass in tissue engineering. *Acta biomaterialia*, *7*(6), 2355-2373.

Rao, L. G., Sutherland, M. K., Reddy, G. S., Siu-Caldera, M. L., Uskokovic, M. R., & Murray, T. M. (1996). Effects of 1α, 25-dihydroxy-16ene, 23yne-vitamin D 3 on osteoblastic function in human osteosarcoma SaOS-2 cells: differentiation-stage dependence and modulation by 17-β estradiol. *Bone*, *19*(6), 621-627.

Razak, S. I. A., Sharif, N., & Rahman, W. A. W. A. (2012). Biodegradable polymers and their bone applications: a review. *Int J Basic Appl Sci*, *12*(1), 31-49.

Ren, D., Yi, H., Wang, W., & Ma, X. (2005). The enzymatic degradation and swelling properties of chitosan matrices with different degrees of N-acetylation. *Carbohydrate Research*, *340*(15), 2403-2410.

Renò, F., Carniato, F., Rizzi, M., Marchese, L., Laus, M., & Antonioli, D. (2013). POSS/gelatin-polyglutamic acid hydrogel composites: Preparation, biological and mechanical characterization. *Journal of Applied Polymer Science*, *129*(2), 699-706.

Rizzi, S. C., Heath, D. J., Coombes, A. G. A., Bock, N., Textor, M., & Downes, S. (2001). Biodegradable polymer/hydroxyapatite composites: surface analysis and initial attachment of human osteoblasts. *Journal of Biomedical Materials Research*, *55*(4), 475-486.

Roudsari, J. M., & Mahjoub, S. (2012). Quantification and comparison of bone-specific alkaline phosphatase with two methods in normal and paget's specimens. *Caspian journal of internal medicine*, *3*(3), 478.

Rungby, J., Kassem, M., Eriksen, E. F., & Danscher, G. (1993). The von Kossa reaction for calcium deposits: silver lactate staining increases sensitivity and reduces background. *The Histochemical Journal*, *25*(6), 446-451.

Sabokbar, A., Millett, P. J., Myer, B., & Rushton, N. (1994). A rapid, quantitative assay for measuring alkaline phosphatase activity in osteoblastic cells in vitro. *Bone and mineral*, *27*(1), 57-67.

Saldaña, L., Bensiamar, F., Boré, A., & Vilaboa, N. (2011). In search of representative models of human bone-forming cells for cytocompatibility studies. *Acta biomaterialia*, *7*(12), 4210-4221.

Saravanan, S., Leena, R. S., & Selvamurugan, N. (2016). Chitosan based biocomposite scaffolds for bone tissue engineering. *International journal of biological macromolecules*.

Sarker, B., Hum, J., Nazhat, S. N., & Boccaccini, A. R. (2015). Combining collagen and bioactive glasses for bone tissue engineering: a review. *Advanced healthcare materials*, *4*(2), 176-194.

Seal, B. L., Otero, T. C., & Panitch, A. (2001). Polymeric biomaterials for tissue and organ regeneration. *Materials Science and Engineering: R: Reports*, *34*(4), 147-230.

Seibel, M. J. (2005). Biochemical markers of bone turnover part I: biochemistry and variability. *The Clinical biochemist. Reviews/Australian Association of Clinical Biochemists.*, *26*(4), 97.

Servoli, E., Maniglio, D., Aguilar, M. R., Motta, A., Vazquez, B., Roman, J. S., & Migliaresi, C. (2009). Comparative methods for the evaluation of protein adsorption. *Macromolecular bioscience*, *9*(7), 661-670.

Shirosaki, Y., Okayama, T., Tsuru, K., Hayakawa, S., & Osaka, A. (2008). Synthesis and cytocompatibility of porous chitosan–silicate hybrids for tissue engineering scaffold application. *Chemical Engineering Journal*, *137*(1), 122-128.

Shirosaki, Y., Tsuru, K., Hayakawa, S., Osaka, A., Lopes, M. A., Santos, J. D., ... & Fernandes, M. H. (2009). Physical, chemical and in vitro biological profile of chitosan hybrid membrane as a function of organosiloxane concentration. *Acta Biomaterialia*, *5*(1), 346-355.

Smith, P., Krohn, R. I., Hermanson, G. T., Mallia, A. K., Gartner, F. H., Provenzano, M., & Klenk, D. C. (1985). Measurement of protein using bicinchoninic acid. *Analytical biochemistry*, *150*(1), 76-85.

Sowjanya, J. A., Singh, J., Mohita, T., Sarvanan, S., Moorthi, A., Srinivasan, N., & Selvamurugan, N. (2013). Biocomposite scaffolds containing chitosan/alginate/nano-silica for bone tissue engineering. *Colloids and Surfaces B: Biointerfaces*, *109*, 294-300.

Subia, B., Kundu, J., & Kundu, S. C. (2010). *Biomaterial scaffold fabrication techniques for potential tissue engineering applications*. INTECH Open Access Publisher.

Subramaniam, M., Jalal, S. M., Rickard, D. J., Harris, S. A., Bolander, M. E., & Spelsberg, T. C. (2002). Further characterization of human fetal osteoblastic hFOB 1.19 and hFOB/ERα cells: Bone formation in vivo and karyotype analysis using multicolor fluorescent in situ hybridization. *Journal of cellular biochemistry*, *87*(1), 9-15.

Strzelczyk, F., Leterq, D., Wilhelm, A. M., & Steinbrunn, A. (1998). Gas–solid chromatographic separation of hydrogen isotopes: a comparison between two palladium bearing materials–alumina and kieselguhr.*Journal of Chromatography A,822*(2), 326-331.

Tang, X. J., Gui, L., & Lü, X. Y. (2008). Hard tissue compatibility of natural hydroxyapatite/chitosan composite. *Biomedical Materials*, *3*(4), 044115.

Tang, D., Tare, R. S., Yang, L. Y., Williams, D. F., Ou, K. L., & Oreffo, R. O. (2016). Biofabrication of bone tissue: approaches, challenges and translation for bone regeneration. *Biomaterials*, *83*, 363-382.

Thein-Han, W. W., & Misra, R. D. K. (2009). Biomimetic chitosan–nanohydroxyapatite composite scaffolds for bone tissue engineering. *Acta Biomaterialia*, *5*(4), 1182-1197.

Tsai, W. T., Lai, C. W., & Hsien, K. J. (2006). Characterization and adsorption properties of diatomaceous earth modified by hydrofluoric acid etching. *Journal of colloid and interface science,297*(2), 749-754.

Tsigkou, O., Hench, L. L., Boccaccini, A. R., Polak, J. M., & Stevens, M. M. (2007). Enhanced differentiation and mineralization of human fetal osteoblasts on PDLLA containing Bioglass® composite films in the absence of osteogenic supplements. *Journal of Biomedical Materials Research Part A*, *80*(4), 837-851.

Tzoneva, R., Faucheux, N., & Groth, T. (2007). Wettability of substrata controls cell–substrate and cell–cell adhesions. *Biochimica et Biophysica Acta (BBA)-General Subjects*, *1770*(11), 1538-1547.

Xu, L. C., & Siedlecki, C. A. (2007). Effects of surface wettability and contact time on protein adhesion to biomaterial surfaces. *Biomaterials*, *28*(22), 3273-3283.

Xu, D., Loo, L. S., & Wang, K. (2011). Characterization and diffusion behavior of chitosan–poss composite membranes. *Journal of Applied Polymer Science*, *122*(1), 427-435.

Xynos, I. D., Edgar, A. J., Buttery, L. D., Hench, L. L., & Polak, J. M. (2001). Gene-expression profiling of human osteoblasts following treatment with the ionic products of Bioglass® 45S5 dissolution. *Journal of biomedical materials research*, *55*(2), 151-157.

Vallet-Regí, M., & Ruiz-Hernández, E. (2011). Bioceramics: from bone regeneration to cancer nanomedicine. *Advanced Materials*, *23*(44), 5177-5218.

Vaz, M. F., Canhão, H., & Fonseca, J. E. (2011). *Bone: a composite natural material*. INTECH Open Access Publisher.

Venkatesan, J., & Kim, S. K. (2010). Chitosan composites for bone tissue engineering—An overview. *Marine drugs*, *8*(8), 2252-2266.

Voegele, T. J., Voegele-Kadletz, M., Esposito, V., Macfelda, K., Oberndorfer, U., Vecsei, V., & Schabus, R. (1999). The effect of different isolation techniques on human osteoblast-like cell growth. *Anticancer research*, *20*(5B), 3575-3581.

Wan, Y., Yu, A., Wu, H., Wang, Z., & Wen, D. (2005). Porous-conductive chitosan scaffolds for tissue engineering II. in vitro and in vivo degradation. *Journal of Materials Science: Materials in Medicine*, *16*(11), 1017-1028.

Wang, W., Sun, X., Huang, L., Gao, Y., Ban, J., Shen, L., & Chen, J. (2014). Structure-property relationships in hybrid dental nanocomposite resins containing monofunctional and multifunctional polyhedral oligomeric silsesquioxanes. *Int J Nanomedicine*, *9*(1), 841-52.

Wang, D., Romer, F., Connell, L., Walter, C., Saiz, E., Yue, S., & Jones, J. R. (2015). Highly flexible silica/chitosan hybrid scaffolds with oriented pores for tissue regeneration. *Journal of Materials Chemistry B*, *3*(38), 7560-7576.

Wang, D., Liu, W., Feng, Q., Dong, C., Liu, Q., Duan, L., & Liang, Y. (2016). Effect of inorganic/organic ratio and chemical coupling on the performance of porous silica/chitosan hybrid scaffolds. *Materials Science and Engineering:C*.

Webb, P. A. (2001). An introduction to the physical characterization of materials by mercury intrusion porosimetry with emphasis on reduction and presentation of experimental data. *Micromeritics Instrument Corp, Norcross, Georgia*.

Wee, K. M., Rogers, T. N., Altan, B. S., Hackney, S. A., & Hamm, C. (2005). Engineering and medical applications of diatoms. *Journal of Nanoscience and Nanotechnology*, *5*(1), 88-91.

Weigel, T., Schinkel, G., & Lendlein, A. (2006). Design and preparation of polymeric scaffolds for tissue engineering. *Expert Review of Medical Devices*, *3*(6), 835-851.

Wu, C. J., Gaharwar, A. K., Schexnailder, P. J., & Schmidt, G. (2010). Development of biomedical polymer-silicate nanocomposites: a materials science perspective. *Materials*, *3*(5), 2986-3005.
Wu, S., Liu, X., Yeung, K. W., Liu, C., & Yang, X. (2014). Biomimetic porous scaffolds for bone tissue engineering. *Materials Science and Engineering: R: Reports*, *80*, 1-36.

Yuan, Y., & Lee, T. R. (2013). Contact angle and wetting properties. In *Surface science techniques* (pp. 3-34). Springer Berlin Heidelberg.

Zhang, Y., & Zhang, M. (2002). Three-dimensional macroporous calcium phosphate bioceramics with nested chitosan sponges for load-bearing bone implants. *Journal of biomedical materials research*, *61*(1), 1-8.

Zhang, L., & Webster, T. J. (2009). Nanotechnology and nanomaterials: promises for improved tissue regeneration. *Nano today*, *4*(1), 66-80.

Zhang, J., Nie, J., Zhang, Q., Li, Y., Wang, Z., & Hu, Q. (2014). Preparation and characterization of bionic bone structure chitosan/hydroxyapatite scaffold for bone tissue engineering. *Journal of Biomaterials Science, Polymer Edition*, *25*(1), 61-74.

Zheng, Z., Zhang, L., Kong, L., Wang, A., Gong, Y., & Zhang, X. (2009). The behavior of MC3T3-E1 cells on chitosan/poly-L-lysine composite films: Effect of nanotopography, surface chemistry, and wettability. *Journal of Biomedical Materials Research Part A*, *89*(2), 453-465.

Zapphu, N., & Chen, X. (2013). *Biofabrication of tissue scaffolds*. INTECH Open Access Publisher.

Zohora, F. T., & Azim, A. Y. M. A. (2014). Biomaterials as porous scaffolds for tissue engineering applications: A review. *European Scientific Journal*, *10*(21).

Zhou, P., Xia, Y., Cheng, X., Wang, P., Xie, Y., & Xu, S. (2014). Enhanced bone tissue regeneration by antibacterial and osteoinductive silica-HACC-zein composite scaffolds loaded with rhBMP-2. *Biomaterials*, *35*(38), 10033-10045.

CURRICULUM VITAE

GENERAL INFORMATION

Sedef TAMBURACI
Telephone: +90 5073661490
E-mail: sedeftamburaci@gmail.com

EDUCATION

PhD in Bioengineering 2009-2016, Izmir Institute of Technology, Izmir, Turkey
MSc in Bioengineering 2006-2009, Ege University, Izmir, Turkey
B.S. in Bioengineering 2002-2006, Ege University, İzmir, Turkey

RESEARCH EXPERIENCE

PhD: Natural and Synthetic Silica Incorporated Chitosan Composite Scaffolds for Bone Tissue Engineering Applications, **Advisor:** Prof. Dr. Funda Tıhmınlıoglu, **Co-advisor:** Prof. Dr. Hasan Havıtcıoglu

M.Sci.: The Optimisation Studies of *Pseudanabaena sp.* Production Isolated From Hot Spring, **Advisor:** Prof. Dr. Meltem Conk Dalay

Undergraduate Thesis: Animal Cell Immobilization**, Advisor:** Prof. Dr. Ismet Deliloglu Gurhan

Internship at Bioengineering Dept. Ege University, "Capari production, plant tissue culture techniques" (2004).

Internship at Institute of FMD (Foot and Mouth Disease), "Vaccine production, virus identification and classification" (2005).

WORK EXPERIENCE

Research Assistance and Teaching Assistance at Izmir Institute of Technology (2012- 2015)

PROJECTS

2008 MUH 005, **Production of *Pseudanabaena sp.* and Investigation of Effects on Cell Culture,** Scientific Research Project supported by. Ege University (2008-2009).

000189.STZ.2007-2 **Development of Skin Cream Including Spirulina Extracts and Investigation of Effects on In Vitro Cell Culture**, Industrial Thesis Project (SAN-TEZ) supported by Ministry of Science, Industry and Technology (2007-2008).

2011İYTE02 **Production and Characterization of Chitosan Based Composites for Orthopedic Applications**, Scientific Research Project supported by Izmir Institute of Technology (IYTE) (2011-2012).

0494.STZ.2013-2 **Production of Dental Composite Materials for Bone Tissue Regeneration**, Industrial Thesis Project (SAN-TEZ) supported by Ministry of Science, Industry and Technology (2013-2015).

PUBLICATIONS

"Determination of Superoxide Dismutase Activities in Different Cyanobacteria for Scavenging of Reactive Oxygen Species"; Gunes S., Tamburaci S., Imamoglu E., Conk Dalay M. Journal of Biologically Active Products from Nature Vol.5, Issue 1, 2015.

"Development of Novel Multilayer Chitosan-Silica Composites for Bone Tissue Engineering Applications" ; Gunes S., Tamburaci S., Tıhmınlıoğlu F.; Regenerative Medicine (Meeting Abstracts) Vol 10, No: 07s, 2015. ISSN 1746-0751

"Zein Based Bilayer Composites for Wound Healing" Tıhmınlıoğlu F., Tamburaci S.; Regenerative Medicine (Meeting Abstracts) Vol 10, No: 07s, 2015. ISSN 1746-0751.

"Development of Skin Creams Including *Spirulina platensis* extract and Its Effect on *In Vitro* Cell Cultures"; Gunes S., Tamburaci S., Conk Dalay M., Deliloglu Gurhan I.; Phythotherapy Research. **In progress.**

PRESENTATION

4-7 May 2008- **14th Biomedical Science and Technology Symposium**, **Mugla** "*In vitro*   Animal Cell Culture Tests For Determination of The Cytotoxic and Genotoxic Effects of Microalgal Products" **Poster presentation.**

1-5 October 2008, **International Enzyme Engineering Symposium, Izmir,**"Superoxide Determination in Some Microalgae" **Poster presentation.**

16-19 June 2010, **Vth International Bioengineering Congress, Ege University**, "Biochemical Composition of *Pseudanabaena sp.* Isolated From a Thermal Spring in Denizli, Turkey" and "Determination and Comparison of Cytotoxic Effects of *Spirulina platensis* and *Pseudanabaena sp.* on Animal Cell Cultures" **Poster presentations.**

3-6 September 2012 **10. National Chemical Engineering Congress (UKMK10-2012) organized by Koc University, Istanbul,** "Characterization of Chitosan/Diatomite Composite Films for Orthopedic Biomaterial Applications, **Oral Presentation.**

09-11 October 2012 **III. International Polimeric Composites Symposium-Exhibition and Workshop, Izmir,** "Production and Characterization of Natural Silica Reinforced Chitosan Composites for Orthopedic Biomaterial Applications, **Oral Presentation.**

17-20 June 2013 **The European Chapter Meeting of the Tissue Engineering and Regenerative Medicine International Society (TERMIS-EU 2013), Istanbul,** "Production and Characterization of Silica Reinforced Chitosan Composites for Orthopedic Biomaterial Applications " **Poster Presentation.**

22 February 2013 **I.Biomaterial Day organized by Boğaziçi University Biyomedical Engineering and Bio³ Research Laboratory, Istanbul,** "Production of Natural Silica Reinforced Polymer Composites for Orthopedic Biomaterial Applications", **Poster Presentation.**

16-17 May 2013 **Inovation in Health; From University to Industry-Workshop organized by Dokuz Eylül University, Izmir** "Production of Natural Silica Reinforced Polymer Composites for Orthopedic Biomaterial Applications" **Poster and Oral Presentation.**

16-19 September 2013 **Advanced Materials World Congress (AMWC 2013) organized by IZTECH, Izmir,** "Production and Characterization of Silica Reinforced Chitosan Composites for Orthopedic Biomaterial Applications" **Oral Presentation.**

24-28 August 2014 **The 2nd International Conference on Bio-Based Polymers and Composites (BiPoCo 2014), Visegrad, Hungary,** "Novel POSS Reinforced Chitosan Composites as Potential Scaffold for Bone Tissue Engineering Applications" **Poster Presentation.**

2-5 September 2014 **11. National Chemical Engineering Congress (UKMK-14) organized by Osmangazi University, Eskisehir,** "Production of Silica Reinforced Chitosan Based Composites for Orthopedic Bone Tissue Engineering Applications", **Oral Presentation.**

2-5 September 2014 **11. National Chemical Engineering Congress (UKMK-14) organized by Osmangazi University, Eskisehir,** "Production of Silica Reinforced Chitosan Based Composites for Orthopedic Bone Tissue Engineering Applications", **Oral Presentation.**

12-14 March 2015 **IBMEC'15 International Biomedical Engineering Congress, Near East University, Grand Library, Nicosia, North Cyprus** "Development of *Spirulina platensis* Extract Incorporated Skin Creams and Its Effect on *In Vitro* Cell Cultures", **Oral Presentation.**

8-11 July 2015 **FBPS'15 11th International Symposium on Frontiers in Biomedical Polymers, Riva del Garda, Italy,** "Production and Characterization of Novel Multilayer Chitosan Based Composite Biomaterial for Bone Regeneration", **Oral Presentation**.

21-23 October 2015, **World Conference on Regenerative Medicine Leipzig, Germany,** "Development of Novel Multilayer Chitosan-Silica Composites for Bone Tissue Engineering Applications"and"Zein Based Bilayer Composites for Wound Healing" **Poster Presentations.**

17-21 July 2016, **World Polymer Congress "MACRO 2016"**,"Development of Novel Bilayer Chitosan-nHap Composite Biomaterial for Guided Bone Regeneration", "Development, Characterization and *In vitro* cell culture studies of Zein Bilayer Composites as Bioactive Wound Dressing Material" and "Production and Characterization of Novel Bilayer Chitosan-Zein Based Composites for Osteochondral Tissue Regeneration" **Poster Presentations.**

23-26 August 2016, **12. National Chemical Engineering Congress (UKMK 2016) organized by İzmir Institute of Technology, İzmir,** "Production and Characterization of Bone Tissue Regeneration Enhancing Bioactive Extract Loaded Chitosan-Carboxymethylcellulose Scaffolds" **Oral Presentation.**